# INVESTIGATION OF THE HIGH-SPEED FINISH-TURNING OF Ti-5Al-5V-5Mo-3Cr ALLOY USING NOVEL MONO/BI-LAYERED PVD-COATED WC TOOLS

# INVESTIGATION OF THE HIGH-SPEED FINISH-TURNING OF Ti-5Al-5V-5Mo-3Cr USING NOVEL MONO/BI-LAYERED PVD-COATED WC TOOLS

By

Hasan Sohail Syed, B.Sc.

A Thesis Submitted to the School of Graduate Studies in Partial Fulfilment of the Requirements for the Degree Master of Applied Science (M.A.Sc.)

McMaster University

MASTER OF APPLIED SCIENCE (2024) McMaster University
(Mechanical Engineering) Hamilton, Ontario

| | |
|---|---|
| TITLE: | Investigation of the High-Speed Finish-Turning of Ti-5Al-5V-5Mo-3Cr Using Novel Mono/Bi-layered PVD-Coated WC Tools |
| AUTHOR: | Hasan Sohail Syed, B. Sc.<br>Mechanical Engineering |
| SUPERVISOR: | Dr. Stephen C. Veldhuis<br>Department of Mechanical Engineering |
| SUPERVISORY COMMITTEE | Dr. Zahra K. Motamed<br>Department of Mechanical Engineering<br>Dr. Maryam Aramesh<br>Department of Mechanical Engineering |
| NUMBER OF PAGES: | xiv, 102 |

## Acknowledgments

Alhamdulillah, praises and thanks belong to the One (swt) most high, without Whom none of what I have achieved would have been attainable. This, followed by my gratitude to Dr. Stephen C. Veldhuis for taking me under his wing, and giving me the opportunity at the McMaster Manufacturing Research Institute (MMRI) to fulfill the requisites for the fulfillment of my MASc degree. His guidance and support have been invaluable in my pursuit towards wanting to publish a sandwich thesis.

To Dr. Jose Mario DePaiva, you put me on the right trajectory and gave me the required support whenever needed; I am truly appreciative of that. Thank you to all my colleagues, friends, and staff members at the MMRI — especially Victor, Andres, Dr. Sharif, Brady, Kevin, and Terry — the technical knowledge and insight imparted onto me by all of you cannot be understated; I will forever be grateful for the perpetual influence it will have on the journey to follow.

My utmost expression of respect and love towards my parents, Sohail Akhtar and Seema Sohail, for their encouragement, guidance, and always being there for me when I needed assurance and emotional support through all the ups and downs I experienced on the path to completion. I owe it to them for raising me to be the man I am today, one with the fortitude and resilience to keep pushing no matter the circumstance arisen.

I look forward to what is to come, and ask Allah (swt) to grant me the best of both worlds. Ameen.

## Lay Abstract

The Ti-5Al-5V-5Mo-3Cr alloy is widely used in aerospace, biomedical, and military applications due to its excellent properties. Nevertheless, its high strength and toughness render it more difficult to machine than traditional titanium alloys. Despite increasing demand, there is limited research on machining this alloy with coated WC tools. This thesis aims to address this gap by investigating the performance of new coated cutting tools during high-speed machining in wet conditions. The study involves three main stages: pre-machining analysis, where existing research is reviewed and experimental methods are developed; machining analysis, which evaluates tool performance and surface finish; and post-machining analysis, which examines tool wear and chip characteristics. The goal is to improve the efficiency and cost-effectiveness of machining the Ti-5Al-5V-5Mo-3Cr alloy.

# Abstract

The Ti-5Al-5V-5Mo-3Cr alloy is used in aerospace, biomedical, and military fields due to its outstanding thermomechanical properties. Nevertheless, its higher strength and toughness make it more challenging to machine compared to traditional Ti alloys like Ti-64. Despite increasing demand, there is a noticeable lack of research on finish turning Ti-5553 with coated carbide tools. This thesis aims to fill that void by thoroughly investigating the tool life and micromechanical performance of new mono/bi-layered PVD-coated WC tools under high-speed finish turning in wet conditions. A commercially applied AlTiN-based coating is used as the baseline reference and compared with mono-layered ta-C (diamond-like carbon, DLC), AlCrN, and TiAlSiN coatings applied over the AlTiN base on three different cutting tools. The study focuses on assessing the tool life and workpiece surface finish outcomes of these coatings and has been divided into the following studies:

Study A - Pre-Machining Analysis: This study begins with a literature review, which informs the development of the experimental methodology, including the selection of coating types, cutting speeds, and other cutting parameters. It also involves characterizing the workpiece by examining its microstructure and mechanical and chemical properties before any cutting operations. Coating characterization includes micromechanical analysis (hardness, elastic modulus, plasticity index), examining the coatings' morphology, measuring adhesion and cohesion strengths, and coating thickness. Surface roughness data are also obtained from topography maps. The primary goal of Study A is to relate the properties of the workpiece and coatings to their respective microstructures.

Study B - Machining Analysis: This study focuses on evaluating tool and coating performance through a comparative analysis of flank wear and the cutting length achieved. It also involves inspecting the surface roughness of the workpiece after each machining pass. Tribological analysis includes collecting and analyzing chips at different stages of the machining cycle using an optical microscope. The main objective of this study is to correlate machining performance with process parameters and the coatings used.

Study C - Post-Machining Analysis: The final stage involves two sets. The first set, tool and coating morphology, includes analyzing morphological wear and elemental composition using SEM and XPS. Chip characterization involves examining the morphological features of the chips (length, thickness, curliness) and the roughness of their back surfaces. The aim of this study is to correlate the effects of cutting conditions on the surface integrity of the workpiece with the mechanical, chemical, and morphological characteristics of the cutting tools and chips.

# Table of Contents

## List of Figures

# List of Tables

## List of Abbreviations and Symbols

| | |
|---|---|
| McMaster Manufacturing Research Institute | MMRI |
| Titanium | Ti |
| Ti-6Al-4V | Ti-64 |
| Ti-5Al-5V-5Mo-3Cr | Ti-5553 |
| Molybdenum | Mo |
| Vanadium | V |
| Aluminum | Al |
| Ultimate Tensile Strength | UTS |
| Yield Strength | YS |
| Physical Vapor Deposition | PVD |
| Cathodic Arc Evaporation | CAE |
| High-power impulse Magnetron Sputtering | HiPIMS |
| X-ray Photoelectron Spectroscopy | XPS |
| Diamond-Like Carbon | DLC |
| Built-up Edge | BUE |
| Built-up Layer | BUL |
| Scalable Pulsed Power Plasma | S3p |
| Secondary Electrons | SE |
| Backscattered Electrons | BSE |
| Field Emission Scanning Electron Microscope | FESEM |
| Energy-dispersive X-ray Spectrometer | EDX/EDS |
| X-ray Diffraction | XRD |

| | |
|---|---|
| Secondary Electron Images | SXI |
| Hardness | H |
| Elastic Modulus | E |
| Acoustic Emissions | AE |
| Atomic Force Microscope | AFM |
| Arithmetical Mean Height | Sa |
| Maximum Height | Sz |
| Face-centred Cubic Structure | fcc |
| Body-centered Cubic Structure | BCC |
| Titanium-molybedenum Alloy | TMA |
| Feed | f |
| Depth of Cut | $a_p$ |
| Speed | $V_c$ |
| Minimum Quantity Lubrication | MQL |
| Cryogenic | Cryo |
| High-pressure Cooling | HPC |
| Material Removal Rate | MRR |
| Data Acquisition | DAQ |
| Three-dimensional | 3D |

# 1 Chapter 1: Introduction

## 1.1 Background

The continual progress in the development and optimization of alloys is fundamental to the growth of the industrial sectors that require the enhancement of thermomechanical properties for their desired applications. From the use of alloys in various industrial applications, to the study of their microstructural variation to uncover intricate deformation mechanisms and consequent effects on properties, all contribute to the ever-growing demands, and drive for the progress in the fields of materials and manufacturing [1], [2].

The effort to make improvements in the development of alloys, and by extension the dependent industries, can only be achieved if complemented with optimal machining and cost reduction practices. Augmenting machining parameters and procedures in relation to cutting speed, depth of cut, feed rate, cutting tool material, as well as the type of cutting fluid selected, while taking into account industry standards can provide a deeper understanding of the alloys being dealt with. The data collected and analyzed from these optimizations can in turn push the limits of potential applications and industrial impact.

Titanium (Ti) alloys have been utilized in several industrial sectors such as aerospace, military, and biomedical. This is owed to their excellent thermomechanical and chemical properties (serviceability). Nevertheless, properties such as high strength, high toughness, and low thermal conductivity classify Ti alloys as 'difficult-to-cut,' indicating poor machinability. [3], [4].

Ti-6Al-4V, abbreviated as Ti-64 has been the focus of extensive research to enhance its machinability. However, other titanium alloys, such as the β-alloy Ti-5Al-5V-5Mo-3Cr (Ti-5553), have not received as much attention or application in comparison to Ti-64. Ti-5553 at present is commonly utilized in the aerospace industry, particularly in landing gears and airframes (Boeing 787 Dreamliner and Airbus 350). While Ti-5553 boasts higher yield (~1300 MPa) and tensile strengths (~1250 MPa)—about 30% more than Ti-64—it has a lower elastic modulus (~10 GPa) and fracture toughness (~55 to 90 MPa). These characteristics result in roughly 25% lower metal removal rates and 15% shorter tool life compared to Ti-64. [5], [6], [7], [8]. As a result, the reduced machining performance hinders its machinability, thereby restricting its potential for further research and industrial application.

The nature of these alloys is such because of their categorization into several different phases, namely, α- and near α-alloys, β- and near β-alloys, α + β alloys, and shape-memory alloys. However, those prioritized for this discussion are β- and near β, and α + β alloys due to their relevancy [5], [9]; shown in Figure 1.1:

**α + β alloys:**

Typical microstructures of Ti-64 and Ti-5553 alloys are shown in Figure 1.2. α + β alloys are the most commonly utilized Ti alloys in the industry. They have β-stabilizers (Mo and V as examples) usually in amounts of 4-6 wt.%. Since they have a higher proportion of β-phase as compared to the near-α type, it can be heat treated to achieve higher mechanical strength. Moreover, they exhibit a binary phase microstructure, with ~20 vol% metastable β-phase, when quenched to the ambient temperature leading to improved

strength of the Ti workpiece. Aging of the alloy is another method through which the alloy is strengthened as a result of the metastable β-phase forming the lamellar α-phase. The most widely employed α + β Ti alloy is the well-established Ti-64.

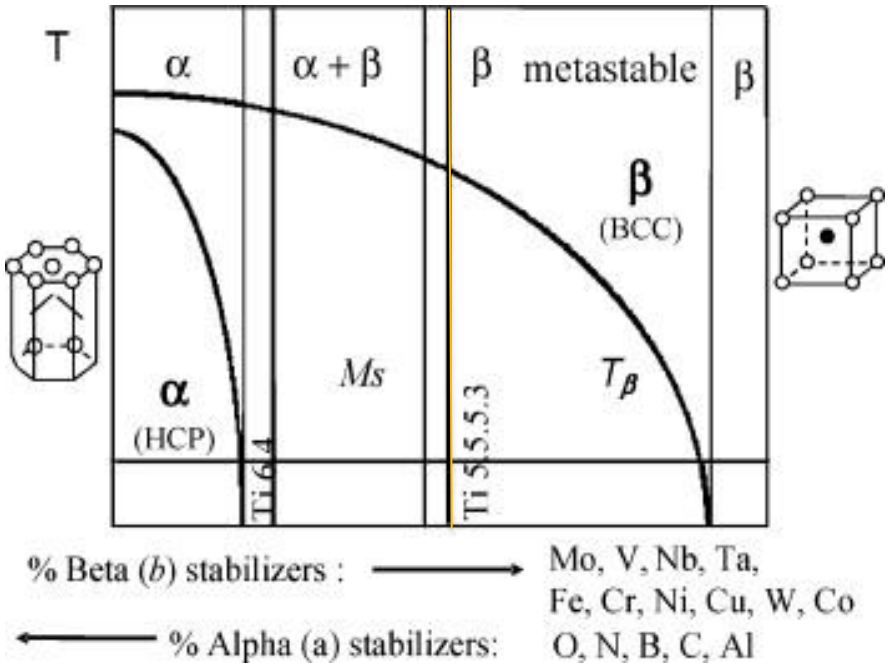


**Figure 1.1: Phase diagram of Ti-5553 and Ti-64 alloys. Reprinted with permission from Arrazola et al. [10]. Copyright © 2009, Elsevier**

**β- and near β (Ti-5553):**

β- or near β-alloys are deemed as Ti alloys with the highest strength. Similar to the α + β- phase alloys, when quenched to ambient temperature from the β-phase state, its strength experiences a rise, however, a higher proportion of metastable β-phase can be preserved (100% if pure Ti). The term "metastable" is associated with some of these β-alloys and are labelled as "metastable β-alloys" because they transform into an α + β- phase, with β- as the matrix and α- particulates, upon going through the aging process. The fraction of each phase is dependent on parameters such as temperature and rate and can significantly affect

the properties of the desired alloy. The relatively higher strengths of near β in comparison to α + β alloys can be attributed to the aforementioned transitional aging process.

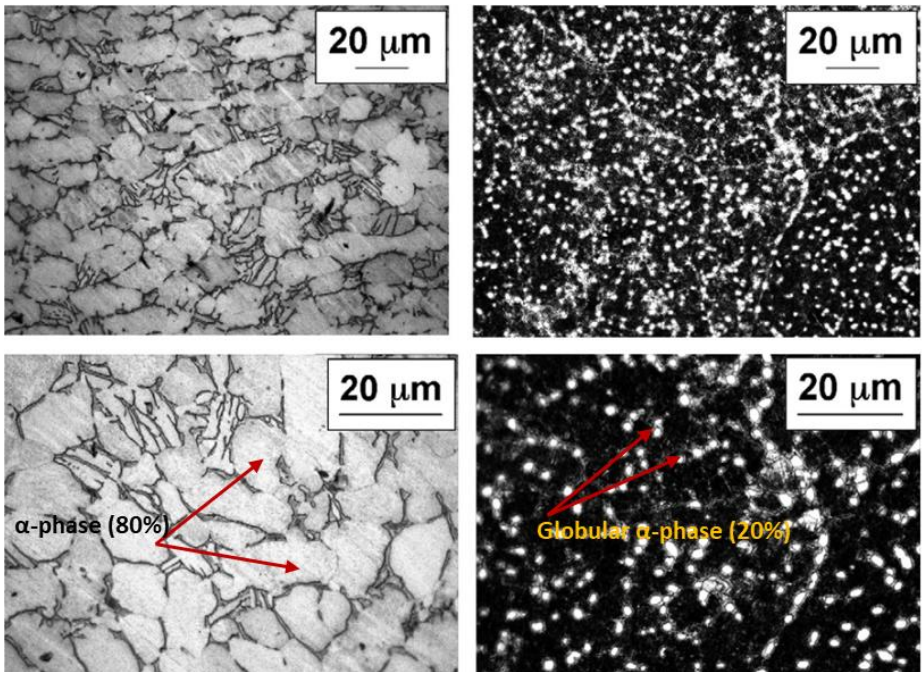


**Figure 1.2: Microstructures of (a) Ti-64 and (b) Ti-5553 . Reprinted with permission from Arrazola et al. [10]. Copyright © 2009, Elsevier**

Apart from the phase compositions, the alloying elements incorporated dramatically change the thermomechanical properties of the alloy. Since the main elements used in forming Ti alloys are aluminum (Al), molybdenum (Mo), and vanadium (Va), adjusting their ratios can significantly affect hardness, ultimate tensile strength (UTS), and yield strength (YS). In terms of Mo content, Ti-5553 contains 7-8 times more than Ti-64, which enhances its mechanical properties by approximately 15-30% in UTS and YS. [7], [10], [11]. While Ti-5553 offers advantages in industrial use, its machining performance suffers

due to its increased mechanical properties (reduced ductility and damage resistance) and modified β-phase structure, making it more difficult to machine than Ti-64

Although Ti-5553 offers properties that are widely applicable in heavy duty applications, its machinability serves as a challenge for the aforementioned reasons:

- While most materials typically produce continuous chips, Ti and its alloys usually generate shear-localized (serrated) chips. Machining Ti-5553 at any cutting speed results in chips with narrow adiabatic shear bands. In contrast, Ti-64 forms partially segmented chips without adiabatic shear bands at low cutting speeds, and segmented chips with adiabatic shear bands, also known as catastrophic thermoplastic shear, at high speeds [12]. Additionally, these adiabatic shear bands can induce force component oscillations, leading to rapid tool wear, with a higher frequency of oscillation in Ti-5553 compared to Ti-64 [10].
- Cutting forces and their components are key criteria for evaluating machinability performance, crucial for optimizing and improving the machining of Ti-5553. The highest mechanical stresses from cutting forces occur at the cutting tool-chip interface due to the brittleness of Ti alloys at high temperatures [11]. Increasing feed rate, depth of cut, and cutting speeds all elevate cutting forces. Depth of cut and cutting speeds interact; at low depths of cut, changes in cutting speed have little effect on cutting forces, whereas at high depths of cut, cutting speeds significantly influence cutting forces. This variation at high depths of cut indicates tool wear's impact on the cutting force needed to form chips [13]. Furthermore, cyclic loading can affect cutting forces, leading to chatter and eventual wear, particularly in β-

alloys [12]. Ti-alloys like Ti-5553 experience nearly twice the deflection of carbon and stainless steels, causing early flank wear due to larger spring-back [11].

- The primary reason Ti-5553 is used in applications demanding high reliability is its surface integrity. Thus, maintaining optimal surface finish is essential. According to Kaynak et al. [13], for Ti-5553 alloys, increasing the depth of cut raises surface roughness, while higher cutting speeds reduce surface roughness. This is due to increased tool wear and the worn cutting tool nose providing a smoother finish. However, despite the reduced surface roughness at higher cutting speeds, the dimensional accuracy of the workpiece worsens because of the worn cutting tool nose.

**Additional points** [12], [14], [15]:

- Ti-5553 has a tendency to chemically react and weld to the cutting tool, leading to rapid tool wear at high cutting speeds.
- The cutting tool and chip have a contact length shorter than that found in steel at the same cutting parameters. This can be attributed to elevated temperatures and stresses at the cutting edge.
- During dry cutting condition and high cutting temperatures, chips have a tendency to ignite.
- Low thermal conductivity of Ti-5553 contributes to elevated cutting temperatures in the machining zone.

- Machining at elevated thermomechanical loads can result in the formation of a few microns thick heated white layer. It is known to lower fatigue life because of its hard and brittle nature, which can lead to surface cracking and propagation.
- It has been reported that the nature of surface residual stresses when machining Ti-5553 alloys is compressive, and their intensity is dependent on the cutting conditions.
- Understanding the effects of cutting temperatures at the tool-chip interface is critical, as increased heat generation in the cutting zone can cause the workpiece and cutting edge to melt, resulting in reduced tool life and elevated wear. The highest temperatures during the machining of Ti alloys are found in the primary and secondary shear zones (tool-chip interface and tip), as illustrated in Figure 1.3. Kaynak et al. [13] reported that, for Ti-5553 alloys, cutting temperatures increase with cutting speed. An increased depth of cut leads to higher temperatures, with the most significant effect observed at cutting speeds above 120 m/min when using WC tools. Additionally, elevated temperatures can cause thermal softening, reducing the hardness of the tool and inducing plastic deformation and severe wear at the cutting edge. The effect of feed rate on temperature is marginal compared to the influence of depth of cut and cutting speeds.
- Having gone through the challenges, it is essential to understand the machining performance and its effect on the surface integrity and tool life of Ti-5553. The impact of varying machining parameters, tool material, cutting fluid, and coatings on the generation of different wear mechanisms, heat dissipation, cutting forces,

and other factors have been analyzed and optimized to present the best machining conditions for improving surface integrity and tool life.

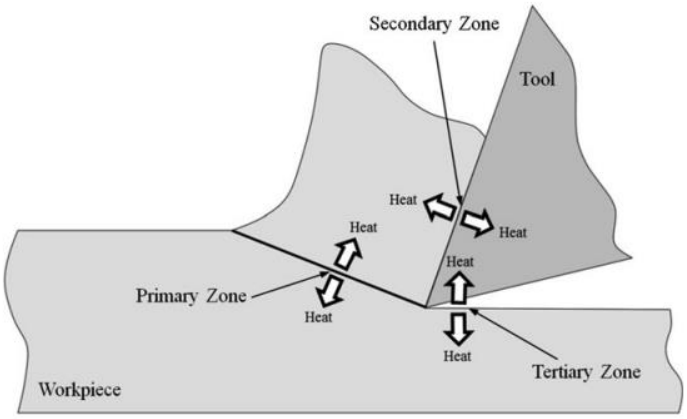


**Figure 1.3: Cutting zone locations in relation to regions of heat dissipation . Reprinted with permission from Hosseini et al. [16]. Copyright © 2014 Springer-Verlag Berlin Heidelberg**

## 1.2 Motivation and Problem Description

Previous studies have not adequately examined the role of physical vapor deposition (PVD) coatings on WC-Co tools in the finish-turning of Ti-5553 alloys. Most studies overlooked coatings as a key factor in machining performance, with only a few even considering their use. Consequently, there is a scarcity of literature on the machinability and the effects of tool materials and coatings during the finish-machining of Ti-5553 alloy. Therefore, a thorough investigation was done on the machining performance, chip morphology, coating properties, among other factors.

- A comparative analysis between different coating types and their influence on the machining performance of Ti-5553 is non-existent in the literature. Hence, the effect of various coating compositions and architecture was investigated on the machining performance of Ti-5553 alloy.

- The dominant wear mechanisms and the resulting tool life under different coating conditions on carbide tools were investigated and their relationship with varying parameters in cutting Ti-5553 established.
- To assess the coatings' performance, morphological analysis of produced chips was performed to relate the various coated tools with the workpiece material under different parameters and flood lubricant.
- A detailed study was conducted to analyze the relationship between the coating properties and the resulting imparted workpiece surface quality.

## 1.3 Research Objectives

The primary goal of this research was to improve the overall finish-turning performance of Ti-5553 alloys by means of different coating types and machining parameters, and in turn increasing the tool life, surface quality, and gain a better understanding of the impact of coatings on Ti-5553 machining. This was achieved by employing a systematic scientific approach to investigate and analyze the many factors that affect a coating's performance, and then discerning the most suitable type. Following are some specific objectives as outcomes of the tasks:

- Synthesis and characterization of CAE and HiPIMS applied PVD coatings on WC-Co tools was done on four different variants of coatings: A monolayer AlTiN, Bi-Layer AlTiN/ta-C, Bi-layer AlTiN/AlCrN, and Bi-layer AlTiN/TiAlSiN coatings. Adhesion, topography, and micromechanical data (Hardness, elastic modulus, and fracture toughness) are some of the factors that were investigated and compared.

- Investigation of wear mechanisms and tool life of the different coating types under varying cutting parameters: The tests were performed at three different levels of high-cutting speeds, 150, 175, and 200 m/min, with a constant depth of cut, and feed rate of 0.25 mm, and 0.15 mm/rev, respectively. A flood lubricant was utilized.
- To assess the coatings' performance, morphological and property assessment of the coated tools were done pre- and post- machining at the high-cutting speeds to assess the coatings' performance.
- Morphology and surface integrity of chips at different stages (start, mid, and end) of the machining process were evaluated to compare chip undersurface quality, shear band formation, and general shape of the coatings, while simultaneously being related to the machining performance.

## 1.4 Experimental Methodology

The following subsection delves into the research and experimental methodology utilized for the completion of the research objectives. Figure 1.4 gives an overview of the steps taken. The studies have been divided into three, namely, Study A: Pre-Machining Analysis, Study B: Machining Analysis, Study C: Post-Machining Analysis. Study A and B were done in no particular order, whereas Study C follows B. The blocks are colored based on the types of experiments and analysis included in each of the sets. Pink represents machining, yellow includes tool and coating, and green tribological and chip analysis.

**Study A, Pre-Machining Analysis**, involves the literature review performed based on which the experimental methodology was developed. This includes the selection of coating types, cutting speeds, and other cutting parameters. Workpiece characterization, as the

name suggests, constitutes the study of the microstructure of the workpiece, and its mechanical, and chemical properties ahead of any cutting operations. Coating characterization includes: micromechanical analysis (hardness, elastic modulus, plasticity index (PI)); investigation of the coatings' morphology; adhesion and cohesion strengths; and coating thickness measurements. Topography maps were also taken to extract surface roughness data. The main purpose of Study A was to relate the various properties of the workpiece and coatings with their respective microstructures.

**Study B, Machining Analysis**, includes investigation of the tool/coating performance. A comparative analysis of the flank wear, as well as the cutting length reached are part of this set. Workpiece analysis considers the inspection of surface roughness after each machining pass. The tribological analysis set includes the collection of chips at the start, mid, and end of the machining cycle (based on flank wear/cutting length), followed by their analysis under an optical microscope. Moreover, this set also includes the extraction of cutting force data by utilizing a dynamometer, and its visualization via a DAS system. The primary goal of this study was to correlate machining performance with the process parameters and coatings employed.

**Study C, Post-Machining Analysis**, is the last stage, and includes two sets. The first set, which is that of tool and coating morphology, involves morphological wear and elemental composition analysis using the SEM, and XPS, respectively. Chip characterization contains the morphological analysis of the chips (i.e. length, thickness, curliness), as well as the back surface roughness. The aim of this study was to correlate the impact of cutting conditions on the surface integrity of the workpiece in relation to the mechanical, chemical, and morphological aspects of the cutting tools and chips.

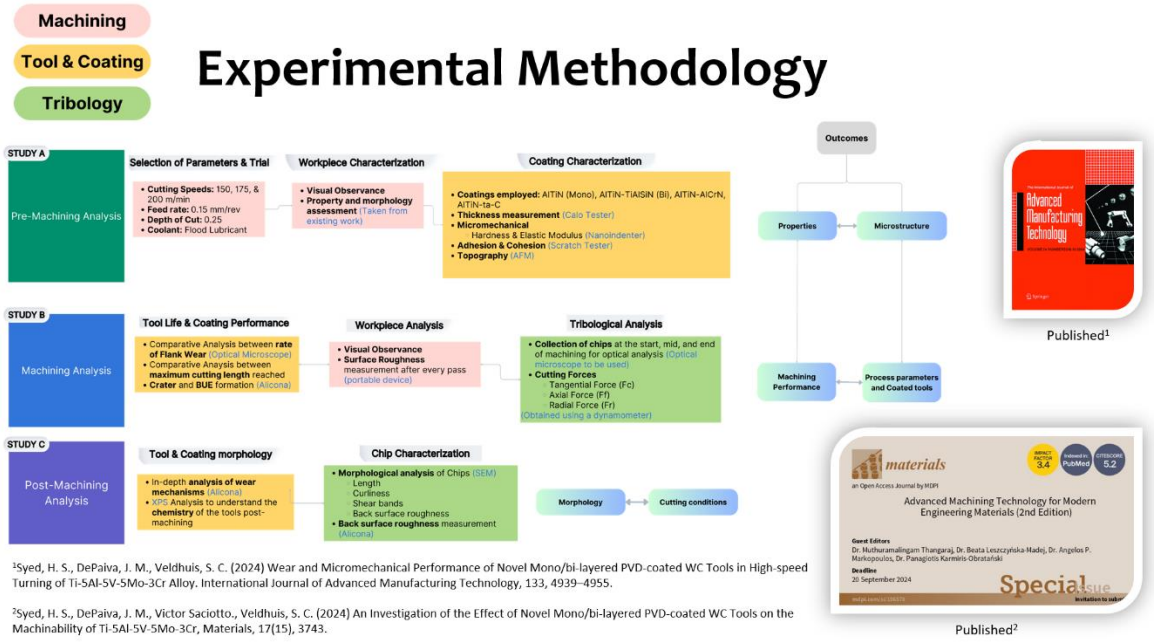


**Figure 1.4: Experimental Methodology**

## 1.5 Thesis Organization

In fulfillment of McMaster University's regulations, the central body of this thesis conforms to a sandwich thesis format. It constitutes an introductory chapter that gives an overview of the topic at hand, existing challenges, objectives, and the experimental methodology. The published articles addressing the objectives of the work are incorporated

into the two subsequent chapters. The last chapter concludes with the major findings and future recommendations. The thesis has been structured as follows:

**Chapter 1:** This chapters introduces the topic with a literature review, motivation, research gaps, and the experimental methodology. The experimental methodology divides the study into three subsets, with each detailing the experimental analysis performed to reach the desired outcomes.

**Chapter 2:** This chapter conducts a comprehensive investigation of the wear and micromechanical performance of PVD coated WC-tools in relation to their machining performance on Ti-5553. The cutting tools involved are composed of a base monolayered AlTiN-coated tool, and AlCrN, ta-C, and TiAlSiN coatings each deposited on top of the base AlTiN coating on three separate cutting tools to form bi-layered AlTiN/AlCrN, AlTiN/ta-C, and AlTiN/TiAlSiN coatings, respectively. The study reveals that a coating's tribological and tool life performance is largely determined by its intrinsic properties.

**Chapter 3:** A detail analysis on the machinability of Ti-5553 has been conducted using the aforementioned sets of coated cutting tools under varying machining conditions. Tool life, cutting forces, workpiece surface quality, and tribological chip analysis were among the subjects of investigation in this study.

**Chapter 4:** The last chapter concludes the thesis by summarizing the major findings extracted from the published articles, and provides the reader with potential pathways to further investigate the machinability of Ti-5553.

## 1.6 Note to the Reader

The nature of the sandwich thesis is such that it is composed of published articles, and therefore, contains repetitions in certain portions, notably in the introduction and experimental sections. Nevertheless, the introduction provides an overview of the contents of the published articles, as well as the research gaps and the experimental methodology employed to address said gaps.

## 1.7 References


1. J. Zhang, X. Li, D. Xu, and R. Yang, "Recent progress in the simulation of microstructure evolution in titanium alloys," *Progress in Natural Science: Materials International*, vol. 29, no. 3, pp. 295–304, Jun. 2019, doi: 10.1016/J.PNSC.2019.05.006.
2. L. C. Zhang and L. Y. Chen, "A Review on Biomedical Titanium Alloys: Recent Progress and Prospect," *Adv Eng Mater*, vol. 21, no. 4, p. 1801215, Apr. 2019, doi: 10.1002/ADEM.201801215.
3. S. D. Bartus, "Evaluation of Titanium-5Al-5Mo-5V-3Cr (Ti-5553) Alloy against Fragment and Armor-Piercing Projectiles," Sep. 2009. doi: 10.21236/ADA516831.
4. Y. Sun, B. Huang, D. A. Puleo, and I. S. Jawahir, "Enhanced machinability of Ti-5553 alloy from cryogenic machining: Comparison with MQL and flood-cooled machining and modeling," *Procedia CIRP*, vol. 31, pp. 477–482, 2015, doi: 10.1016/J.PROCIR.2015.03.099.
5. J. C. Williams and R. R. Boyer, "Opportunities and Issues in the Application of Titanium Alloys for Aerospace Components," *Metals 2020, Vol. 10, Page 705*, vol. 10, no. 6, p. 705, May 2020, doi: 10.3390/MET10060705.

**6.** J. D. Cotton *et al.*, "State of the Art in Beta Titanium Alloys for Airframe Applications," *JOM*, vol. 67, no. 6, pp. 1281–1303, Jun. 2015, doi: 10.1007/S11837-015-1442-4/FIGURES/25.

**7.** V. Wagner, M. Baili, and G. Dessein, "The relationship between the cutting speed, tool wear, and chip formation during Ti-5553 dry cutting," *International Journal of Advanced Manufacturing Technology*, vol. 76, no. 5–8, pp. 893–912, Feb. 2015, doi: 10.1007/S00170-014-6326-1/METRICS.

**8.** "Titanium 2005 conference proceedings, 21st Annual International Titanium Association, Scottsdale, Arizona, September 25-27, 2005.," Broomfield, Colo. : International Titanium Association.

**9.** L. C. Zhang, L. Y. Chen, and L. Wang, "Surface Modification of Titanium and Titanium Alloys: Technologies, Developments, and Future Interests," *Adv Eng Mater*, vol. 22, no. 5, p. 1901258, May 2020, doi: 10.1002/ADEM.201901258.

**10.** P.-J. Arrazola, A. Garay, L.-M. Iriarte, M. Armendia, S. Marya, and F. Le Maître, "Machinability of titanium alloys (Ti6Al4V and Ti555.3)," *J Mater Process Technol*, vol. 209, no. 5, pp. 2223–2230, Mar. 2009, doi: 10.1016/j.jmatprotec.2008.06.020.

**11.** E. O. Ezugwu and Z. M. Wang, "Titanium alloys and their machinability—a review," *J Mater Process Technol*, vol. 68, no. 3, pp. 262–274, Aug. 1997, doi: 10.1016/S0924-0136(96)00030-1.

**12.** A. R. Machado and J. J Wallbank, "Machining of Titanium and its Alloys—a Review," *http://dx.doi.org/10.1243/PIME_PROC_1990_204_047_02*, vol. 204, no. 1, pp. 53–60, Aug. 2016, doi: 10.1243/PIME_PROC_1990_204_047_02.

**13.** Y. Kaynak and A. Gharibi, "The effects of cutting parameters on machining performance of titanium alloy Ti-5553," *Advances in Materials and Processing Technologies*, vol. 5, no. 2, pp. 317–328, Apr. 2019, doi: 10.1080/2374068X.2019.1585071.

**14.** E. Moor and W. Paul Kenneth, *Metal cutting*, 4th ed. Butterworth-Heinemann, 2000. Accessed: Jan. 03, 2023. [Online]. Available: https://ebookcentral.proquest.com/lib/mcmu/detail.action?pq-origsite=primo&docID=296697

**15.** M. Rahman, Y. Wong, and R. Zareena, "Machinability of titanium alloys," *JSME International Journal Series C Mechanical Systems, Machine Elements and Manufacturing*, 2003.

**16.** J. P. Davim, "Materials Forming, Machining and Tribology Machining of Titanium Alloys," *Springer*, 2014, Accessed: Feb. 16, 2023. [Online]. Available: http://www.springer.com/series/11181

# 2 Chapter 2: Wear and Micromechanical Performance of Novel Mono/bi-layered PVD-coated WC Tools in High-speed Turning of Ti-5Al-5V-5Mo-3Cr Alloy

Syed, H.S.[1,*], DePaiva, J.M.[1], Veldhuis, S.C.[1]

1 - McMaster Manufacturing Research Institute (MMRI), Department of Mechanical Engineering, McMaster University, 230 Longwood Rd S, Hamilton, ON L8P0A6, Canada.

* Corresponding author: syedh39@mcmaster.ca (Syed, H.S.).

*This paper is published in the International Journal of Advanced Manufacturing Technology (IJAMT) - (IF 2.9) 133, 4939–4955*

*https://doi.org/10.1007/s00170-024-14045-1*

**Author's Contribution**

| | |
|---|---|
| Hasan Sohail Syed | Investigation, methodology, validation, formal analysis, writing—original draft, writing—review and editing, visualization. |
| Jose Mario DePaiva | Resources, supervision. |
| Stephen C. Veldhuis | Conceptualization, supervision, project administration, funding acquisition. |

**Abstract**

The Ti-5Al-5V-5Mo-3Cr alloy is utilized in the aerospace, biomedical, and military industries for its exceptional thermomechanical properties. However, its comparatively higher strength and toughness render it more difficult-to-cut than traditionally employed Ti alloys such as Ti-64. Despite its growing demand, a noticeable gap concerning the finish

turning of Ti-5553 using coated carbide tools was identified. This paper aims to address this gap by conducting a comprehensive investigation of the tool life and micromechanical performance of novel mono/bi-layered PVD-coated WC tools under high-speed finish turning and wet conditions. A commercial AlTiN-based coating serves as the baseline reference layer and was compared with mono-layered ta-C (diamond-like carbon, DLC), AlCrN, and TiAlSiN coatings deposited atop the AlTiN base on three separate cutting tools. The study focused on evaluating the tool life and surface finish results of all the coatings. Demonstrating that the AlTiN/AlCrN coated tool exhibited the longest tool life, improvement of ~ 9.02% with reference to the baseline, while imparting the smoothest surface finish, an improvement of ~ 31.81%, on the workpiece material due to its optimal micromechanical properties and conducive oxide formation. The results obtained offer valuable insight into understanding the relationship between machining performance and coating properties, consequently allowing the industrial sector to refine its selection criteria to aid with productivity and quality assurance.

## 2.1 Introduction

Titanium (Ti) and its alloys have been employed in industries such as aerospace, military, biomedical, and marine due to the several thermomechanical and chemical properties they provide (serviceability). However, many of these properties, including but not limited to, high strength, high toughness (due to low oxygen content), and low thermal conductivity deem the classification of titanium alloys as “difficult-to-cut” and lower their machinability performance [1, 2].

For this very reason, Ti-6Al-4V, abbreviated as Ti-64, has been studied and covered extensively in the literature to improve its machinability. However, many other titanium-based (Ti-based) alloys exist, yet they are not studied or applied as much as Ti-64. Amongst these is a β-alloy known as Ti-5Al-5V-5Mo-3Cr, abbreviated as Ti-5553. Ti-5553 has excellent properties such as high strength, high toughness, exceptional corrosion resistance, and elevated temperature stability, and is reported to be half as heavy as steel- or nickel-based alloys giving excellent strength-to-weight ratio [3, 4]. These properties have allowed for its use in the aerospace industry, particularly in landing gears and airframes (Boeing 787 Dreamliner and Airbus 350), as well as in biomedical applications such as 3D printed implants [5, 6]. Although it has comparatively higher yield (~ 1300 MPa) and tensile strengths (~ 1250 MPa) than Ti-64, which is a difference of approximately 30% for each standard, it has lower elastic modulus (~ 10 GPa) and fracture toughness (~ 55 to 90 MPa). These properties cause it to have ~ 25% lower metal removal rates, and ~ 15% lower tool life than Ti-64 [7,8,9,10]. Hence, the lower machining performance hinders its machinability performance and thus limits its potential to be studied and implemented in the industry at a wider scale. The mechanical superiority of Ti-5553 over Ti-64 can partly be attributed to the alloying elements incorporated. Considering that the primary elements utilized in the formation of Ti-based alloys are aluminum (Al), molybdenum (Mo), and vanadium (V), as is evident from Table 1 [6, 9, 11, 12], varying their proportions can drastically impact the hardness, ultimate tensile (UTS) and yield strengths (YS), respectively. When comparing the Mo content of Ti-5553 and Ti-64, it can be observed that the former has a value 7–8 times greater than the latter, contributing to its improvement

in mechanical properties by about ~ 15–30% (UTS and YS) as shown in Table 2 [8, 11, 16]. However, despite its positive impact on service in the industry, machining performance experiences a decline, as Ti-5553 now having higher mechanical properties (lower ductility and damage resistance) and metamorphosed morphology of the β-phase, is more difficult-to-cut than the traditionally machined Ti-64. Moreover, according to Stephenson et al. [17], alloys with higher contents of β-phase concentration generally have improved strength which leads to poor machinability than their α-phase counterparts, hence, reaffirming the aforementioned points about its more difficult-to-cut nature.

**Table 2.1: Table 1 Chemical composition of Ti-5553 and Ti-64 alloys [6, 9, 11, 12]**

| **Composition** (wt.%) | **Al** | **V** | **Mo** | **Cr** | **Fe** | **Z** | **O** | **N** | **C** |
|---|---|---|---|---|---|---|---|---|---|
| Ti-5553 alloy | 4.5–6 | 4–5.5 | 4–5.5 | 2.5–3.5 | 0.3-0.5 | <0.4 | <0.2 | <0.1 | <0.1 |
| Ti-64 alloy | 4.5-6 | 3.5-4.5 | - | - | 0.3-0.8 | - | <0.2 | <0.1 | <0.1 |

**Table 2.2: Table 2 Thermomechanical properties of Ti-5553 and Ti-64 at ambient temperature [9, 11, 12, 13, 14, 15]**

| **Properties** | **Ultimate Tensile Strength** *(MPa)* | **Yield strength** (*MPa)* | **Elongation** *(%)* | **Fracture Toughness** *($K_{1C}$)* | **Thermal Conductivity** (*$W/m^{-1}C^{-1}$)* | **Specific heat** *($J.\ Kg^{-1}C^{-1}$)* |
|---|---|---|---|---|---|---|
| Ti-5553 alloy | ~1300 | ~1250 | 6-10 | 55-70 | 5.3-6.2 | 400-500 |
| Ti-64 alloy | ~950 | ~880 | 14-18 | 60-85 | 6.7-7.3 | 520-710 |

The study of wear is of great importance for such alloys as it has a direct impact on the quality of the workpiece, and cost. For instance, high wear-resistant tools have longer serviceability, resulting in lower production costs, improved workpiece surface quality, and dimensional accuracy. Tools with rapid wear, on the other hand, tend to get scrapped and have unpredictable service lives and costs [17]. Ti-5553 like many of the other Ti-based alloys is prone to certain common wear mechanisms such as adhesion, abrasion, and

diffusion/oxidation. Abrasion wear primarily occurs on the flank side of the cutting tool due to hard particles rubbing between the workpiece and the cutting tool during the machining process. The particles causing the abrasion can either be remnants of the workpiece or the cutting tool. Primary causes of abrasion wear are high cutting speeds and the use of a soft cutting tool material. Wagner et al. [8] reported that for Ti-5553, abrasive wear resulting from abrasive chips caused a change in the cutting tool geometry close to the cutting edge and that it got progressively worse because of BUE formation, leading to high cutting forces and temperatures, facilitating the formation of more BUE due to rise in ductility. Adhesion wear happens on both the flank and rake faces because fragments of a softer workpiece substance adhere to the tool while the workpiece and cutting tool are in relative motion. Subsequently, when the adhered material accumulates (leading to BUE formation) and comes off, it can cause the cutting tool material to be peeled off resulting in further wear. This wear type is mainly attributed to low cutting speeds (affects chip flow), low feed rate (causes ploughing), and poor application of lubricants. According to Ugarte et al. [18] adhesion severity was higher for Ti-5553 as compared to Ti-64 due to poorer machinability. Moreover, cutting-edge fracture leading to cutting material peel-off was attributed to adhesion wear. However, Liu et al. [19] mentioned that adhesion can, under certain circumstances, protect the tool from wearing by reducing the contact length between the rake face and the chip. Some elements can diffuse from the tool to the workpiece or vice versa at high temperatures in the tool-workpiece contact zone, from the region of high to low concentration. It often happens as a result of improper selection of cutting tools, and lack of coolant application. Diffusion wear has been reported as the most frequent wear

mechanism for all cutting tool materials in the machining of Ti alloys [8, 11]. According to Hartung et al. [20], for Ti alloys, at low cutting speeds a stable built-up layer (BUL) forms which reduces diffusion wear owing to a reduction in sliding between the workpiece and tool, however, at higher cutting speeds (~> 90 m/min) the BUL deteriorates leading to rapid tool wear. Oxidation is another tribo-chemical wear that occurs due to the chemical reaction of some of the elements of the cutting tool material with oxygen. It transpires on surfaces openly exposed to oxygen and can lead to notch wear on the region of the highest depth of cut. The major causes of this wear type are high cutting temperatures, low feed rates and depth of cut, and a high work-hardening tendency of the material.

Literature indicates that very limited research has been performed on the turning machining of the Ti-5553 alloy, and even less so on the tribological comparative analysis of physical vapor deposition (PVD)-coated WC-Co tools in relation to the machining performance on said workpiece material. PVD is an atomistic deposition process, which means that the material transitions to a vapor phase form from either a solid or liquid state. Subsequently, the vaporized material travels through a low vacuum or plasma chamber from the target material to the substrate, where it condenses, as depicted in Fig. 1. The evaporation of the target material may be done by vacuum deposition which includes resistance heating, electron beam heating, induction heating, and arc evaporation, sputtering, or ion plating [21, 22]. The typical coatings applied to carbide tools are TiN, TiC, TiCN, TiAlN, $Al_2O_3$, CrN, and $TiB_2$. They can be applied as a single/monolayer or in multiple layers, also referred to as multi-layered coatings. The application of multiple layers helps to improve the compatibility between the coating and substrate as it optimizes

the chemical bond and thermal expansion coefficient, and in turn, gives varying properties for their respective conditions [17]. A balanced multi-layer would improve mechanical wear resistance, and improve thermomechanical performance under high loads and temperatures.

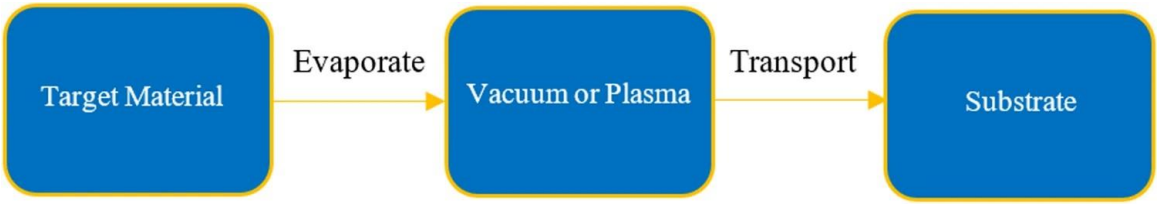


**Figure 2.1: Fig. 1 A flowchart depicting a typical PVD process**

The coating types selected in this study are based on their effectiveness in the machining of other Ti-based alloys in published works, commercial usage, and/or the novelty factor. The commercial PVD coatings chosen for this study are divided into two categories: mono-layered, and bi-layered. The mono-layered coating was AlTiN-based, whereas the three bi-layered coatings all had the same base layer of AlTiN with the second layers being ta-C, AlCrN, and TiAlSiN, respectively. Totaling to four distinct coating types; one mono-layered, and three bi-layered. It has been reported [23] that AlTiN provides excellent thermal and chemical stability, oxidation resistance, and higher hardness and hot hardness (up to ~ 900 °C) as compared to TiN and TiCN. Moreover, a study performed on the use of TiN, TiCN, and TiAlN on WC-6%Co in the turning of Inconel 718 showed that the best tool life was that of TiAlN, followed by TiCN, and TiN-coated tools. This was owed to TiAlN's relatively higher resistance to abrasion and cratering due to better hot hardness and resistance to oxidation [24]. It was reported by Wang et al. [25] that during the diffusion phenomenon when machining Ti-17 using TiAlN PVD coated WC tool, W and C diffuse

into the cutting tool's adhesion layer, Ti and Al diffuse into the tool substrate, and Mo, Sn, Zr, and Cr within the workpiece material are unaffected. The base AlTiN layer (chosen for this study) is a high-Al alternative to TiAlN that is likely to affect the coating's thermomechanical properties at different concentrations. The higher the Al content the better the thermal and oxidation resistance, as well as higher hot hardness (up to Ti:Al ratio of 40:60 [23], after which a soft hexagonal TiN phase forms) within a certain temperature range [26]. TiAlN coating performance has the potential to be improved by doping with functional elements such as Si, Y, B, V, and Cr. B adds to the hardness, Si helps to improve high-temperature performance, V improves the tribological behavior, and Cr and Y aid with improving the oxidation resistance and thermal stability. Doping with such elements yields compounds such as AlTiCrYN, AlTiCrN, and TiAlSiN, each of which has its unique set of properties [26]. CrN coatings exhibit exceptional tribological and mechanical properties that aid in preventing delamination. This is partly a result of CrN coatings forming a $Cr_2O_3$ tribo-layer during machining, which minimizes crater wear (with reference to the high-speed finish turning of Ti-64) [27]. The Al in AlCrN has a similar effect to that of having a higher composition of Al in TiAlN. They are suitable for conditions requiring high oxidation resistance and toughness. The DLC ta-C coating was primarily selected due to its novelty and lack of usage in the turning machining of Ti-based alloys.

PVD coatings are often employed when an increase in tool life or improved surface quality is desired. This has generally been the approach taken to enhance the machining performance of Ti-64, as is evident from the literature. However, studies have not thoroughly investigated the effectiveness of PVD coatings on WC-Co tools for the finish-

turning of Ti-5553 alloys. The existing literature has not considered coatings as a primary factor when analyzing machining performance, and only a few of them employed coatings in their studies. Limited research is available in the open literature on the machinability and effect of tool materials and coatings during the finish-turning of the Ti-5553 alloy. Therefore, this paper prioritizes the wear and micromechanical properties of the coatings in relation to their machining performance in the finish-turning of Ti-5553.

## 2.2 Materials and Experimental Methods

### 2.2.1 Coating Selection and Deposition

The coatings selected for this study were deposited on Kennametal CNGG120408 K313 cutting tool inserts and polished WIDIA SNUN120408 cemented carbide coupons, both having the same microstructural composition and cemented carbide grade. The former was utilized for the machining tests whereas the latter for coating characterization. The commercial AlTiN-based (BALIQ® ALTINOS) coating layer was deposited by Oerlikon Balzers on all inserts and coupons as a base layer. This coating has been designed for turning applications and utilizes the HIPIMS s3p (scalable pulsed power plasma) coating technology which combines the benefits of arc and sputtering technologies providing a smoother finish with virtually no macro-particles. The substrate was heated to a temperature < 500 °C and has been imparted with a maximum service temperature of 1000 °C, which is well below the expected machining operating range. This ceramic coating has been reported to exhibit high hardness and in turn excellent wear resistance under extreme thermal loads [28]. In addition to the base layer reference coating, three varying compositions of mono-layered commercial coatings were deposited on top of three separate

AlTiN-based (BALIQ® ALTINOS) tools. Namely, DLC ta-C (Ionbond Tetrabond$^{TM}$ Plus), AlCrN (Ionbond Crosscut$^{TM}$ Plus), and TiAlSiN (Kyocera HDT). ta-C is a diamond-like (DLC) extremely hard coating (> 5000 HV) designed for machining non-ferrous metals and sticky materials to help reduce the formation of BUE. It was deposited at sub-300 °C temperatures with the maximum operating temperature being approximately 500 °C. AlCrN is optimized for both dry and wet conditions at temperatures exceeding 1000 °C. It has been deposited at temperatures within the range of 450–500 °C. Both of these coatings were deposited using the PVD Advanced Arc Technology, which aims to deposit at higher energy levels and densities than conventional arc technologies to improve the overall surface smoothness, as well as the abrasion and chipping resistance. The TiAlSiN was synthesized to perform at temperatures beyond ~ 1150 °C.

### 2.2.2 Coating Characterization

The unpolished WIDIA SNUN120408 cemented carbide coupons were hot-mounted using a SimpliMET$^{TM}$ XPS1 Compression Mounting System (Lake Bluff, IL, USA) in a black phenolic thermosetting powder by MetLab Corporation (Niagara Falls, NY, USA). The temperature was set to 170 °C, at a pressure of 3.65 psi, with heat and cool time of 10 and 5 min, respectively. Subsequently, the samples were polished in steps on a Struers Tegramin-25 semi-automatic polishing/grinding machine (Copenhagen, Denmark). The first step involved a disc speed of 300 rpm, force of 30 N, holder speed of 180 rpm, and water as the lubricant, for a total duration of 6 min. The next three steps were all done with the following parameters: disc speed of 150 rpm, DP-Lubricant Blue (Struers), force of 30 N, holder speed of 150 rpm, duration of 5 min, with DP-Lubricant Blue, and 9, 3, and 1 μm

abrasive disc pads in succession to obtain a smooth reflective surface finish. The samples after thorough inspection were then sent off for coating deposition.

The coating thickness was measured using a BC-2 MIBA Coating Group ball crater device (Droitwich Spa, England) with a 25-mm diameter AISI 52100m Grade 25 Chromium steel ball on the WIDIA SNUN120408 polished WC-Co inserts. The thicknesses of the coatings AlTiN (Monolayer), AlTiN/ta-C, AlTiN/TiAlSiN, AlTiN/AlCrN were observed to be 5.57, 6.23, 6.35, and 7.01 μm, respectively. The surface topography and morphology of the coatings were obtained using the tapping mode of an Anton Parr Tosca$^{TM}$ 400 atomic force microscope (AFM) (Graz, Austria). Commercial silicon probes with a resonant frequency of 278 kHz were utilized to perform the line scans at a scan speed of 0.3 lines/second with a force of 42 N/m. The scan size was set to 25 μm × 25 μm. Data analysis and image processing of the scans were conducted in the Tosca$^{TM}$ analysis software (Version 7.4.8341).

Micro-scratch tests were conducted with an Anton Paar-RST3 Revetest® Scratch Tester (Graz, Austria). A Rockwell diamond indenter with a diameter of 200 μm was selected for the tests. At least 3 scratch tests per coating insert were performed in a 3-scan progressive mode procedure to investigate the coating delamination behavior. The 3-scan procedure is divided into 3 modes: pre-topography scan, progressive load scratch scan, and post-topography scan. The pre-topography scan occurs at a load of 0.5 N to get a gauge of the surface profile (waviness, roughness, and form), followed by a progressive load scratch where the parameters were configured such that the load ramped up from 0.5 N to 100 N over a distance of 3 mm, and finally ending off with a post-topography scan to measure the

residual depth to obtain more insight into the deformation behavior. The loading rate was set to ~ 199 N/min at a scan speed of 6 mm/min. The morphology and elemental distribution of the scratch tracks were observed with secondary (SE) and backscattered (BSE) modes in a FESEM (FEI, USA, and Tescan, Lraya3 Czech Republic) equipped with an energy-dispersive X-ray spectrometer (EDX).

The micromechanical properties of the mono/bi-layered coatings were assessed at room temperature by a Micro Materials NanoTest P3 system (Wrexham, UK) based on the Oliver-Pharr method. A Berkovich diamond indenter was utilized to perform a minimum of 20 indents for each of the coatings. The calibration of the indenter was done as per the ISO14577-4 [29] standard to accommodate for load, displacement, indenter shape, and frame compliance. The load parameter was optimized such that the surface roughness of the coating, as well as the substrate effect, would be minimized or negated to obtain data most representative of the coatings themselves. To minimize the substrate effect the indentation contact depth was set to $1/10^{th}$ of the coating's thickness, which in the current study was around 450 nm. This in turn ensured that the coatings' load-invariant hardness and elastic modulus were taken into account. The nanoindentation was done at a loading rate of 200 mN/min with a max load of 100 mN where it was dwelled for 2.0 s before being released. This was subsequently followed by 60 s of post-indentation time to allow for thermal drift correction.

The coatings' 3D surface roughness measurements were performed with an Alicona Infinite Focus G5 3D surface measurement system (Alicona Manufacturing Inc., Bartlett, IL, USA). It utilized the focus-variation technology of the Alicona 3D optical system to

generate real color information highlighting the peaks and valleys of the surface. A lens with a magnification of 100 x was used to image an average area of 180,000 $\mu m^2$ for each of the coated samples. Phase analysis of the coatings was performed using the X-ray diffraction technique on The Rigaku Miniflex II X-ray diffractometer (Tokyo, Japan) with the XRD peak identification and verification done through a database. The XRD phase analysis data was conducted and collected at 15 mA current, 30 kV voltage with the 2θ angle ranging between 20° and 80°. A copper anode λ Cu Kα = 1.5418 Å radiation source was used to determine the crystallographic structure and orientation of the coatings.

### 2.2.3 Experimental Setup and Machining Studies

Turning machining tests were performed under wet (flood) lubricant conditions (~ 9% coolant concentration) on a Grandis Ti-5553 workpiece (starting diameter 55 mm and length 250 mm) with different sets of coated single/bi-layered Kennametal CNGG120408FS K313 cutting tool inserts to analyze the wear behavior and surface quality of the tool and workpiece, respectively. The Boehringer VDF 180 CM CNC (FFG Europe & Americas, Eislingen, Germany) turning lathe (Fig. 2) was employed at high cutting speeds of 150, 175, and 200 m/min and fixed feed rate and depth of cut (0.15 mm/rev, and 0.25 mm, respectively). The tool inserts were fixed to a Kenloc$^{TM}$ MCLNL164D NJ9 5° (rake angle) tool holder, nose radius of 0.8 mm, and an average edge radius of 22 ± 3 μm mounted to a Kistler Type 9129AA 3-component piezoelectric dynamometer for resultant cutting force measurements. A Kistler LabAmp Type 5167A charge amplifier was connected to the dynamometer. The signal was converted from analog to digital with a National Instruments (NI) Type 9215 data acquisition card in a National Instruments (NI)

cDAQ-9172 DAQ system. The sampling rate for data collection was set to 10 kHZ to then be processed using the National Instruments (NI) LabView 2014 data analysis system. The data was acquired from an average of 3 trials for each of the coating variants. The coolant used was a Castrol Hysol MB50 Semi-Synthetic with a concentration of 9% and a pressure of ~ 7 bar.

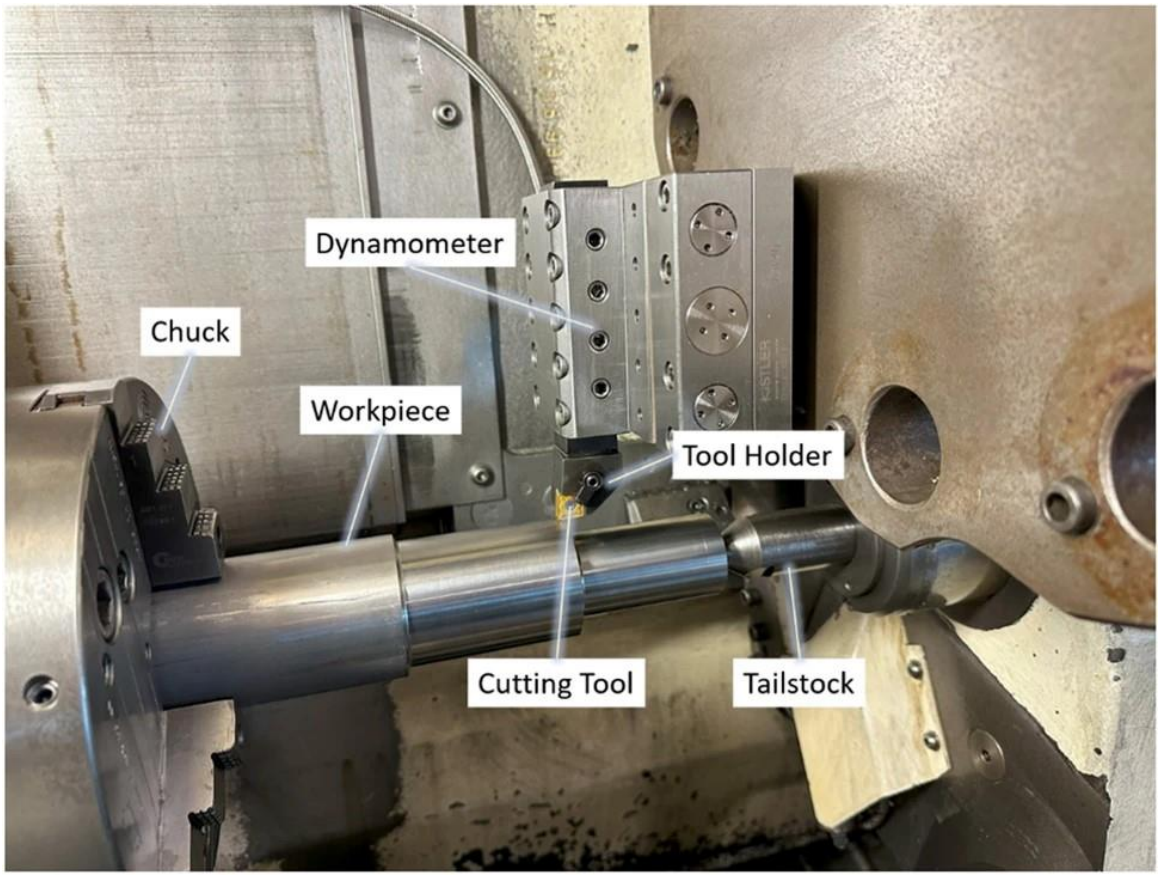


**Figure 2.2: Fig. 2 Experimental Setup for Machining of Ti-5553**

Tool life in terms of flank wear progression was measured after every 30 m of linear pass using a VHX-5000 Keyence optical microscope (KEYENCE Corporation of America, Elmwood Park, NJ, USA). The flank wear data was recorded until the tool reached a maximum flank wear of 300 μm, as per the ISO 3685:1993 standard [30]. The cutting-edge

radius and the end-of-life crater wear and BUE measurements (volumetric wear) of the coated cutting inserts were analyzed using the Edge Master module, and the focus-variation technology + Measure Suite module, respectively, of the Alicona Infinite Focus G5 3D surface measurement system (Alicona Manufacturing Inc., Bartlett, IL, USA). The Measure Suite module layers a reference cutting tool 3D dataset of the same geometry as the worn coated tools to generate 3D volumetric variations to compare the volumetric transformation post-machining. Subsequently, the module juxtaposes the worn and reference images to give a measure for the volume of BUE/crater wear formation relative to the reference dataset. The surface roughness of the workpiece was measured after every 30 m pass using the Mitutoyo SJ-201 portable surface roughness device (Mitutoyo America Corporation, Japan). Readings after every pass were taken an average of 4 times with the cut-off length set to 0.8 mm, in accordance with the optimal finish turning conditions as per the ISO 21920-3:2021 (previously ISO 4288) standard [31].

The X-ray photoelectron Spectroscopy (XPS) technique was employed on the rake face of worn coated cutting inserts to determine the chemical composition and formation of tribo-oxides in a PHI Quantera II Scanning XPS Microprobe (Physical Electronics Inc, Chanhassen, MN, USA). The spectrometer is equipped with an Al anode source on which a Raster Scanned Electron Gun® shoots electrons, resulting in the formation and release of X-rays. The generated X-rays are focused on the coated samples using a quartz crystal monochromator. Consequently, secondary electrons are generated from the sample and directed towards a multi-channel detector through a hemispherical energy analyzer to form secondary electron images (SXI). The monochromatic Al K-α X-ray source was set to a

constant acceleration voltage of 1486.6 eV while the 50 μm X-ray beam was operated at 12.5 W and 15 kV to collect all the relevant data. The system's base pressure was at the lowest noted as $5 \times 10^{-9}$ torr whereas the maximum sputtering pressure was recorded to be $1 \times 10^{-9}$ torr. The samples were sputter-cleaned with Ar+ gas beam prior to the collection of spectral data. The spectral survey data was collected at a pass energy of 224 eV whereas the high-resolution spectral data at 55 eV, in step sizes of 0.8 and 0.1 eV, respectively. The take-off angle (angle between the analyzer axis and sample surface) was adjusted to 45°. A dual-beam charge compensation system was employed to ensure neutralization of the coated samples. Calibration of the equipment for high-resolution data was done by setting the C1s C-C peak to 284.8 eV. The PHI Multipak software (Version 9.5) was utilized for data analysis.

## 2.3 Results and Discussion

### 2.3.1 Micromechanical and Structural Properties of the Coatings

The micromechanical and structural properties of the various coating types are discussed in the following subsection. The coatings' architecture, thickness, and mechanical properties, among other characteristics, are provided in Table 3. A coating's micromechanical properties are typically a good basis for making inferences about their resulting machining performance concerning wear mechanisms and workpiece surface quality. The H/E and $H^3/E^2$ ratios were calculated from coatings' hardness (H) and elastic modulus (E), with the former being a representation of a material's elastic strain to failure, which in the context of nanoindentation is the measure of the elasticity at the contact point between the indenter and coating, whereas the latter indicates the ability of the coating to

resist plastic deformation. Both of these properties can be well correlated with a coating's wear resistance (i.e., if disregarding other variables, the higher the H/E ratio the more wear-resistant the coating) [32, 33]. It can be observed from the results that AlTiN/AlCrN has the lowest H/E and $H^3/E^2$ ratios whereas AlTiN/ta-C has the highest. The considerably low, and high hardness values of AlTiN/AlCrN and AlTiN/ta-C, respectively, can be attributed to their ratios being on the opposite ends of the spectrum. The general rule is that the higher these ratios are, the better the resistance to wear, however, under high-load machining conditions with adhesion wear being the dominant wear mechanism, the opposite trend has been found to be true (i.e., lower H/E equating to better tool life) due to the formation of a stable adhesive layer of the workpiece material on the cutting tool resulting in a reduction of frictional forces in the workpiece-tool interaction zone. Ding et al. [34] further mention that the variation in wear resistance of a material is not solely dependent—tribological and temperature-related factors need to be considered—on the micromechanical properties (H/E, $H^3/E^2$) and should hence be optimized rather than prioritizing an increase in hardness value with the desire to achieve improved wear resistance. This is substantiated by the current analysis where AlTiN/AlCrN, having low H/E and $H^3/E^2$, was found to provide reasonable improvement in tool life, whereas AlTiN/ta-C, having the highest H/E and $H^3/E^2$ (indicative of brittleness), at times had comparatively lower life, but was prone to sudden failure at high cutting speeds, as further elaborated in Section 3.2 (Machining performance and tool life) AlTiN/TiAlSiN was only slightly higher in hardness than the base mono-layer with the resulting H/E and $H^3/E^2$ ratios being similar, and this is further evinced by their

having comparable tool life. The marginally higher hardness can be attributed to the Si dopant as it is known to impart improved strength [35, 36].

**Table 2.3: Table 3 Micromechanical and Structural Properties of the Coatings**

| **Coating Type** | **Properties** | | | | | | | |
|---|---|---|---|---|---|---|---|---|
| | **Architecture** | **Total Thickness** (µm) | **Hardness** (GPa) | **Elastic Modulus** (GPa) | **H/E** | **$H^3/E^2$** | **Plasticity Index** | **$S_a$** (nm) |
| AlTiN | Monolayer | 5.57 | 33.87±3.78 | 503.84±47.25 | 0.0672 | 0.153 | 0.470 | 36.91 |
| AlTiN/AlCrN | Bilayer | 6.60 | 24.23±4.96 | 450.35±72.24 | 0.0538 | 0.070 | 0.515 | 33.59 |
| AlTiN/ta-C (DLC) | Bilayer | 6.05 | 41.88±6.46 | 487.54±71.60 | 0.0859 | 0.309 | 0.354 | 43.47 |
| AlTiN/TiAlSiN | Bilayer | 6.54 | 36.44±6.73 | 588.01±112.56 | 0.0620 | 0.140 | 0.473 | 45.38 |

These results can't be investigated in a vacuum and must be complemented by examining the Plasticity Index (PI) values for each of the coatings. The PI is the quotient of the plastic work done over the total work done (inclusive of plastic and elastic) obtained during the indentation process, which in this investigation's framework serves to give a gauge for a coating's ability to dissipate frictional heat energy during its deformation in a cutting process. A higher PI in the case of AlTiN/AlCrN for the machining of Ti-5553 entails substantial energy dissipation, indicative of the coating being soft and tough/durable leading to the best tool life and overall smoothest surface finish of the workpiece. On the contrary, AlTiN/ta-C having the lowest PI, corroborates the conclusion established by the H/E and $H^3/E^2$ ratios of the brittle nature of said coating resulting in occasional catastrophic failure, as also observed in previous studies using ceramic-based cutting tools [37, 38].

The Microscratches further support the aforementioned discussion by providing data pertaining to plastic deformation, friction, and delamination/spallation behavior of the coatings by applying progressively increasing loads over a specified distance. Trends and changes in surface morphology in relation to the acoustic emissions (AE) are depicted in Fig. 3 along with coefficient of friction data shown in Fig. 4. The cohesive (internal) failure of the coatings is represented by $Lc_1$ and is primarily based on the variation in the AE signals as they are indicative of rapid release of energy (acoustic/ultrasonic elastic waves) from within the internal structure of the coatings due to irreversible changes such as plastic deformation or crack formation [39], and also because a clear visual demarcating point along the scratch track was not observed, whereas $Lc_2$ has been identified by the first instance of adhesive failure of the coating (substrate exposure and spallation) [40]. Based on the AE data, AlTiN/ta-C coating has the earliest observance of cohesive failure at a distance of ~ 0.11 mm and a load of 4.51 N, followed by AlTiN at ~ 0.35 mm and 12.07 N, AlTiN/TiAlSiN at ~ 0.43 mm and ~ 14.81 N, and with the longest period of resistance to crack initiation by the AlTiN/AlCrN coating at ~ 0.60 mm and ~ 20.40 N. Relating this to the micromechanical properties of the coatings and it becomes evident that the extremely high H/E and low PI of AlTiN/ta-C render it exceptionally brittle, consequently leading to proneness and catastrophic failure during machining. On the other hand, the balanced micromechanical properties of AlTiN/AlCrN aid with resistance to the relatively early onset of internal plastic deformation, and by extension external cracking. Additionally, throughout the $Lc_1$ to $Lc_2$ zone, the acoustic emissions of AlTiN/AlCrN remain the lowest. As for the slight delay in the spike of acoustic emissions of AlTiN/TiAlSiN as compared

to the base layer AlTiN coating, this can be attributed to the Si dopant's tendency to impart additional strength and by extension resistance to wear. The adhesion ($Lc_2$) of the soft AlTIN/AlCrN coating was the highest with cracking observed at a distance of ~ 1.77 mm at 59.39 N, AlTiN/TiAlSiN at ~ 1.38 mm and 46.86 N, base layer AlTiN ~ 1.34 mm at 45.42 N, and AlTiN/ta-C coating at ~ 1.32 mm and 44.76 N. The delayed onset of external spallation of the soft AlTiN/AlCrN coating can strongly be correlated to the cutting tests performed in this study, such that because it stays adhered to the cutting tool for a longer period, less adverse chipping results in a smoother surface finish as less of the relatively rougher substrate is exposed. Further details are discussed in Sections 3.2 and 3.3. In other words, the delayed flaking or delamination of the coating during the cutting process explains the comparatively longer tool life and improved tribological performance (smoother workpiece finish). A similar phenomenon has also been reported elsewhere [41].

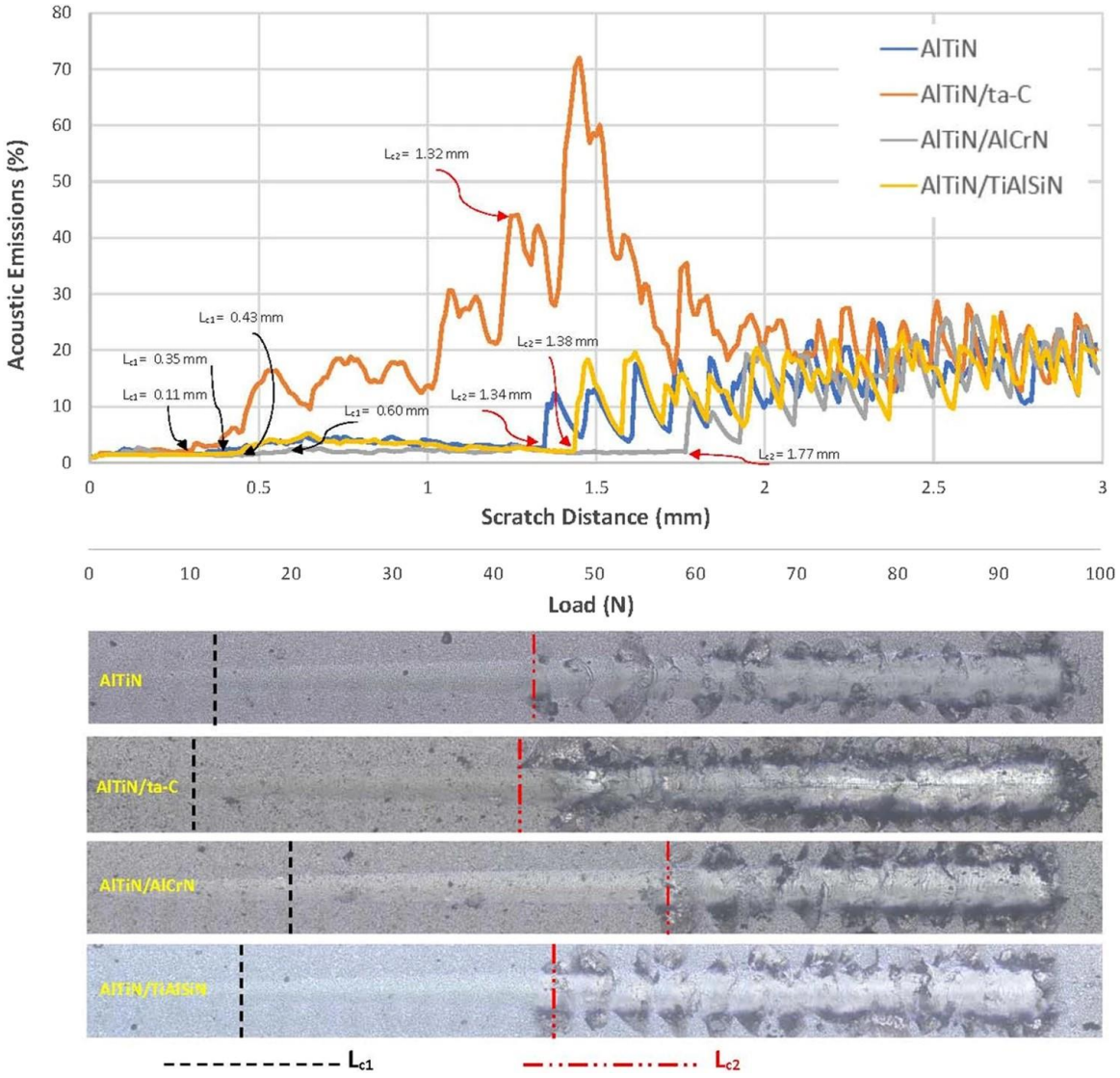


**Figure 2.3: Fig. 3 Optical images of the scratch test tracks in relation to scratch length and loads along with the acoustic emission data of the coatings: mono-AlTiN, AlTiN/ta-C, AlTiN/AlCrN, and AlTiN/TiAlSiN**

As can be noted from Fig. 4, the coefficient of friction data of the AlTiN/ta-C coating is the highest which is a contributing factor to its early failure due to worsened wear performance. The remaining three coatings all follow a similar frictional behavior trend. The rate of increase in the coefficient of friction of the AlTiN/ta-C coating from 0 mm to 1.5 mm (until external spallation) is twice that of the other three coatings. Additionally, the

significantly higher variation in the frictional behavior of said coating may be attributed to the nature of scattered peak topography which is discussed next.

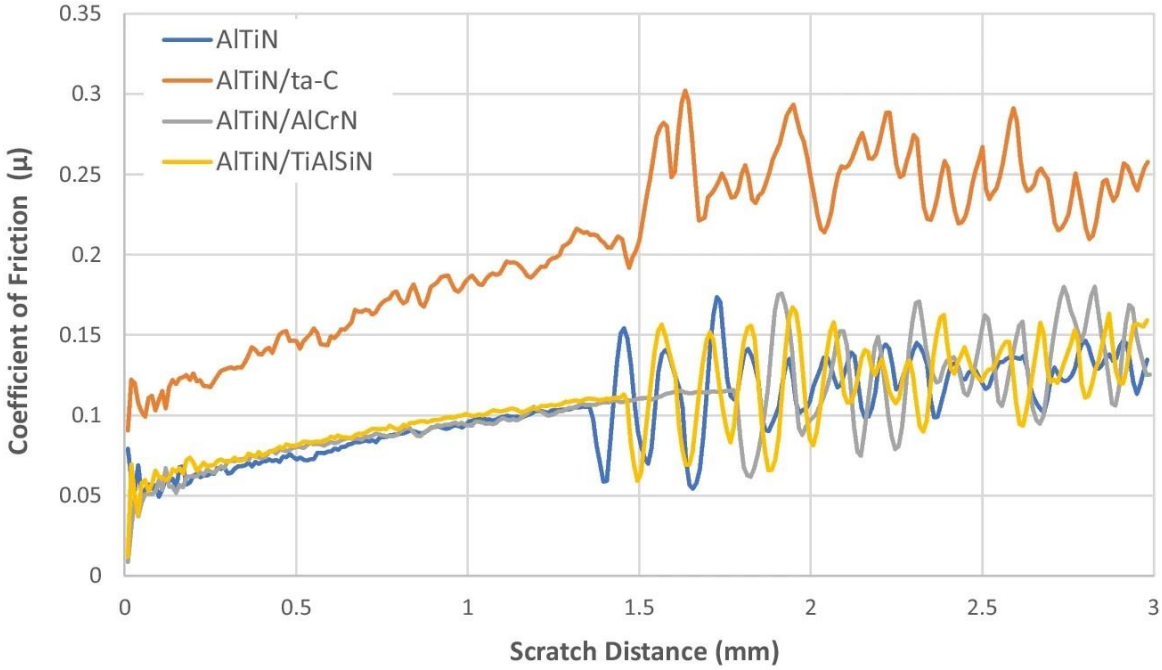


**Figure 2.4: Fig. 4 Coefficient of friction data of the coatings: mono-AlTiN, AlTiN/ta-C, AlTiN/AlCrN, and AlTiN/TiAlSiN**

The surface morphologies of the coatings measured via AFM are presented in Fig. 5. Factors that may influence a coating's behavior during a cutting process are their variation in topographies, and surface smoothness (sharp or rounded peaks). The surface roughness values shown in Fig. 5 are taken from the Alicona Infinite Focus G5 3D surface measurement system based on a surface area of 180,000 $\mu m^2$ as it is a more accurate representation of the overall surface roughness of the coating. The smoother/rounded topology of the AlTiN/AlCrN coating could be causative to its coefficient of friction being lower than the AlTiN/ta-C coating. The AlTiN/ta-C coating, however, when compared with the base layer has longer and more scattered spikes all across its morphology. The

topographical characteristics of the AlTiN/ta-C and AlTiN/AlCrN coating are reflected in their surface roughness ($S_a$ and $S_z$) values, with the former being 43.47 nm and 6.88 nm, and the latter 33.59 nm and 4.60 nm. These differences by extension could be a cause for the differences in their cutting tool performance.

Further investigation of the tracks was performed by studying the surface morphology and compositional analysis using SEM and EDX as shown in Figs. 6 and 7, respectively. The tracks of the AlTiN/ta-C and soft AlTiN/AlCrN coating illustrate the exposure of the substrate and base layer, indicated by the W (inner magenta), Ti + Al (red and cyan, respectively) in EDX mapping as shown in Fig. 7. The primary difference between the AlTiN/ta-C and AlTiN/AlCrN coatings is that the former has a smaller substrate exposure spread and the pattern is more consistent as depicted in Fig. 6. This may be attributed to the AlTiN/ta-C coating's brittle nature. The AlTiN/AlCrN, albeit having a similar trend, seems to have experienced more plastic flow (plastic deformation before failure) as indicated in Fig. 7 considering that the substrate exposure is patchier (due to adherence) and more spread as can be noted by the magenta W spectral dots. The aforementioned qualities of the softer AlTiN/AlCrN coating hinder the propagation of internal cracks and aid with coating adherence, thereby providing a longer tool life.

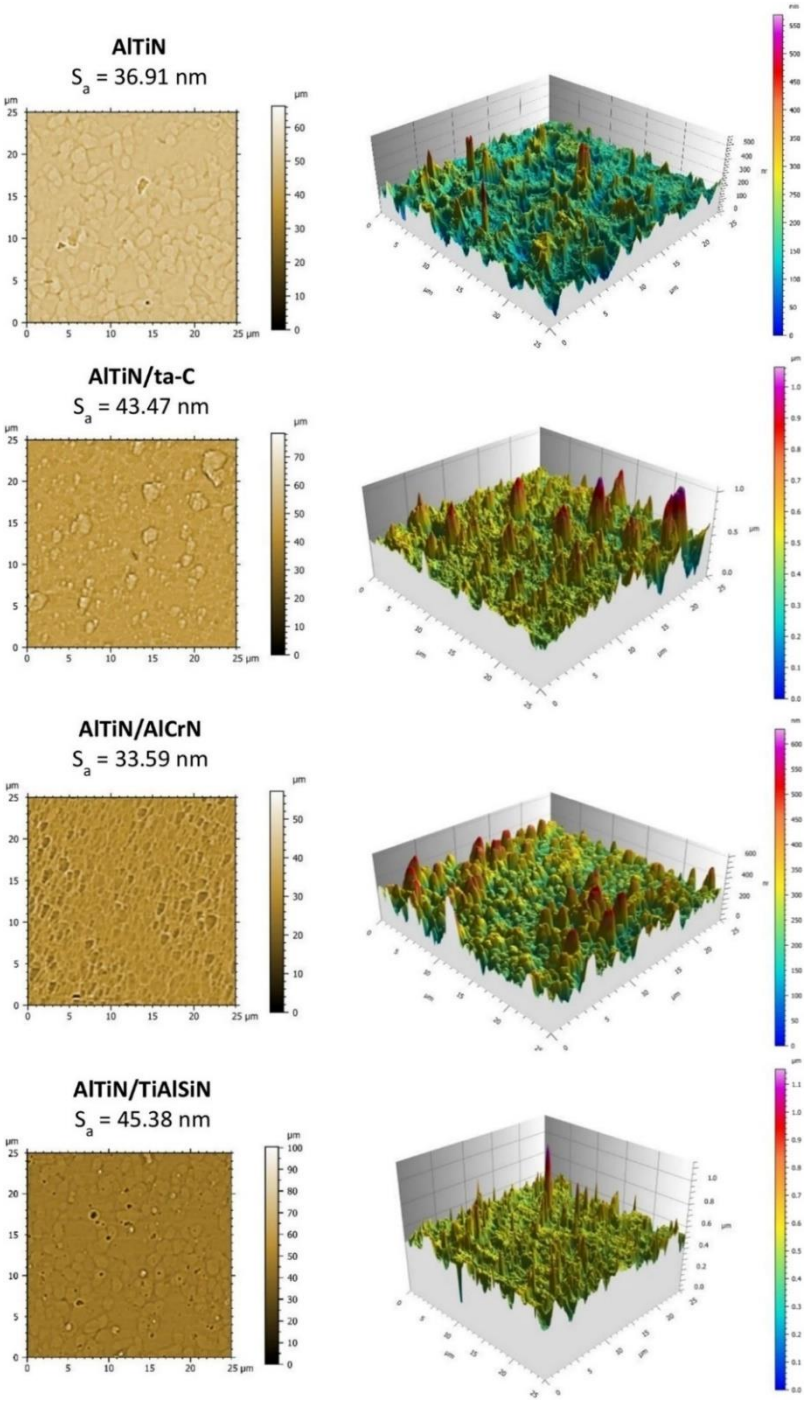


**Figure 2.5: Fig. 5 AFM images that show coating surface topography and structure in 2D and 3D views of mono-AlTiN, AlTiN/ta-C, AlTiN/TiAlSiN, and AlTiN/AlCrN coatings**

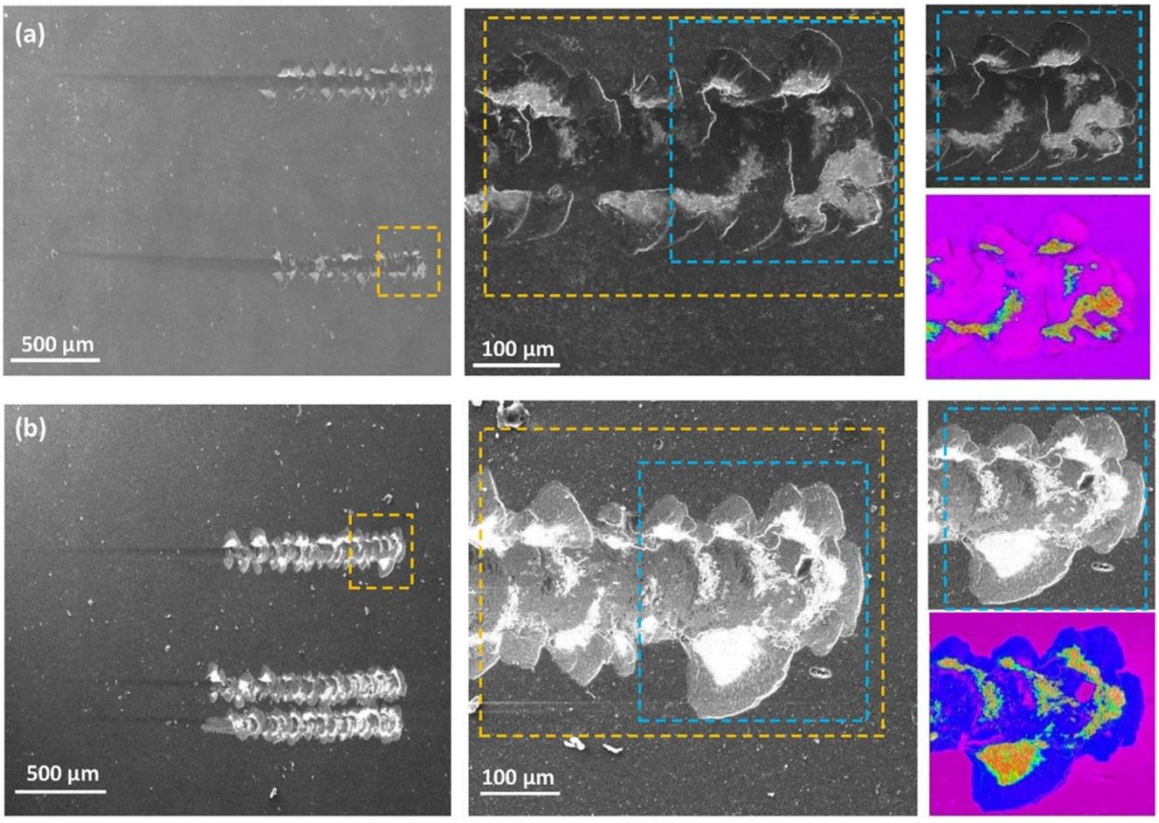


**Figure 2.6: Fig. 6 SEM morphologies of coating surfaces after nanoscratch tests: (a) AlTiN/AlCrN, (b) AlTiN/ta-C. Black & White (SE mode), Chrome (BSE mode)**

XRD phase crystallographic patterns of all the coating types are depicted in Fig. 8. In addition to the peaks identified from the substrate, diffraction patterns of all coating types contain two main phases, TiN and AlN. As can be observed, the AlTiN appears as a single fcc structure with different sets of crystallographic orientations in (111), (200), (220), and (311) crystal planes. The diffraction peaks fall between those of the fcc TiN (PDF# 25-1495) and AlN (PDF# 38-1420) phases, demonstrating that the fcc (Al, Ti)N solid solution phase does in fact exist. AlTiN coating containing a higher concentration of Al than Ti, is a cause for its diffraction peaks being more similar to those of AlN, noted to have a lower

lattice constant than the TiN phase. The XRD patterns of AlTiN/AlCrN coating corresponding with two diffraction peaks of the CrN phase at 36.5° and 42° of 2θ can be observed. These peaks have a B1 NaCl structure with planes (111) and (200), respectively, which is consistent with the literature findings [42]. The ta-C peaks correspond to the DLC AlTiN/ta-C coatings with orientations in the (111) and (220) planes along with CN and TiC peaks with orientations in the (200) crystal planes. The peaks identified as ta-C and TiC affirm the high hardness characteristics of these coatings. In addition to these crystal phases, the coatings contain the crystal phase CN (200) which further validates the resulting hardness values achieved in the coating. It is worth noting that the most intense peak of TiN identified in the TiAlN/TiAlSiN bi-layered coatings, at 2θ of 36.51°, is consequent of the (111) orientation somewhat shifting to lower angles as compared to the typical TiN peak (PDF#00-038-1420) in the mono-layered AlTiN coating. This confirms that the TiN phase's unit cell characteristics have changed due to the partial substitution of Al (or Si) in place of Ti atoms, the former having smaller atomic radii [43].

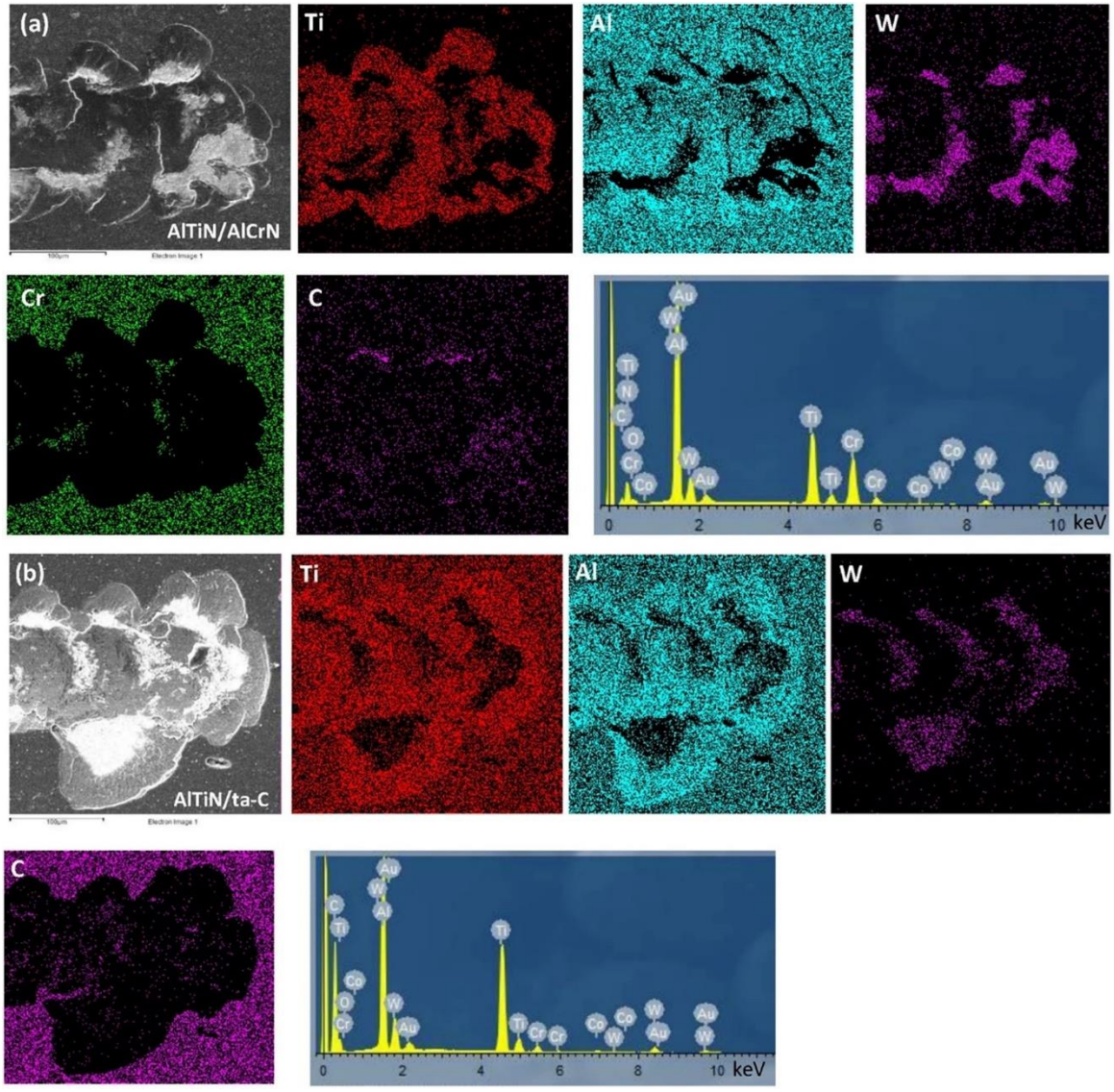


**Figure 2.7: Fig. 7 EDS mapping analyses of tool coating surfaces after microscratch tests: (a) AlTiN/AlCrN, (b) AlTiN/ta-C. Images taken in SE mode**

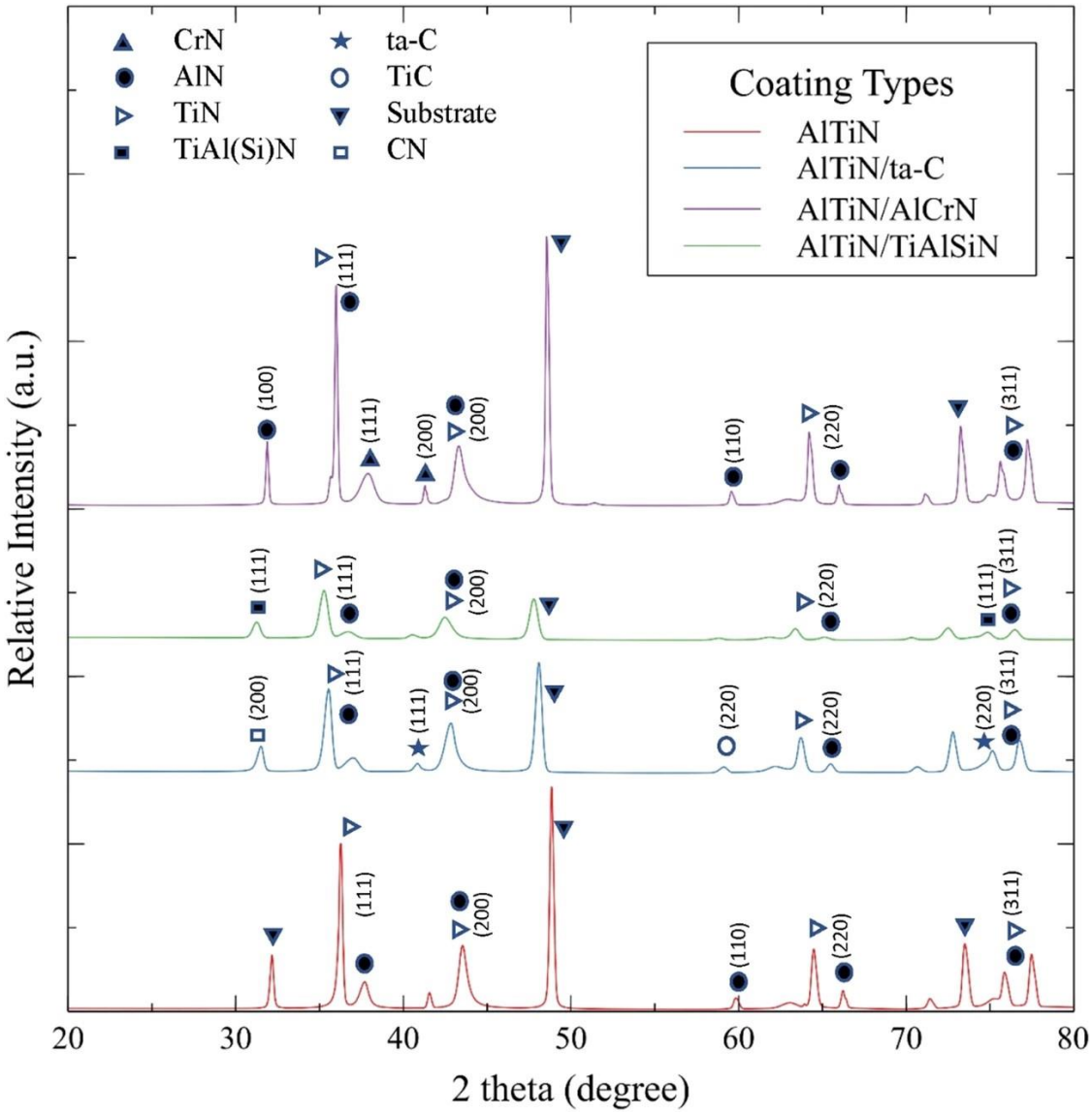


**Figure 2.8: Fig. 8 XRD Diffractogram of mono-AlTiN, AlTiN/ta-C, AlTiN/TiAlSiN, and AlTiN/AlCrN**

### 2.3.2 Machining Performance and Tool Life

Tool life, surface roughness, and wear severity studies were initially conducted at three high cutting speeds (150, 175, and 200 m/min) under wet conditions, however, this discussion hones its focus on the results obtained at the speed of 150 m/min as it has been deemed to be most representative of what could be considered as the maximum limit of

"high-speed" for carbide-based tools, both based on literature and experimentation, as the unpredictability in tool life and surface quality was observed to increase at the higher speeds as reported by Kaynak Y et al. [44, 45]. Nonetheless, the trends for tool life and surface roughness measurements were found to be similar at the higher cutting speeds for the AlTiN/AlCrN coating. They also report that the wear rate dramatically increases past a cutting speed of 120 m/min for Ti-5553 alloys at all depths of cut values, with the potential for abrupt failure. Moreover, they further mention that carbide-based tools experience extreme wear and forces beyond the cutting speed of 150 m/min [46].

Figure 9 illustrates life comparisons as a function of cutting lengths of the four coated tools discussed in the sections prior. The criterion for tool life was taken as flank wear land of 300 μm. The optical images shown in the figure were taken corresponding to the first pass (~ 30 m) at a magnification of × 150. Obtaining large tool life differences at extremely high cutting speeds amongst coatings is not as feasible as it may be at sub-100 m/min cutting speeds due to the higher coating peel-off rate. At such high speeds, the immediate influence of coatings is most pronounced for the first couple of passes, nevertheless, this initial influence significantly contributes to the overall tool life and workpiece surface quality. Comparing tool wear intensity with the monolayered AlTiN coating as the baseline reference, the coatings have been ranked as follows: AlTiN/ta-C exhibits the highest intensity of wear by experiencing catastrophic failure, followed by monolayered AlTiN, and the bi-layered AlTiN/TiAlSiN coating being in close proximity by following a similar trend, albeit with a marginally shorter tool life. The longest tool life was noted with the AlTiN/AlCrN coating. The AlTiN/ta-C coating as highlighted in the discussions within the

section former has shown, from the tool life perspective, inhibitive thermomechanical properties: lowest PI, and highest H/E, $H^3/E^2$ ratios. This contributes to its higher potential for sudden failure. It, with respect to tool life, in comparison to the baseline monolayer and AlTiN/AlCrN (longest tool life) underperformed by ~ 39.6%, and ~ 44.6%, respectively. As for the AlTiN/TiAlSiN coating, it experienced a marginal decrement of 2.65% in relation to the baseline, and ~ 10.7% to AlTiN/AlCrN. As mentioned previously, the lower tool life can be attributed to the Si dopant imparting brittleness, leading to an increase in wear rate [35, 36]. The AlTiN/AlCrN coating achieved the longest life and outperformed the base monolayer by ~ 9.02% at 150 m/min, and ~ 19% when taking an average of three trials across all the cutting speeds.

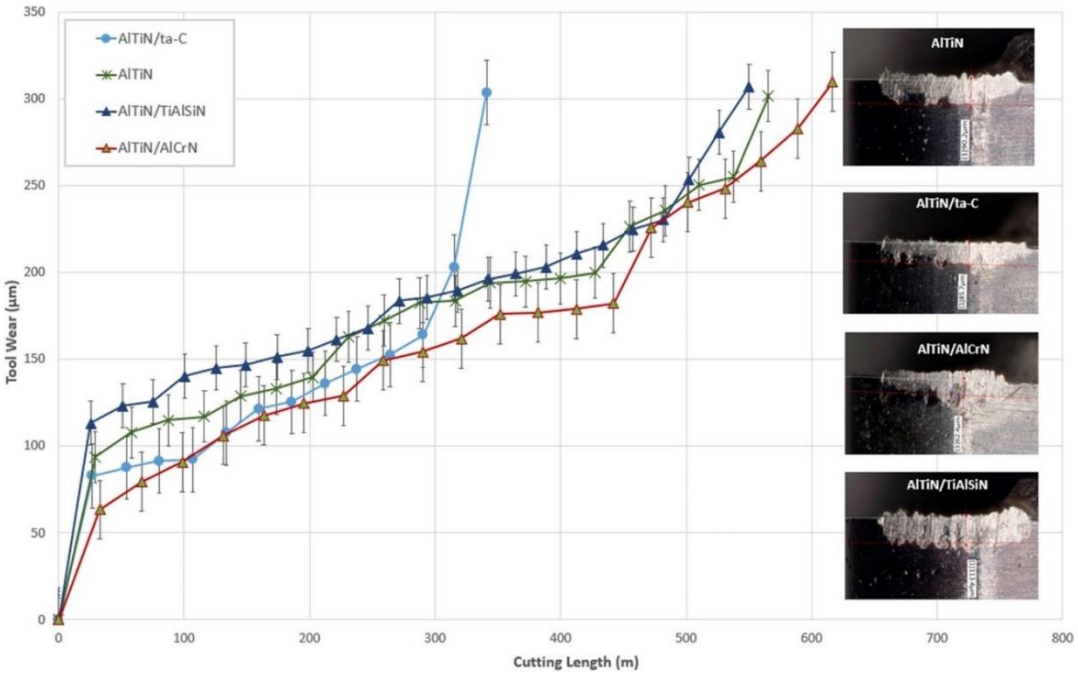


**Figure 2.9: Fig. 9 Tool life comparison with respect to the flank wear for mono-layered AlTiN and bi-layered coated tools, namely AlTiN/ta-C, AlTiN/AlCrN, and AlTiN/TiAlSiN. The optical images correspond to the first cutting pass (~30 m)**

The most common wear mechanisms of the coated tools as depicted by the first-pass optical images in Fig. 10, with the subsequent passes having a similar visual appearance, were adhesion, abrasion, and attrition. With abrasion and attrition allowing for the adhesive material to settle into the grooves. The cycle of adhesive sticking and peel-off, in other words, BUE and sticking, resulted in rapid coating and substrate peel-off, as well as chipping, hindering prolonged tool life for all sets of coatings. A byproduct of adhesion sticking and peel-off was tool wear by cratering, which was by far the most dominant wear mechanism observed among all the coatings. Figure 10 depicts 3D images with volume of crater wear and depth, as well as BUE formed at the end of tool life. The volumetric datasets taken and generated by the Alicona microscope revealed notable distinctions. Results indicate that the largest crater volume and deepest crater are that of the AlTiN/TiAlSiN coating ($1.03 \times 10^7$ $\mu m^3$, and 168.74 μm, respectively), while the smallest is presented by the AlTiN/ta-C coating ($5.71 \times 10^6$ $\mu m^3$, and 105.95 μm, respectively). However, the apparent smallest crater volume and depth result from its susceptibility to abrupt failure preventing the formation of larger and deeper craters. Hence, in effect, the true smallest crater volumes and depths are observed in the soft AlTiN/AlCrN coating ($7.35 \times 10^6$ $\mu m^3$, and 120.52 μm). This leaves the reference monolayer to be the median with crater volume and depth of $9.50 \times 10^6$ $\mu m^3$ and 150.84 μm, correspondingly.

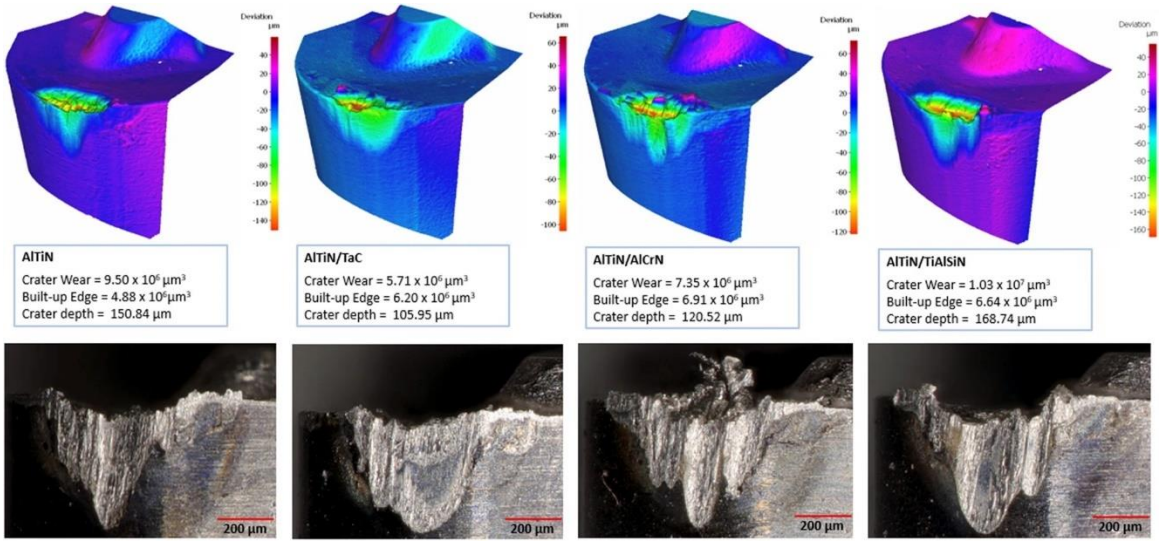


**Figure 2.10: Fig. 10 3D volumetric datasets of the coated cutting tools highlighting the amount of crater and BUE formation at the end of tool life. The optical images show the end-of-life flank wear**

The extreme crater wear generated on the rake face can partially be attributed to the elevated temperatures at the high cutting speeds during the machining process leading to tool-softening and consequent cratering [47]. The severity of crater wear far exceeded that of flank wear for all coatings except the AlTiN/ta-C coating as it experienced abrupt failure. The AlTiN/AlCrN coating's low crater volumes and depths can primarily be owed to its high PI and low H/E ratios as they allowed for the tool to undergo prolonged plastic deformation, as opposed to brittle fracture, as was observed in the diamond-like AlTiN/ta-C coating. The AlTiN/TiAlSiN coating resulted in the largest and deepest craters, despite it having a marginally lower H/E ratio and higher PI than the base monolayer, because of the inclusion of the element Si in the coating potentially having led to excessive abrasion, exacerbating the formation of craters. Overall, in light of the discussion above it can be

concluded that the AlTiN/AlCrN provided the best tool life and resistance to wear, more specifically crater wear.

### 2.3.3 Tribological Studies

Surface roughness (Ra) measurements of the workpiece were taken after every cutting tool pass as it is a good indicator of the workpiece surface quality as a function of cutting length. Figure 11 depicts the variation in surface roughness at different intervals along a cutting length distance of 300 m for the coated tools. The overview depicts that across the cutting length distance, the AlTiN/AlCrN coating, excluding the first pass, has the lowest surface roughness values whereas AlTiN/TiAlSiN has the highest. Additionally, all coatings see a drop in their roughness values after ~ 30 m of cutting length distance. The AlTiN/AlCrN coating has a decreasing trend, decrementing from ~ 0.83 μm down to ~ 0.30 μm up to a distance of 150 m, and then fluctuating within a range of ~ 0.37 μm and ~ 0.49 μm past that distance. Similarly, the base AlTiN (~ 0.95 μm to ~ 0.44 μm), AlTiN/ta-C (~ 0.82 μm to ~ 0.64 μm), and AlTiN/TiAlSiN (~ 1.16 μm to ~ 0.75 μm) coated tools see a decreasing trend up to and close to a cutting length distance of 150 m, with a spike (except AlTiN/TiAlSiN) and unpredictable trend observed thereafter. The relatively higher initial surface roughness values can be attributed to the nature of PVD-based coated tools having a thicker edge radius than uncoated tools and thus requiring a break-in period for the coated surface and tool geometry to stabilize, and thereafter adapt for subsequent passes [48]. The decreasing trend of surface roughness is owed to the aforementioned reason for the coating and tool geometry settling. Similarly, the rise and fluctuation in surface roughness values

past the cutting length of 150 m can be attributed to extensive geometrical deviations of the cutting edge as a consequence of extensive crater wear formation.

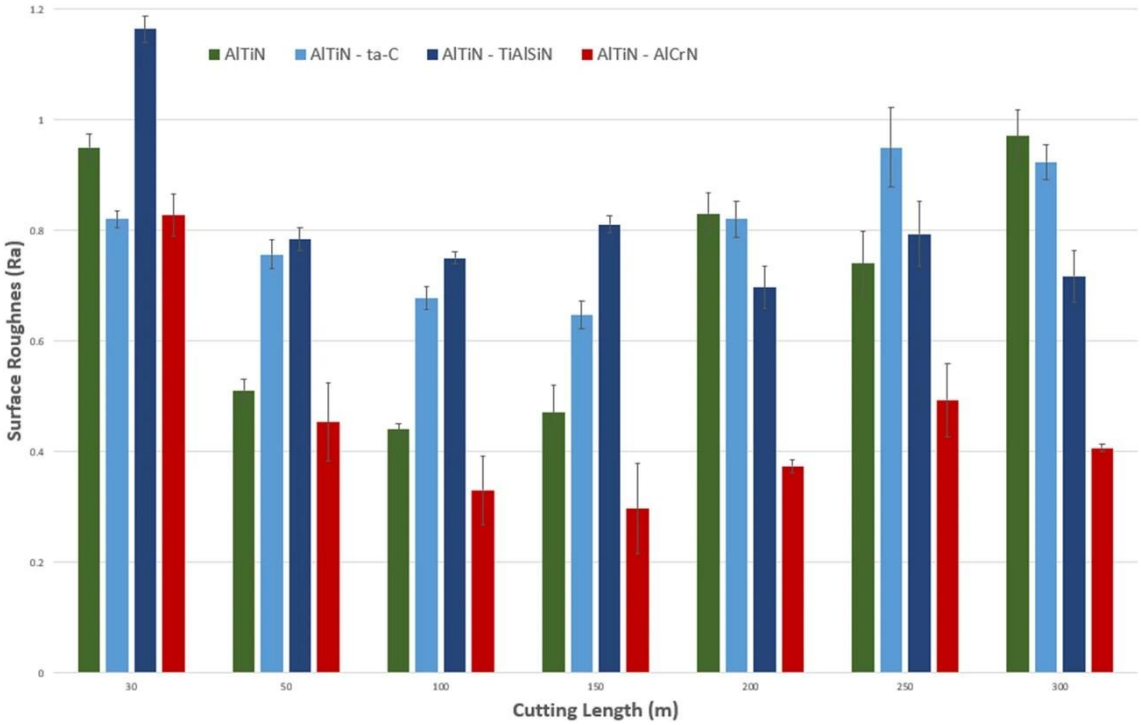


**Figure 2.11: Fig. 11 Surface roughness measurements of the workpiece as a function of cutting length across a distance of 300 m**

The extensive crater formation is partially a result of extremely high cutting temperatures and the diffusion/oxidation process between the elements within the workpiece and the WC tool. The presence of oxygen and high temperatures, primary catalysts for diffusion/oxidation, leads to the formation of tribo-oxides. Tribo-oxides can either be detrimental or beneficial depending on the constituent elements of the workpiece and/or cutting tool. One of the most common determinantal tribo-oxides formed during the machining of the Ti-5553 alloy is $TiO_2$, illustrated in the Ti2p XPS fittings of one of the representative coated tools in Fig. 12a. The formation of $TiO_2$ oxide is reported [32] to expedite the wearing process as it imparts worsened frictional characteristics.

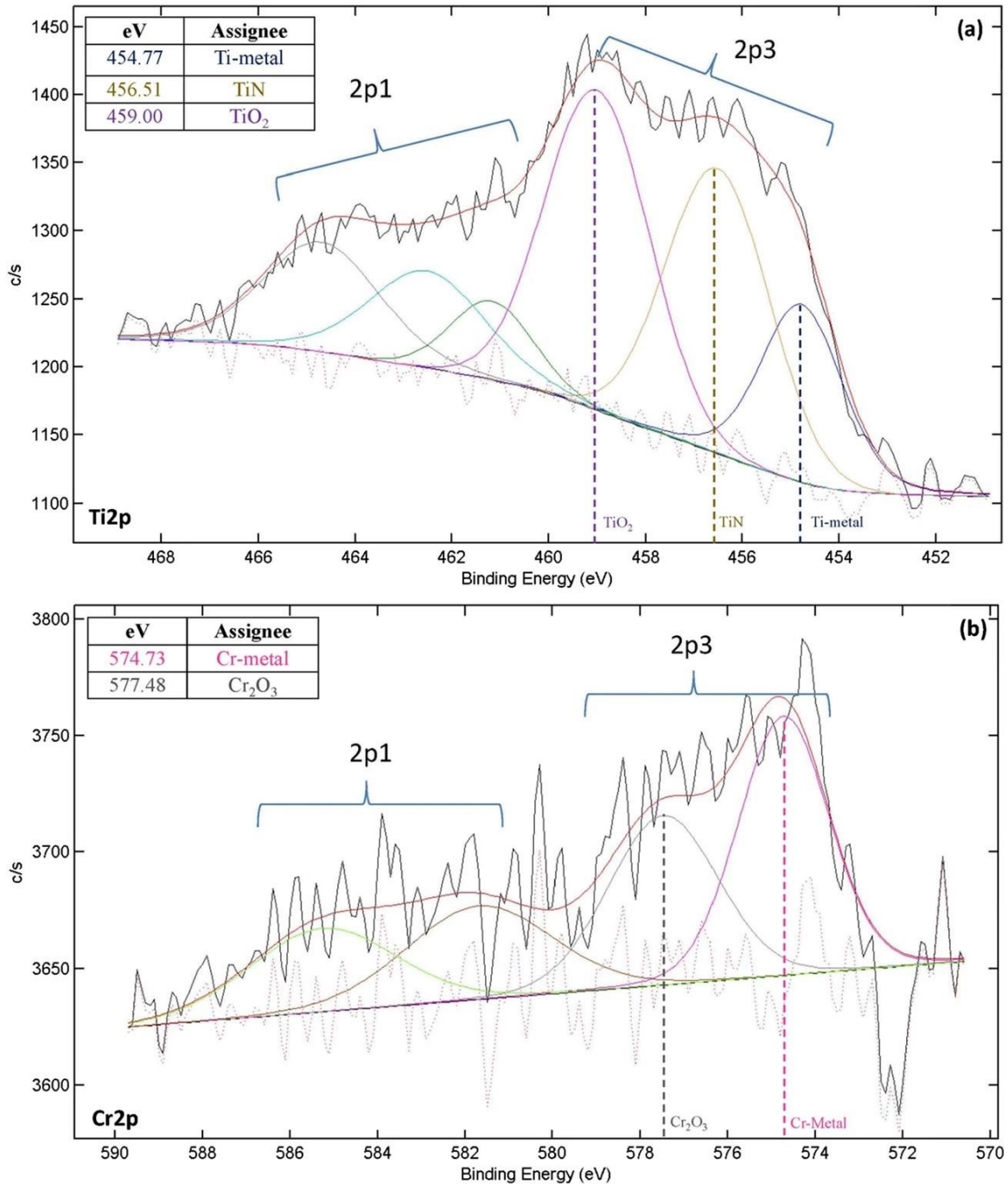


**Figure 2.12: Fig. 12 High-resolution XPS spectrum data collected using the (a) Ti2p, and (b) Cr2p fittings on the rake faces of the AlTiN (monolayer) and AlTiN/AlCrN coatings, respectively**

A coated tool's performance to a certain extent depends on its ability to form beneficial tribo-oxides at the tool-chip interface during the cutting process as it aids by providing in-situ lubrication along with thermal barrier properties. These thermal barrier properties are reportedly a product of the typically low thermal conductivity of the coating material as well as the low thermal diffusivity of the substrate [49]. The Cr2p fitting XPS analysis as shown in Fig. 12b performed on the rake face of the worn AlTiN/AlCrN coated tool indicates that at high temperatures, resulting from the interaction between the workpiece material and coated tool, lubricious $Cr_2O_3$ and $(Al, Cr)_2O_3$ (Cr and Al being amongst the constituent elements) tribofilms form. The resulting lowest workpiece surface roughness and improved wear performance (lowest crater wear intensity) during the machining of Ti-5553 using AlTiN/AlCrN can be attributed to the formation of said tribofilms as they lower frictional characteristics [50] at the tool-chip interface by imparting lubricious and thermal barrier properties at elevated temperatures. The evidently superior protection of the AlTiN/AlCrN coated tool during the initial stages of the cutting process contributed to its comparatively prolonged tool life.

## 2.4 Conclusion

Limited studies conducted on the machining of Ti-5553 using coated WC-based tools, along with the growing industrial demand underscore the necessity for the development and testing of novel PVD-coated tools. To address this, several novel mono/bi-layered PVD-coated WC-based cutting tools were employed in the turning machining of the Ti-5553 alloy to investigate their impact on wear performance, tool life, as well as workpiece surface quality.

A commercial AlTiN-based coating serves as the baseline reference layer and is compared with mono-layered DLC ta-C, AlCrN, and TiAlSiN coatings deposited on the AlTiN base on three separate cutting tools. Results indicate that the AlTiN/AlCrN bi-layered coating provided the longest tool life, an increment of approximately 9% compared to the baseline reference. In contrast, the AlTiN/ta-C showed proneness to sudden failure, a decrement of ~ 39.6%, compared to the baseline reference, and ~ 44.6% compared to the AlTiN/AlCrN coating. Similarly, the AlTiN/AlCrN yielded the smoothest surface finish on the workpiece material, a plus of ~ 31.81% over the baseline reference monolayer. The optimal micromechanical properties (H/E, $H^3/E^2$, and PI) further supported by the microscratch tests of the AlTiN/AlCrN coating contributed to the improvements mentioned. By reducing delamination and consequently inhibiting crater wear formation, relatively longer tool life and improved tribological performance were achieved. Furthermore, In-situ lubrication and thermal barrier properties resulting from the formation of $Cr_2O_3$ oxides when machining with AlTiN/AlCrN coated tools also provided superior protection of the coated tool during the initial stages of the cutting process, thus prolonging tool life. A coating's tribological and tool life performance is highly dependent on its underlying characteristics—adaptation post-break-in period, micromechanical properties, as well as the constituent elements having a bearing on the types of oxides formed.

## 2.5 References

1. Sun Y, Huang B, Puleo DA, Jawahir IS (2015) Enhanced machinability of Ti-5553 alloy from cryogenic machining: Comparison with MQL and flood-cooled machining and modeling. Procedia CIRP 31:477–482. https://doi.org/10.1016/J.PROCIR.2015.03.099

2. Bartus SD (2009) Evaluation of Titanium-5Al-5Mo-5V-3Cr (Ti-5553) Alloy Against Fragment and Armor-Piercing Projectiles

3. Kolli R, Devaraj A (2018) A Review of Metastable Beta Titanium Alloys. Metals (Basel) 8:506. https://doi.org/10.3390/met8070506

4. Wang L, Wang Y, Xu X, Liu C (2015) Dynamic behaviour and shock-induced martensite transformation in near-beta Ti-5553 alloy under high strain rate loading. EPJ Web Conf 94:02026. https://doi.org/10.1051/epjconf/20159402026

5. Micheletti C, Lee BEJ, Deering J, et al (2020) Ti–5Al–5Mo–5V–3Cr bone implants with dual-scale topography: a promising alternative to Ti–6Al–4V. Nanotechnology 31:235101. https://doi.org/10.1088/1361-6528/AB79AC

6. Veeck S, Lee D, Boyer R, Briggs R (2004) The castability of Ti-5553 alloy: the microstructure and properties of cast titanium alloy Ti-5553 were evaluated in a joint program by Howmet and Boeing. Advanced Materials & Processes 162:47–49

7. Cotton JD, Briggs RD, Boyer RR, et al (2015) State of the Art in Beta Titanium Alloys for Airframe Applications. JOM 67:1281–1303. https://doi.org/10.1007/S11837-015-1442-4/FIGURES/25

8. Wagner V, Baili M, Dessein G (2015) The relationship between the cutting speed, tool wear, and chip formation during Ti-5553 dry cutting. International Journal of Advanced Manufacturing Technology 76:893–912. https://doi.org/10.1007/S00170-014-6326-1/METRICS

9. (2005) Titanium 2005 conference proceedings, 21st Annual International Titanium Association, Scottsdale, Arizona, September 25-27, 2005. In: Broomfield, Colo. : International Titanium Association

10. Williams JC, Boyer RR (2020) Opportunities and Issues in the Application of Titanium Alloys for Aerospace Components. Metals (Basel) 10:705. https://doi.org/10.3390/met10060705

11. Arrazola P-J, Garay A, Iriarte L-M, et al (2009) Machinability of titanium alloys (Ti6Al4V and Ti555.3). J Mater Process Technol 209:2223–2230. https://doi.org/10.1016/j.jmatprotec.2008.06.020

12. Nouari M, Makich H (2014) On the Physics of Machining Titanium Alloys: Interactions between Cutting Parameters, Microstructure and Tool Wear. Metals (Basel) 4:335–358. https://doi.org/10.3390/met4030335

13. Imam MA (2011) The 12th world conference on titanium presents research and applications of "Wonder Metal." JOM 63:16–23. https://doi.org/10.1007/S11837-011-0166-3/METRICS

14. Parida AK, Maity K (2019) Analysis of some critical aspects in hot machining of Ti-5553 superalloy: Experimental and FE analysis. Defence Technology 15:344–352. https://doi.org/10.1016/J.DT.2018.10.005

15. ASM Material Data Sheet. https://asm.matweb.com/search/SpecificMaterial.asp?bassnum=mtp641. Accessed 3 Jan 2023

16. Ezugwu EO, Wang ZM (1997) Titanium alloys and their machinability—a review. J Mater Process Technol 68:262–274. https://doi.org/10.1016/S0924-0136(96)00030-1

17. Stephenson DA, Agapiou JS (2018) Metal Cutting Theory and Practice. CRC Press

18. Ugarte A, M'Saoubi R, Garay A, Arrazola PJ (2012) Machining Behaviour of Ti-6Al-4 V and Ti-5553 All0oys in Interrupted Cutting with PVD Coated Cemented carbide. Procedia CIRP 1:202–207. https://doi.org/10.1016/J.PROCIR.2012.04.035

19. Liu E, Wang R, Zhang Y, An W (2021) Tool wear analysis of cutting Ti-5553 with uncoated carbide tool under liquid nitrogen cooling condition using tool wear maps. J Manuf Process 68:877–887. https://doi.org/10.1016/j.jmapro.2021.06.016

20. Hartung PD, Kramer BM, von Turkovich BF (1982) Tool Wear in Titanium Machining. CIRP Annals 31:75–80. https://doi.org/10.1016/S0007-8506(07)63272-7

21. Shaw MC (Milton C (2005) Metal cutting principles. Oxford University Press

22. Chatti S, Laperrière L, Reinhart G, Tolio T (2019) CIRP Encyclopedia of Production Engineering. Springer Berlin Heidelberg, Berlin, Heidelberg

23. Mrkvica I, Neslušan M, Čep R, Sléha V (2016) Properties and comparison of PVD coatings. Tehnički vjesnik 23:569–574. https://doi.org/10.17559/TV-20140509105317

24. Proost J (2018) Mechanical and electrostrictive effects in anodic films. In: Encyclopedia of Interfacial Chemistry: Surface Science and Electrochemistry. Elsevier, pp 302–318

25. Wang B, Li A, Liu G (2020) Cutting performance and wear mechanisms of TiAlN PVD-coated cemented carbide tool in high speed turning of Ti-5Al-2Sn-2Zr-4Mo-4Cr alloy. Journal of Mechanical Science and Technology 34:2997–3006. https://doi.org/10.1007/s12206-020-0631-4

26. Inspektor A, Salvador PA (2014) Architecture of PVD coatings for metalcutting applications: A review. Surf Coat Technol 257:138–153. https://doi.org/10.1016/j.surfcoat.2014.08.068

27. Chowdhury MSI, Bose B, Yamamoto K, et al (2020) Wear performance investigation of PVD coated and uncoated carbide tools during high-speed machining of TiAl6V4 aerospace alloy. Wear 446–447:203168. https://doi.org/10.1016/j.wear.2019.203168

28. Khoei AA, He Q, DePaiva JM, et al (2023) Assessment of the tribological and wear performance of new duplex AlTiN-based coating systems at high temperatures when threading super duplex stainless steel. J Manuf Process 98:285–301. https://doi.org/10.1016/j.jmapro.2023.05.042

29. ISO 14577-4:2016 - Metallic materials — Instrumented indentation test for hardness and materials parameters — Part 4: Test method for metallic and non-metallic coatings. https://www.iso.org/standard/61823.html. Accessed 25 Dec 2023

30. ISO 3685:1993 - Tool-life testing with single-point turning tools. https://www.iso.org/standard/9151.html. Accessed 26 Dec 2023

31. ISO 21920-3:2021 - Geometrical product specifications (GPS) — Surface texture: Profile — Part 3: Specification operators. https://www.iso.org/standard/72228.html. Accessed 9 Jun 2024

32. Patel U, Rawal S, Bose B, et al (2022) Performance evaluations of Ti-based PVD coatings deposited on cermet tools for high-speed dry finish turning of AISI 304 stainless steel. Wear 492–493:204214. https://doi.org/10.1016/j.wear.2021.204214

33. Fang W, Chen J, Cai F, et al (2023) Reduced crater wear and improved high-speed dry cutting performance of B-containing AlTiBN coatings against Ti-6Al-4 V alloy. Tribol Int 187:108730. https://doi.org/10.1016/j.triboint.2023.108730

34. Ding F, Wang C, Zhang T, et al (2023) Adhesive wear mechanism of coated tools and its influence on cutting performance during machining of Zr-based bulk metallic glass. Journal of Materials Research and Technology 27:5489–5506. https://doi.org/10.1016/j.jmrt.2023.11.073

35. Sun X, Liu ZR, Chen L (2023) Influence of Si and Ta mixed doping on the structure, mechanical and thermal properties of TiAlN coatings. Surf Coat Technol 461:129428. https://doi.org/10.1016/J.SURFCOAT.2023.129428

36. Ardila LC, Dueñas R, Orozco G, et al (2023) Influence of Si Addition on the Chemical and Tribological Performance of TiAlCrN Coating Deposited by Co-Sputtering. Crystals (Basel) 13:1666. https://doi.org/10.3390/cryst13121666

37. Jun Z, Jianxin D, Jianhua Z, Xing A (1997) Failure mechanisms of a whisker-reinforced ceramic tool when machining nickel-based alloys. Wear 208:220–225. https://doi.org/10.1016/S0043-1648(96)07476-5

38. Yu Z, Chen G, Wang J, et al (2023) Research status and development trend of tungsten alloy cutting. International Journal of Advanced Manufacturing Technology 125:4435–4451. https://doi.org/10.1007/S00170-023-11025-9/TABLES/3

39. Scruby CB (1987) An introduction to acoustic emission. J Phys E 20:946. https://doi.org/10.1088/0022-3735/20/8/001

40. C1624 Standard Test Method for Adhesion Strength and Mechanical Failure Modes of Ceramic Coatings by Quantitative Single Point Scratch Testing. https://www.astm.org/c1624-22.html. Accessed 2 Jan 2024

41. Chowdhury MSI, Bose B, Fox-Rabinovich G, Veldhuis SC (2021) Investigation of the Wear Performance of TiB2 Coated Cutting Tools during the Machining of Ti6Al4V Alloy. Materials 14:2799. https://doi.org/10.3390/ma14112799

42. Lü W, Li G, Zhou Y, et al (2020) Effect of high hardness and adhesion of gradient TiAlSiN coating on cutting performance of titanium alloy. J Alloys Compd 820:153137. https://doi.org/10.1016/J.JALLCOM.2019.153137

43. Zhao F, Ge Y, Wang L, Wang X (2020) Tribological and mechanical properties of hardness-modulated TiAlSiN multilayer coatings fabricated by plasma immersion ion implantation and deposition. Surf Coat Technol 402:126475. https://doi.org/10.1016/J.SURFCOAT.2020.126475

44. Kaynak Y, Gharibi A (2019) The effects of cutting parameters on machining performance of titanium alloy Ti-5553. Advances in Materials and Processing Technologies 5:317–328. https://doi.org/10.1080/2374068X.2019.1585071

45. Kaynak Y, Gharibi A (2019) Cryogenic Machining of Titanium Ti-5553 Alloy. J Manuf Sci Eng 141:. https://doi.org/10.1115/1.4042605

46. Kaynak Y, Gharibi A, Yılmaz U, et al (2018) A comparison of flood cooling, minimum quantity lubrication and high pressure coolant on machining and surface integrity of titanium Ti-5553 alloy. J Manuf Process 34:503–512. https://doi.org/10.1016/j.jmapro.2018.06.003

47. He Q, DePaiva JM, Kohlscheen J, Veldhuis SC (2021) A study of mechanical and tribological properties as well as wear performance of a multifunctional bilayer AlTiN PVD coating during the ultra-high-speed turning of 304 austenitic stainless steel. Surf Coat Technol 423:127577. https://doi.org/10.1016/j.surfcoat.2021.127577

48. Kumar Bhushan R (2022) Effect of tool wear on surface roughness in machining of AA7075/ 10 wt.% SiC composite. https://doi.org/10.1016/j.jcomc.2022.100254

49. Zhao J, Liu Z (2018) Effects of Thermo-physical properties of Ti0.41Al0.59N coating on transient and steady cutting temperature distributions in coated cemented carbide tools. International Communications in Heat and Mass Transfer 96:80–89. https://doi.org/10.1016/j.icheatmasstransfer.2018.05.024

50. Morton TJ (2017) Development of high temperature/oxidation- resistant PVD coatings for cutting tools using HIPIMS. Sheffield Hallam University

# 3 Chapter 3: An Investigation of the Effect of Novel Mono/Bi-Layered PVD-Coated WC Tools on the Machinability of Ti-5Al-5V-5Mo-3Cr

Syed, H.S.[1,*], DePaiva, J.M.[1], Saciotto, V.[1], Veldhuis, S.C.[1]

1 - McMaster Manufacturing Research Institute (MMRI), Department of Mechanical Engineering, McMaster University, 230 Longwood Rd S, Hamilton, ON L8P0A6, Canada.

* Corresponding author: syedh39@mcmaster.ca (Syed, H.S).

*This paper is published in Materials MDPI - (IF 3.1) 17(15), 3743 https://doi.org/10.3390/ma17153743*

**Author's Contribution**

| | |
|---|---|
| Hasan Sohail Syed | Investigation, Methodology, Validation, Formal Analysis, Writing—Original Draft, Writing—Review and Editing, Visualization. |
| Jose Mario DePaiva | Resources, Supervision. |
| Victor Saciotto | Methodology, Validation, Writing—Review and Editing, Resources. |
| Stephen C. Veldhuis | Conceptualization, Supervision, Project Administration, Funding Acquisition, Writing—Review and Editing. |

**Abstract**

The Ti-5Al-5V-5Mo-3Cr (Ti-5553) alloy is a relatively novel difficult-to-cut material with limited machinability and tool life analysis available in the literature, and hence requires further investigation. This study focuses on the machining and tribological performance of Ti-5553 under high-speed finish turning (150 m/min, 175 m/min, and 200

m/min) via novel mono/bi-layered PVD-coated WC tools. A base AlTiN coating is used as the reference monolayer coating, with AlCrN, diamond-like ta-C, and TiAlSiN coatings each deposited on top of a base AlTiN coating, totaling four separate coated tools (one monolayer and three bi-layer). Tool life, cutting forces, workpiece surface quality, and tribological chip analysis are among the subjects of investigation in this study. Overall, the AlTiN/AlCrN coated tool outperformed all the other combinations: an improvement of ~19% in terms of tool life in reference to the base AlTiN coating when averaging across the three speeds; lowest surface roughness values: ~0.30, 0.33, and 0.64 µm; as well as the lowest chip back surface roughness values: ~0.80, 0.68, and 0.81 µm at 150, 175, and 200 m/min, respectively. These results indicate that the AlTiN/AlCrN coating is an excellent candidate for industrial applications involving high-speed machining of Ti-5553.

## 3.1 Introduction

The VSPO-AVISM Corporation developed a metastable (up to ~850 °C) body-centered cubic (BCC) near-beta Ti alloy (commercially branded as titanium–molybdenum alloy or "TMA") called Titanium-5Al-5V-5Mo-3Cr (Ti-5553) that has excellent properties such as high strength, high toughness, exceptional corrosion resistance, elevated temperature stability, and is reported to be effectively lighter than steel- or nickel-based alloys, providing an excellent strength-to-weight ratio [1,2]. Ti-5553 at present is commonly utilized in the aerospace industry, particularly in landing gears (Boeing 787 Dreamliner and Airbus 350), and to a certain extent in biomedical applications, 3D printed implants being an example [3,4]. The superior mechanical properties achieved through the formation of the metamorphosed β-phase and higher concentration of certain elements over Ti-64

facilitates its serviceability in heavy duty applications; however, these very properties hinder its machinability and in turn result in worsened tool life and workpiece surface quality, a decrement of ~25% in terms of metal removal rates, and ~15% lower tool life [5,6,7,8].

Ti-5553 belongs to the β-alloy group, unlike the most commonly used Ti-64 alloy, which is categorized as having the α + β microstructure. It has a metastable β-structure and comes under the class of near-beta alloys due to beta stabilizers (V, Mo, Cr, and Fe), shown in Table 1, which lower the temperature required to stabilize the beta phase and contribute to the superior mechanical properties (~15–30% higher tensile and yield strengths) that Ti-5553 has over Ti-64 (Table 2) [9,10]. Compared to the 80% α-phase concentration in Ti-64, a proportion of only 20% exists in Ti-5553 in the form of α + β Widmanstätten, or bimodal/globular residual α microstructure [10]. In addition, the thermomechanical properties of any given alloy are not only defined by the microstructural phases, but also the chemical composition of the integrated elements. Table 1 and 2 show the elemental composition and mechanical properties, respectively, of the Ti-5553 alloy used in this study (Grandis Titanium), and a typical Ti-64 alloy. The elements involved in the alloying of a near β-titanium alloy are generally categorized as β-stabilizers, α-stabilizers, and neutral [11,12].

**Table 3.1: Table 1. Chemical composition of Ti-5553 and Ti-64 at ambient temperature [7, 10, 13, 14]**

| Composition (wt.%) | Al | Mo | V | Cr | Fe | Z | O | N | C |
|---|---|---|---|---|---|---|---|---|---|
| **Ti-5553 alloy** | 4.5–6 | 4–5.5 | 4–5.5 | 2.5–3.5 | 0.3–0.5 | <0.4 | <0.2 | <0.1 | <0.1 |
| **Ti-64 alloy** | 4.5–6 | - | 3.5–4.5 | - | 0.3–0.8 | - | <0.2 | <0.1 | <0.1 |

**Table 3.2: Table 2. Thermomechanical properties of Ti-5553 and Ti-64 at ambient temperature [7, 10, 13, 14, 15, 16, 17]**

| Properties | Tensile Strength *(MPa)* | Yield Strength (*MPa)* | Elongation (%) | Hardness (*HV*) | Thermal Conductivity ($W/m^{-1}C^{-1}$) |
|---|---|---|---|---|---|
| Ti-5553 alloy | 1290 | 1170 | 6 | 415 | 5 |
| Ti-64 alloy | ~950 | ~880 | 14–18 | ~300 | 6.7–7.3 |

Machining Ti-5553 at any cutting speed yields chips that have narrow adiabatic shear bands, unlike Ti-64, which forms partially segmented chips without any adiabatic shear bands (transitional chips) at low cutting speeds and segmented with adiabatic shear bands (also known as catastrophic thermoplastic shear [18]) at high cutting speeds. Moreover, these adiabatic shear bands can cause oscillations in force components resulting in rapid tool wear [10]. The size and shape of the chips are highly dependent on controllable machining factors, and analyzing the chips can aid in understanding the dynamics that contribute to the formation of chips [19]. The shear bands and back surface roughness are some of the factors that can be analyzed to give us details in relation to their effect on chips. Chips that are curly, thin, and have a low undersurface roughness, for instance, would be indicative of low friction at the tool–chip interface and improved chip flow [20].

Cutting forces and their components are amongst the major criteria for evaluating the machinability performance to aid with optimizing and improving machining of Ti-5553. The highest mechanical stresses due to cutting forces are found in the region of the cutting tool–chip interface due to the resistance to deformation (brittleness) of titanium alloys at high temperatures [12]. Increasing the feed rate, depth of cut, and cutting speeds all lead to an increase in the cutting forces. However, at low depths of cut, varying the cutting speed has little influence on the cutting forces, whereas the opposite is true at high depths of cut.

Increased variability in cutting forces with changing cutting speeds at high depths of cut is indicative of tool wear rate influencing the requirements for the cutting forces to form chips [21]. Moreover, cutting forces can be influenced by cyclic loading resulting in chatter (common in finishing operations) and eventually wear, and is more prominent in β-alloys [18]. Additionally, Ti-alloys such as Ti-5553 experience deflection almost two times that in carbon and stainless steels, which can result in the early onset of flank wear due to larger machined surface spring-back [12]. For this study, a low depth of cut was chosen to minimize the impact of cutting force variation with increasing speed in order to reduce the number of variables.

The highest temperatures in the machining of Ti-alloys are observed in the primary and secondary shear zones (tool–chip interface and tip). It has been reported by Kaynak et al. [21] that for Ti-5553 alloys, the cutting temperatures increase with an increase in cutting speed. As for the depth of cut, it causes the temperature to increase with its increase, with the highest influence at cutting speed above 120 m/min (for tungsten carbide tools (WC)). Moreover, the tool's hardness can decrease due to thermal softening at high temperatures, and stresses at the cutting edge, which can cause plastic deformation and extreme wear [18]. The effect of feed rate is marginal as compared to the depth of cut and cutting speed.

The surface integrity of Ti-5553 is primarily why it is used in applications requiring excellent reliability; hence, it is crucial to ensure that the surface finish is monitored and kept within an optimal range. Kaynak et al. [21] mention that for Ti-5553 alloys, increasing the depth of cut results in an increase in surface roughness, whereas increasing the cutting speed decreases the surface roughness, owing to high tool wear, and a worn cutting tool

nose giving a smoother surface finish, respectively. Although with increasing cutting speed the surface roughness of the workpiece decreases, its dimensional accuracy deteriorates due to the worn cutting tool nose.

The type and material of cutting tool utilized are highly dependent on the workpiece being machined and the limitations imposed by the equipment, amongst other factors. To resist sudden failure, the cutting tool material should have high resistance to abrasion, fracture toughness, and resistance to plastic deformation. The chipping resistance as well as the feed rate and depth of cut permitted are contingent on the cutting tool's resistance to fatigue and fracture. As for the maximum allowable cutting speed, the tool material is required to have high thermal conductivity, chemical inertness, and high hardness (i.e., penetration resistance) [22]. Coatings are applied as a means to enhance the properties of the surface layer of the tool material. Depending on the application, they can be applied to reduce the friction coefficient, improve the thermomechanical properties, or resist corrosion and oxidation. The primary focus of this discussion is on thin coatings (0.1–10 μm) deposited via physical vapor deposition (PVD).

The available literature primarily pertains to the challenges faced with the use of uncoated WC tools during the turning machining of Ti-5553. Limited research is available on the use of coated tools, or a comparative analysis of PVD-coated WC tools for cutting Ti-5553, as is evident from Table 3. A comprehensive study comparing coatings with different chemical compositions and architectures in terms of their performance for high-speed machining of Ti-5553 has not been reported. Hence, this study delves into performing a comparative analysis of single and bi-layered PVD-coated WC tools in the finish turning

of Ti-5553 in relation to tool life, surface quality, and tribological conditions. Highlighting the effect of the coatings' micromechanical properties, such as hardness, H/E, $H^3/E^2$, plasticity index (PI), and the importance of reducing the adhesion levels during the machining of this type of material.

**Table 3.3: Table 3. Summary of existing research on turning machining of Ti-5553**

| Paper Details | | | Cutting Tool and Workpiece | | Machining Conditions | | Testing Outputs | | |
|---|---|---|---|---|---|---|---|---|---|
| **No.** | **Reference** | **Objective** | **Cutting tool material** | **Coating** | **Feed** (f), **Depth of Cut** ($a_p$), **Speed** ($V_c$) | **Coolant** | **Thermomechanical** | **Visual** | **Important Conclusions** |
| **1.** | Kaynak Y. [23] | To analyze the impact of cutting parameters on machining of Ti-5553 | 883 Carbide - CNMG120408 M1 | Uncoated | $V_c$: 40, 80, 120, 160, 200 m/min<br>$a_p$: 0.8, 1.4, 2<br>f: 0.1, 0.15, 0.2 mm/rev | Dry | Surface roughness, cutting forces | Tool wear, cutting temperature, chips | • Depth of cut and cutting speed have a profound effect on the machining performance<br>• Feed rate has minimal effect on the machining performance, but does impact the surface roughness of the material<br>• Common wear mechanism is BUE on the rake face<br>• Nose wear increases considerably above 120 m/min |
| **2.** | Sun Y. [24] | Assessing different cutting fluid mechanisms on machining performance of Ti-5553 | SANDVIK 432-MM (Carbide) | Coated (TiCN) | $V_c$: 20, 50, 80 m/min<br>f: 0.05, 0.125, 0.2 mm/rev | Cryo (10g/s, 1.5 MPa), Flood, and MQL | Cutting forces | Tool wear, surface roughness | • Cutting forces were reduced by 30% with cryogenic cooling as compared to flood and MQL<br>• Nose wear reduced in cryogenic cooling due to reduced adhesion of material<br>• The lowest surface roughness values were found by using MQL due to high temperature and lubricity effects resulting in softening of the workpiece<br>• Cutting forces increased with feed rate<br>• Flank wear was insensitive to cooling conditions and was found in all<br>• Adhesion was the primary wear mechanism of the nose |
| **3.** | Tascioglu E. [25] | Assessing different cutting fluid mechanisms on machining performance of Ti-5553 | 883 Carbide - CNMG120408 M1 | Uncoated | $V_c$: 90 (Dry and lubrication), 120 (Cryogenic) m/min<br>$a_p$: 0.6 (Finishing), 1.2 (Roughing)<br>f: 0.15 mm/rev | Dry, Flood (400 L/h), HPC (50 bar), MQL (21 ml/h, 0.4 MPa), and Cryo (10 g/s, 15 bar) | Cutting forces | Tool wear, cutting temperature, chips, surface roughness | • Greatest tool life observed under HPC, followed by Cryo<br>• HPC was found to be the best coolant in reducing friction and temperature, and consequently wear, and cutting forces<br>• Cryo cooling is more effective at lower depths of cut (finishing) |
| **4.** | Kaynak Y. [26] | Assessing different cutting fluid mechanisms on machining performance of Ti-5553 | 883 Carbide - CNMG120408 M1 | Uncoated | $V_c$: 30, 90, 120, 150, 210 m/min<br>$a_p$: 1.2<br>f: 0.15 mm/rev | Flood (400 L/h, MQL (21 ml/h, 5 bar), and HPC (50 bar) | Cutting forces, microhardness, | Tool wear, chips, surface roughness | • Beyond 150 m/min extreme wear and forces were observed<br>• HPC provides the best results<br>• Reduced hardness observed after machining<br>• No strain hardening observed<br>• Phase transformation does not occur hence post-treatment is not needed |
| **5.** | Yan D.P. [27] | Examining chip formation, and calculating shear strains, and rates | WNMG carbide | Uncoated | $V_c$: 37, 49, 66 m/min<br>$a_p$: 0.2 mm<br>f: 0.05, 0.1, 0.2 mm/rev | Dry | Shear stress and strain | Chip formation | • Shear strain within the bands was observed to be greater than in segments<br>• Shear strain rate increased with cutting speed<br>• Shear strain increased with material removal rate (MRR) |

| | | | | | | | | | |
|---|---|---|---|---|---|---|---|---|---|
| **6.** | Kaynak Y. [28] | Assessing different cutting fluid mechanisms on chip formation of Ti-5553 | TCMW16T308H13A (Carbide) | Uncoated | $V_c$: 20, 60, 120, and 210 m/min<br>f: 0.1 mm/rev | Cryo (15 bar), MQL (21 ml/h), and HPC (50 bar) | Cutting forces | Cutting temperature, tool wear, chip formation | • Increased cutting speeds lead to segmented chips in all conditions<br>• Chip thickness was larger at low cutting speeds<br>• Cryogenic condition produced the thinnest chips and smallest tool-chip contact length<br>• Shear angle becomes larger with increased cutting speeds resulting in thinner chips<br>• Cutting forces decreased with increasing cutting speeds<br>• Only HPC helped with improving chip breaking |
| **7.** | Liu E. [29] | A novel approach to assess tool wear | CNMG120408-SMRH13A (Carbide) | Uncoated | $V_c$: 30, 60, 90 m/min<br>$a_p$: 0.5, 1, 1.5 mm<br>f: 0.05, 0.1, 0.15, 0.2, 0.25 mm/rev | Cryo (5.5 g/s) | | Tool wear (Keyence for wear modes, SEM for microscopic wear morphology, EDS to analyze wear modes) | • Primary wear mechanisms on rake face were BUE, BUL, crater, notch, chip flow damage, and burr damage |
| **8.*** | Arrazola P.-J. [10] | Machinability comparison between Ti-5553 and Ti-64 | CNMG 120408-2 (Carbide) | Uncoated | $V_c$: 40-60 (Ti-5-5-5-3), 90 (Ti-6-4) m/min<br>$a_p$: 2 mm<br>f: 0.1 mm/rev | Conventional | Cutting forces | Tool wear, chips | • Machinability of Ti-64 was observed to be higher than Ti-5553<br>• Higher cutting forces when machining Ti-5553<br>• SEM observations of the worn tool detected the presence of titanium carbide. The presence of carbon in the adhered material on the tool indicates diffusion of carbon from insert to workpiece |
| **9.** | Wagner V. [6] | Effect of cutting parameters during machining of Ti-5553 | Tungsten carbide | Coated (TiAlN) | $V_c$: 35-65 m/min<br>$a_p$: 3 mm<br>f: 0.2 mm/rev | Dry | Cutting forces | Tool wear, chips | |
| **10.** | Wang L. [30] | Chip morphology comparison between dry and HPC in machining of Ti-5553 | CNMG 432-SMR H13A | Uncoated | $V_c$: 30, 60, 120 m/min<br>$a_p$: 0.5 mm<br>f: 0.1, 0.2 mm/rev | Dry, and HPC (105 bar) | | Chips | • HPC improved machinability<br>• Better chip morphology and chip breaking under HPC<br>• Serrated chips (adiabatic shear phenomenon) more severe under HPC<br>• The degree of chip sawtooth intensifies with increasing cutting speed and feed rate<br>• HPC chips had a mix of ductile + quasi-cleavage fracture whereas dry cutting chips had ductile fracture |
| **11.** | Liu E. [31] | A novel approach to assess tool wear | CNMG120408-SMRH13A (Carbide) | Uncoated | $V_c$: 30, 60, 90 m/min<br>$a_p$: 0.5, 1, 1.5 mm<br>f: 0.05, 0.1, 0.15, 0.2, 0.25 mm/rev | Cryo (5.5 g/s) | | Tool wear (Keyence for wear modes, SEM for microscopic wear morphology, average value of flank wear VB to evaluate wear) | |
| **12.** | Kaynak Y. [32] | Cryogenic coolant to assess machinability of Ti-5553 | 883 Carbide - CNMG120408 M1 | Uncoated | $V_c$: 30, 90, 120, 150, 210 m/min<br>$a_p$: 1.2<br>f: 0.15 mm/rev | Dry, and Cryo (Ln2: 1.5 MPa, 10g/s CO2: 5.4 MPa) | Cutting forces, surface integrity | Cutting temperature, tool wear | • Up to 120 m/min similar tool wear was observed for all 3 conditions<br>• In terms of material removal rate and cutting force 120 m/min was deemed the best<br>• Cryogenic cooling shortened chip contact length and improved breakability<br>• Reduced dimensional deviation in cryogenic due to reduced wear<br>• Surface and subsurface hardness of the workpiece decreased under all conditions<br>• XRD showed that the crystal structure and |

| | | | | | | | | | |
|---|---|---|---|---|---|---|---|---|---|
| | | | | | | | | | phases on the surface were affected during machining<br>• Cutting forces increased above 120 m/min due to tool wear |
| **13.** | Yan D.P. [33] | Investigated chip formation mechanisms, morphology, and microstructure evolutions | WNMG carbide | Uncoated | $V_c$: 27, 39, 55 m/min<br>ap: 2 mm<br>f: 0.08, 0.11, 0.2 mm/rev | Dry | Shear strain, strain rate | Chips, shear angle, shear | • Chip serration occurs during high-speed machining of Ti-5553, which is found to be attributed to the periodic formation of shear bands caused by thermoplastic instability within the primary shear zone.<br>• Effect of feed rate was found to be greater than cutting speed on shear angle |
| **14.** | Zhao X. [34] | Effect of surface integrity on fatigue life under cryogenic cooling in machining of Ti-5553 is analyzed | CNMG 12 04 08-SMR H13A | Uncoated | $V_c$: 30, 60, 90 m/min<br>$a_p$: 0.5 mm<br>f: 0.10, 0.20 mm/rev | Dry and Cryo (0.09 MPa) | Surface roughness, surface topography, fatigue, residuals stress | | • As the cutting speed increased from 30-90 m/min the surface roughness first decreased followed by an increase<br>• At constant cutting speed, surface roughness increased with increasing feed<br>• Cryogenic cooling extended fatigue life |
| **15.** | Liu E. [35] | Experimental and numerical approach to studying the effect of dry and cryogenic machining of Ti-5553 | CNMG 12 04 08-SMR H13A | Uncoated | $V_c$: 50, 60 m/min<br>$a_p$: 0.2, 0.4, 0.6, 0.8 mm<br>f: 0.10, 0.12, 0.14, 0.16, 0.18, 0.20 mm/rev | Dry and Cryo | | Cutting temperature | • At 50 and 60 m/min, and ap = 0.8 mm, an increase in feed rate under both cryo and dry conditions results in temperature increase (simulation and experimental)<br>• Marginal increase in temperature with change in depth of cut |
| **16** | Liu E. [36] | Effect of different cooling mechanisms on the surface integrity during machining of Ti-5553 | CNMG1204 08-SMR H13A | Uncoated | $V_c$: 30, 60, 90 m/min<br>$a_p$: 0.5 mm<br>f: 0.10, 0.15, 0.20 mm/rev | Dry, Cryo, (0.09 MPa) and HPC (8 MPa) | Surface roughness, plastic deformation, work hardening, residual stresses | | • As the cutting speed increased the surface roughness first decreased followed by an increase<br>• At constant cutting speed, surface roughness increased with increasing feed<br>• Surface hardness is mostly affected by cutting speed, followed by the cooling condition, and finally feed rate<br>• Max tensile residuals stress under dry whereas max compressive residual stress under HPC condition |
| **17.** | Liu E. [37] | A numerical approach to assess surface morphology of Ti-5553 | CNMG120408-MJ | Uncoated | $V_c$: 30, 50, 70 m/min<br>$a_p$: 0.5 mm<br>f: 0.05, 0.15, 0.25 mm/rev | Dry, and Cryo | Cutting forces | Surface roughness, surface morphology | • Cryogenic cooling affects low- and high-frequency surface roughness<br>• Cutting parameters affect low-frequency surface roughness<br>• Better 3D surface morphology found in Cryo than in dry<br>• Increase in cutting speed led to decrease followed by an increase of low-frequency surface roughness<br>• Increase in feed resulted in the increase of low- and high- frequency surface roughness |
| *** Indicates use of both Ti-64 and Ti-5553 workpieces. Green background indicates the use of a coating** | | | | | | | | | |

## 3.2 Materials and Methods

### 3.2.1 Experimental Setup and Machining Studies

Sets of single and bi-layered coated Kennametal CNGG120408FS K313 cutting inserts were used in the finish turning of Ti-5553 alloy supplied by Grandis Titanium, under flood lubrication with a coolant concentration of ~9%. The Boehringer VDF 180 CM CNC (FFG Europe & Americas, Eislingen, Germany) turning lathe was the machine employed for this study (Figure 1), with the cutting parameters and tools used provided in Table 4. To measure cutting forces, a piezoelectric Kistler Type 9129AA 3-component dynamometer was mounted to a KenlocTM MCLNL164D NJ9 5° tool holder. The analog data was fed into a National Instruments (NI) Type 9215 data acquisition card, converted to digital, and then acquired by the National Instruments (NI) cDAQ-9172 DAQ system. The data were processed via a National Instruments (NI) LabView 2014 data analysis system collected at a sampling rate of 10 kHz.

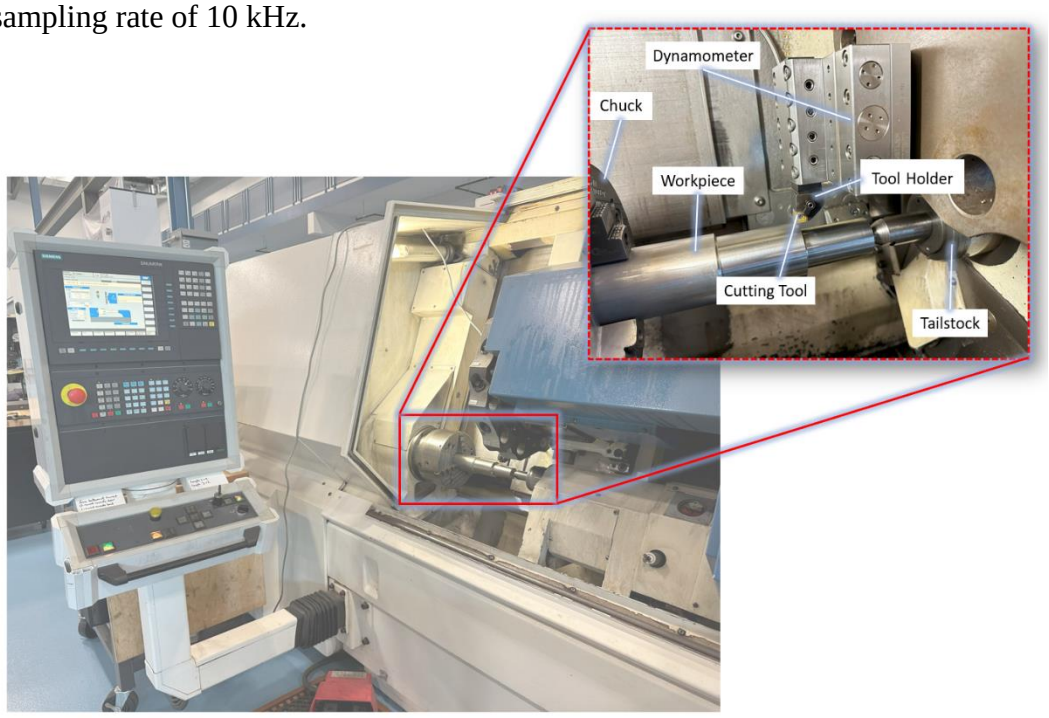


**Figure 3.1: Figure 1. Experimental machining setup for machining of Ti-5553**

**Table 3.4: Table 4. Cutting parameters and conditions**

| Cutting Conditions | | | | |
|---|---|---|---|---|
| **Cutting Speed (m/min)** | **Feed Rate (mm/rev)** | **Depth of Cut (mm)** | **Coolant Type** | **Workpiece Material** |
| 150 | 0.15 | 0.25 | Castrol Hysol MB50 Semi-Synthetic (9%) | Ti-5553 Grandis Titanium |
| 175 | | | | |
| 200 | | | | |

### 3.2.2 Coating Deposition and Cutting Tools

A monolayered commercial AlTiN-based (BALIQ® ALTINOS, Lake Orion, MI, USA) coating was used as the reference, with TiAlSiN (Kyocera HDT, Cuyhoga Falls, OH, USA), AlCrN (Ionbond CrosscutTM Plus, Duncan, SC, USA), and DLC ta-C (Ionbond Tetrabond$^{TM}$ Plus, Duncan, SC, USA) coatings deposited on top of the base AlTiN layer, for machining and characterization tests. Kennametal CNGG120408 K313 inserts were used for the cutting tests whereas polished WIDIA SNUN120408 WC coupons were utilized for the micromechanical and characterization tests to assess coating performance. The base monolayer coating designed for turning was deposited using s3p (scalable pulsed power plasma) HIPIMS technology, which incorporates both arc and sputtering technologies, resulting in excellent surface quality with minimal macroparticles. The AlCrN layer is an extremely versatile coating suitable for usage under both dry and wet cutting conditions at temperatures up to 1050 °C. The ta-C coating is optimal for the machining of non-ferrous metals such as titanium alloys and can be operated at temperatures in proximity of 500 °C. Both, having been deposited by Ionbond, employed PVD Advanced Arc Technology. The TiAlSiN coating was engineered to provide high performance solutions for titanium and super alloys at operating temperatures exceeding 1000 °C.

The WC coupons were hot-mounted in a black phenolic powder supplied by the MetLab Corporation (Niagara Falls, NY, USA) in a SimpliMET$^{TM}$ XPS1 Compression Mounting System (Lake Bluff, IL, USA). The mounting procedure was as follows: The heat and cool times were set to 10 and 5 min, with the maximum temperatures and pressures being 170 °C and 3.65 psi, respectively. Thereafter, a Struers Tegramin-25 semi-automatic machine (Copenhagen, Denmark) was used to polish the mounted sample in four steps: Step (1) disc speed: 300 rpm; force: 30 N; holder speed: 180 rpm; lubricant type: water; and duration: 6 min. Steps (2–4) disc speed: 150 rpm; force: 30 N; holder speed: 150 rpm; duration: 5 min; lubricant type: DP-Lubricant Blue with 9, 3, and 1 µm diamond suspensions; in series for steps 2, 3, and 4, correspondingly. After attaining a smooth reflective surface, the samples were coated.

### 3.2.3 Tool Wear Measurements

The VHX-5000 Keyence optical microscope (KEYENCE Corporation of America, Elmwood Park, NJ, USA) was used to inspect flank wear progression in increments of 30 m linear passes, with failure marked at 300 µm wear land in accordance with the ISO 3685:1993 standard [36]. The focus variation technology of the Alicona Infinite Focus G5 3D surface measurement system (Alicona Manufacturing Inc., Bartlett, IL, USA) was used to analyze cutting edge wear and create volumetric datasets using the EdgeMaster and MeasureSuite modules. In order to create and compare the 3D volumetric transformation of the tools before and after machining, the modules layer the worn tool dataset on top of the reference cutting tool of a similar geometry. The difference gives information related to edge and crater volume removal at the end of tool life. The Mitutoyo SJ-201 portable

surface roughness device (Mitutoyo America Corporation, Aurora, IL, USA) was used to measure the workpiece surface roughness an average of 3–4 times as per the ISO 21920-3:2021 standard [37] after every cutting pass.

### 3.2.4 Characterization and Chip Analysis

The coating thicknesses were measured by placing the samples at an angle in a BC-2 MIBA Coating Group ball crater device (Droitwich Spa, UK). An AISI 52100M Grade 25 mm Chromium steel ball was used to wear away at multiple spots on the coated samples, which were then inspected using a digital microscope. The coatings' surface topography were obtained using an Anton Parr Tosca$^{TM}$ 400 atomic force microscope (AFM) (Graz, Austria). Line scans were performed over a scan range of 25 µm × 25 µm at a scan speed of 0.3 lines/second using commercial silicon probes. The resonant frequency was set to 278 kHz, and force of 42 N/min. Data were analyzed and processed in Tosca$^{TM}$ analysis software (Version 7.4.8341).

Scratch tests were performed using an Anton Paar-RST3 Revetest® Scratch Tester (Graz, Austria). An average of 3 scratch tests were performed using a 200 µm Rockwell diamond indenter using a 3-scan progressive mode to understand the coatings' delamination behavior. Pre-topography scan, progressive load scratch scan, and post-topography scan are the three modes that make up the 3-scan procedure. The pre-topography scan gauged the surface profile by applying an initial load of 0.5 N; thereafter, the load was ramped up to 100 N over a distance of 3 mm, with load rate set to ~200 N/min and scan speed to 6 mm/min under progressive load scratch scan, and finally ending off with the post-topography scan for residual depth measurement to extract more details

related to the deformation behavior. The morphology and elemental distribution of the scratch tracks were observed with secondary (SE) and backscattered (BSE) modes in a FESEM (FEI, Hillsboro, Oregon, USA and Tescan, Lraya3, Brno, Czech Republic) equipped with an energy-dispersive X-ray spectrometer (EDX).

The micromechanical properties of the mono/bi-layered coatings were evaluated under ambient conditions using a Micro Materials NanoTest P3 system (Wrexham, UK) employing the Oliver–Pharr method. A Berkovich diamond indenter was employed to conduct a minimum of 20 indentations per coating. The indenter was calibrated in accordance with the ISO14577-4 [38] standard, encompassing load displacement, indenter geometry, as well as frame compliance. The indentation contact depth was fixed to $1/10^{th}$ of the coatings' thickness such that the substrate effect would be negligible and thus obtain values truly representative of the thin coatings. In other words, the coatings' load-invariant hardness and elastic modulus were solely considered. A maximum load of 100 mN was achieved at a loading rate of 200 mN/min during the indentation process. This was followed by a dwell time of 2.0 s, and 60.0 s of post-indentation to account for thermal drift.

Three-dimensional surface roughness measurement of the coatings was conducted using the focus variation technology of an Alicona Infinite Focus G5 3D surface measurement system (Alicona Manufacturing Inc., Bartlett, IL, USA). For all the coated samples, an area of ~180,000 $\mu m^2$ was captured at a magnification of 100× with highlights to the peaks and valleys via real color information.

The chemical composition and tribo-oxide formation during the machining process on coated tools' rake faces were extracted by means of the X-ray photoelectron spectroscopy

(XPS) technique using a PHI Quantera II Scanning XPS Microprobe (Physical Electronics Inc., Chanhassen, MN, USA). The spectrometer is equipped with an Al anode source acting as a receiver to electrons targeted towards it via a Raster Scanned Electron Gun®, with the generated X-rays redirected towards the samples using a quartz crystal monochromator. Thereafter, the secondary electrons generated pass through a hemispherical energy analyzer in a multi-channel detector to produce secondary electron images (SXI). A monochromatic Al K-α X-ray source in a 50 μm X-ray beam was used to collect data at a constant acceleration voltage of ~1486 eV while being operated at 12.5 W and 15 kV. The max sputtering pressure was reported as $1 \times 10^{-9}$ torr, whereas the lowest base pressure was recorded at $5 \times 10^{-9}$ torr. The spectral data were collected after having sputter-cleaned the samples with Ar+ gas. Spectral survey data were acquired at pass energy of 224 eV in step sizes of 0.8 eV, whereas the high-resolution data were acquired at 55 eV, in step sizes of 0.1 eV. The take-off angle was set to 45° and the dual-beam charge compensation system was utilized to neutralize the coatings. The C1s C-C peak was set to 248.8 eV to calibrate the equipment for high-resolution data acquisition. Post-acquisition data analysis was conducted in PHI Multipak software (Version 9.5).

Chips formed during the machining process were collected after the first pass for each of the coatings to assess their tribological characteristics in relation to the machining process and workpiece surface quality. The chip undersurface roughness, shear band morphology, curliness, and length were observed under a TESCAN VEGA-II LSU SEM. The back surface roughness (Sa) values for the chips were extracted via an Alicona Infinite Focus G5 3D surface measurement system for all the coated tools and cutting speeds.

## 3.3 Results and Discussion

### 3.3.1 Tool Performance and Cutting Forces

High-speed cutting tests were performed under wet conditions at 150, 175, and 200 m/min to obtain tool life and other complementing data—cutting forces and wear—for the four different coating types. Figure 2 depicts the tool life trends in terms of flank wear as a function of cutting length, with failure classified as flank wear reaching 300 µm. The overall trends across all three speeds supported the AlTiN/AlCrN coating providing the longest tool life, followed by the base layer AlTiN coating, then AlTiN/TiAlSiN, and AlTiN/ta-C being prone to abrupt failure due to its brittle nature. AlTiN/AlCrN had an average tool life improvement of ~19% as compared to the reference monolayer coating when taking all three cutting speeds into account. This improvement in tool life is attributed to its favorable thermomechanical properties (lowest H/E and $H^3/E^2$ ratios, and highest plasticity index (PI)) and tribo-oxide formation as evident from the micromechanical (Table 5) and XPS analysis [39]. The AlTiN/TiAlSiN coating's tool life was marginally lower across all the speeds when compared to the reference coating. This is owed to the Si inclusion exacerbating the wear rate due to its brittle nature [40], and hence resulting in a shorter tool life. The AlTiN/ta-C coating's behavior was a lot more unpredictable as it experienced occasional catastrophic failure as a result of its diamond-like nature, with the highest H/E and $H^3/E^2$ ratios, and lowest PI. Overall, as can be observed from Figure 2, for all the coatings, the tool life decremented by approximately 200 m at each instance of increase in speed, which was to be expected, as higher speeds expedite the wear process due to an increase in temperature and stresses. This is evinced by Kaynak Y et al. [26]

reporting extreme forces and wear when machining Ti-5553 using carbide tools at cutting speeds above 150 m/min.

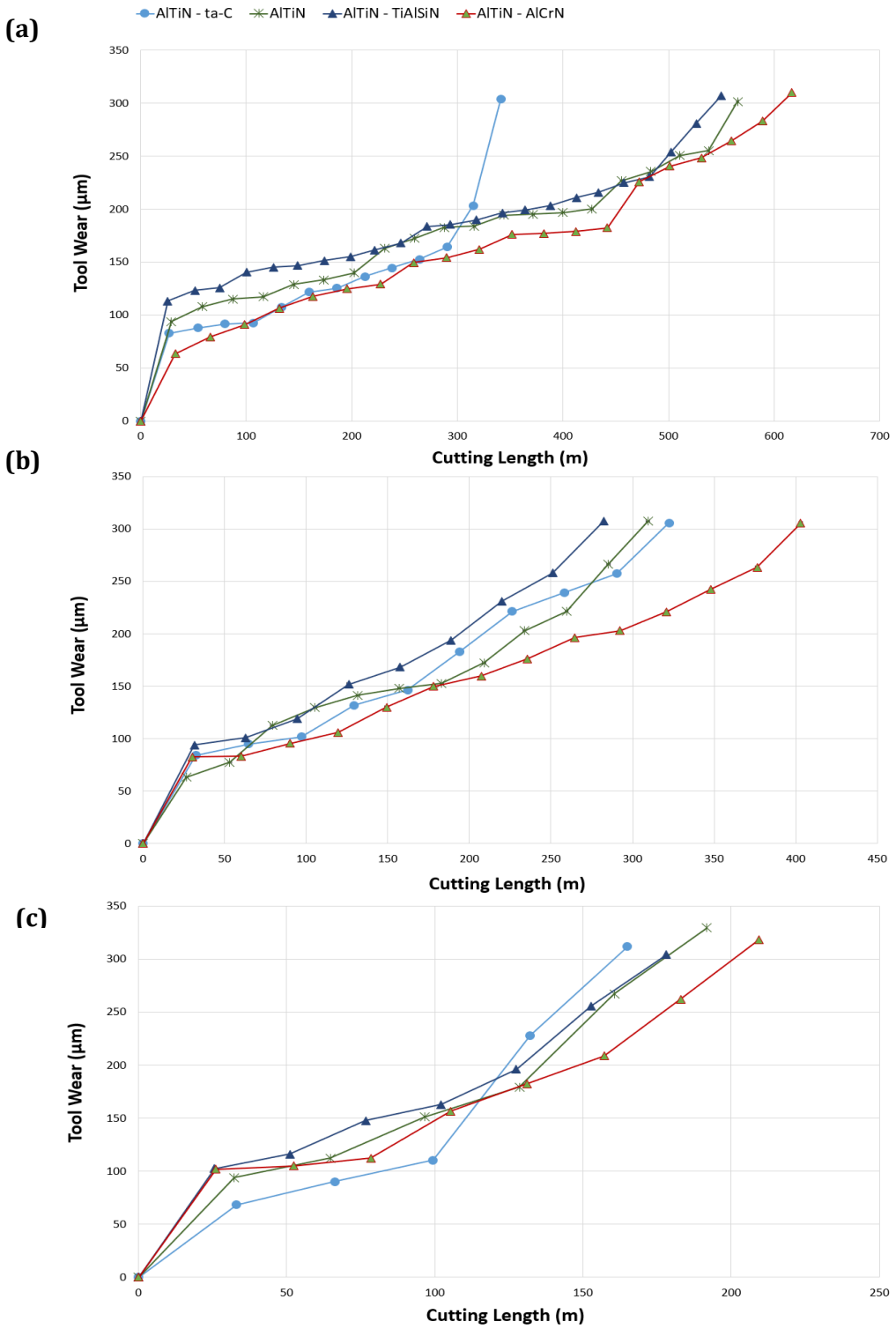


**Figure 3.2: Figure 2. Comparison of tool life curves in terms of flank wear (µm) as a function of cutting length (m) for AlTiN/AlCrN, base AlTiN, AlTiN/ta-C, and AlTiN/TiAlSiN coated tools at the cutting speeds of (a) 150 m/min, (b) 175 m/min, and (c) 200 m/min**

**Table 3.5: Table 5. Mechanical, architectural, and surface properties of the coated tools.**

| **Coating Type** | **AlTiN** | **AlTiN/AlCrN** | **AlTiN/ta-C (DLC)** | **AlTiN/TiAlSiN** |
|---|---|---|---|---|
| Architecture | Monolayer | Monolayer | Monolayer | Monolayer |
| Thickness (µm) | 5.57 | 6.6 | 6.05 | 6.54 |
| Hardness (GPa) | 33.87 ± 3.78 | 24.23 ± 4.96 | 41.88 ± 6.46 | 36.44 ± 6.73 |
| Elastic modulus (GPa) | 503.84 ± 47.25 | 450.35 ± 72.24 | 487.54 ± 71.60 | 588.01 ± 112.56 |
| H/E | 0.0672 | 0.0538 | 0.0859 | 0.0620 |
| $H^3/E^2$ | 0.153 | 0.070 | 0.309 | 0.140 |
| Plasticity index (PI) | 0.470 | 0.515 | 0.354 | 0.473 |
| $S_a$ (nm) | 36.91 | 33.59 | 43.47 | 45.38 |

Cutting forces typically have a significant impact on the rate of wear progression of a cutting tool, as an increase or decrease in cutting forces is commensurate to changes in frictional forces. Therefore, the higher the cutting forces during the machining process, the worse the frictional characteristics [41]. Cutting forces being high during the machining of superalloys such as Ti-5553 is partially due to their work-hardening nature. Lowering the work-hardening behavior of the workpiece would in turn result in a decrease in cutting forces, temperature, and chatter, and consequently obtaining improved workpiece surface quality and longer tool life. Figure 3 is representative of tangential cutting forces as a function of cutting length at the speed of 150 m/min. It can be noted that, albeit marginal, the lowest cutting forces up to a cutting length of 250 m were obtained by the AlTiN/AlCrN coating. This behavior can primarily be owed to its mechanical properties allowing for higher amounts of plastic deformation before coating delamination and failure. The same trend, however, was not reflected past a cutting length of 250 m, where the behavior was much more unpredictable. The trend for all the coatings was that of cutting forces being an average of 100 N before 250 m of cutting length, and then incrementally increasing by approximately 5 N after each 50 m of cutting length increase until 550 m, where the average force value was found to be 129 N. The rise and unpredictability of cutting forces past the

midway point is a result of geometrical distortions at the cutting edge superseding the coatings' influence on the cutting forces during the cutting process. As indicated by the yellow arrow, a peak of 132 N was observed for AlTiN/ta-C at 350 m of cutting length as it experienced sudden failure due to its extremely hard brittle nature. It is evident from Figure 3 and Figure 4 that across all the speeds, the general trend is that of cutting forces being in the same value range up to the approximate halfway point, and then increasing until the end of life. Moreover, the force variation between the coatings became more unpredictable at the speeds of 175 m/min and 200 m/min due to excessive geometrical deviations at the tool cutting edge. This is further substantiated by the comparatively higher end of life forces found at 175 and 200 m/min: an average of 143 N and 136 N at 200 m/min and 175 m/min, respectively, and 129 N at 150 m/min.

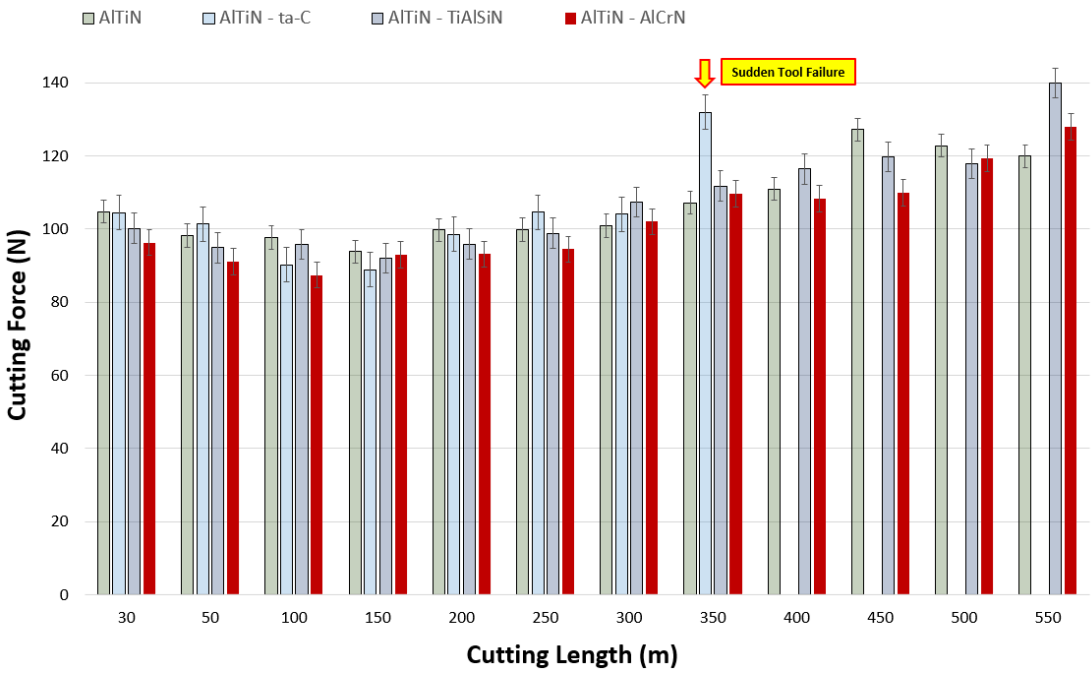


**Figure 3.8: Figure 3 Comparison of cutting force data for AlTiN, AlTiN/ta-C, AlTiN/TiAlSiN, and AlTiN/AlCrN coated tools during the machining of Ti-5553 at the cutting speed of 150 m/min**

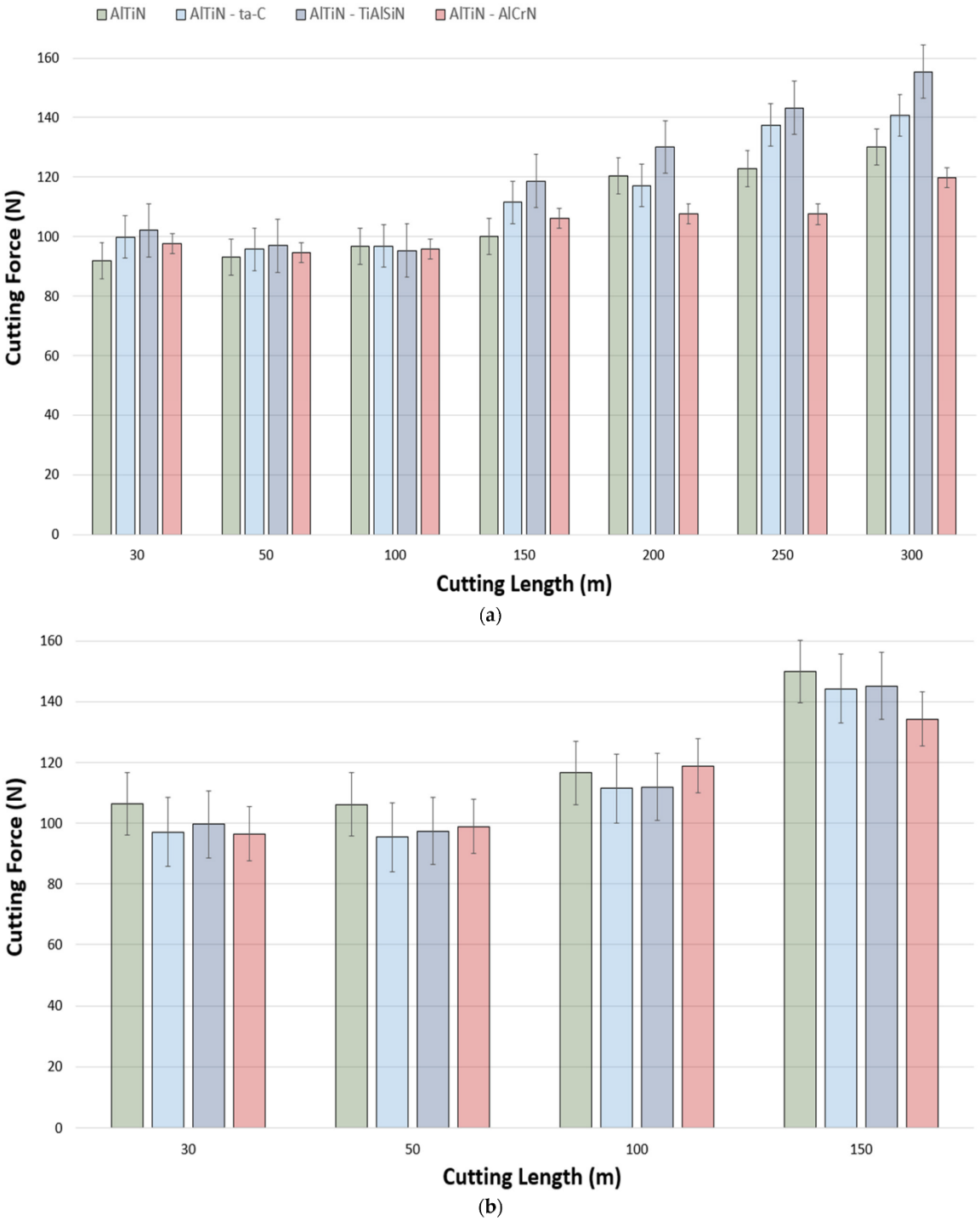


**Figure 3.9: Figure 4. Comparison of cutting force data for AlTiN-, AlTiN/ta-C-, AlTiN/TiAlSiN-, and AlTiN/AlCrN-coated tools during the machining of Ti-5553 at cutting speeds of (a) 175 m/min and (b) 200 m/min**

### 3.3.2 Tool Wear Analysis and Workpiece Surface Quality

Figure 5 illustrates the end of life volumetrically generated models, and optically taken images of the coated tools at the end of tool life as per the ISO 3685:1993 standard [36]. The two most common wear mechanisms found on all the coatings were flank and crater wear. This was primarily a result of abrasion and attrition forming intense grooves on the cutting edge, allowing for workpiece material to adhere on, and then subsequently being peeled off. Over the many repetitive machining cycles, the adherence and removal of workpiece material from the tools resulted in coating and tool substrate delamination from the flank and rake sides, with each corresponding to flank and crater wear, respectively. The crater wear formation on the rake face is partly a consequence of high temperature generation enabling tool softening and chemical reaction between the tool and workpiece. This leads to diffusion-dominated wear, resulting in crater formation on the rake face of the tool [42,43]. At the speed of 150 m/min, disregarding the abruptly failed AlTiN/ta-C coating, the smallest crater wear and depth were of the AlTiN/AlCrN coating at $7.35 \times 10^6$ $\mu m^3$ and 120.52 µm, and largest and deepest crater wear and depth were of the AlTiN/TiAlSiN coating at $1.03 \times 10^7$ $\mu m^3$ and 168.74 µm. The AlTiN/AlCrN coating had an advantage in terms of crater wear resistance because it has a relatively high resistance to plastic deformation, stemming from it having the highest PI and lowest H/E ratios. As for AlTiN/ta-C experiencing sudden failure, and AlTiN/TiAlSiN obtaining large and deep crater volumes, this can be attributed to their constituent elements (Si in the case of AlTiN/TiAlSiN, and hard C in AlTiN/ta-C), high $H^3/E^2$ ratios, lesser plastic deformation, and hence proneness to brittle fracture. At higher speeds, however, the end-of-life wear patterns became less predictable and saw a transition from regular flank wear to large and

deep notch wears, along with high volume craters, from an average magnitude of $\times 10^6$ $\mu m^3$ at 150 m/min, to $\times 10^7$ $\mu m^3$ at 200 m/min. This was to be expected as higher cutting forces and friction during machining cause extreme tool chipping, and hence, as a result, intensified wear rate.

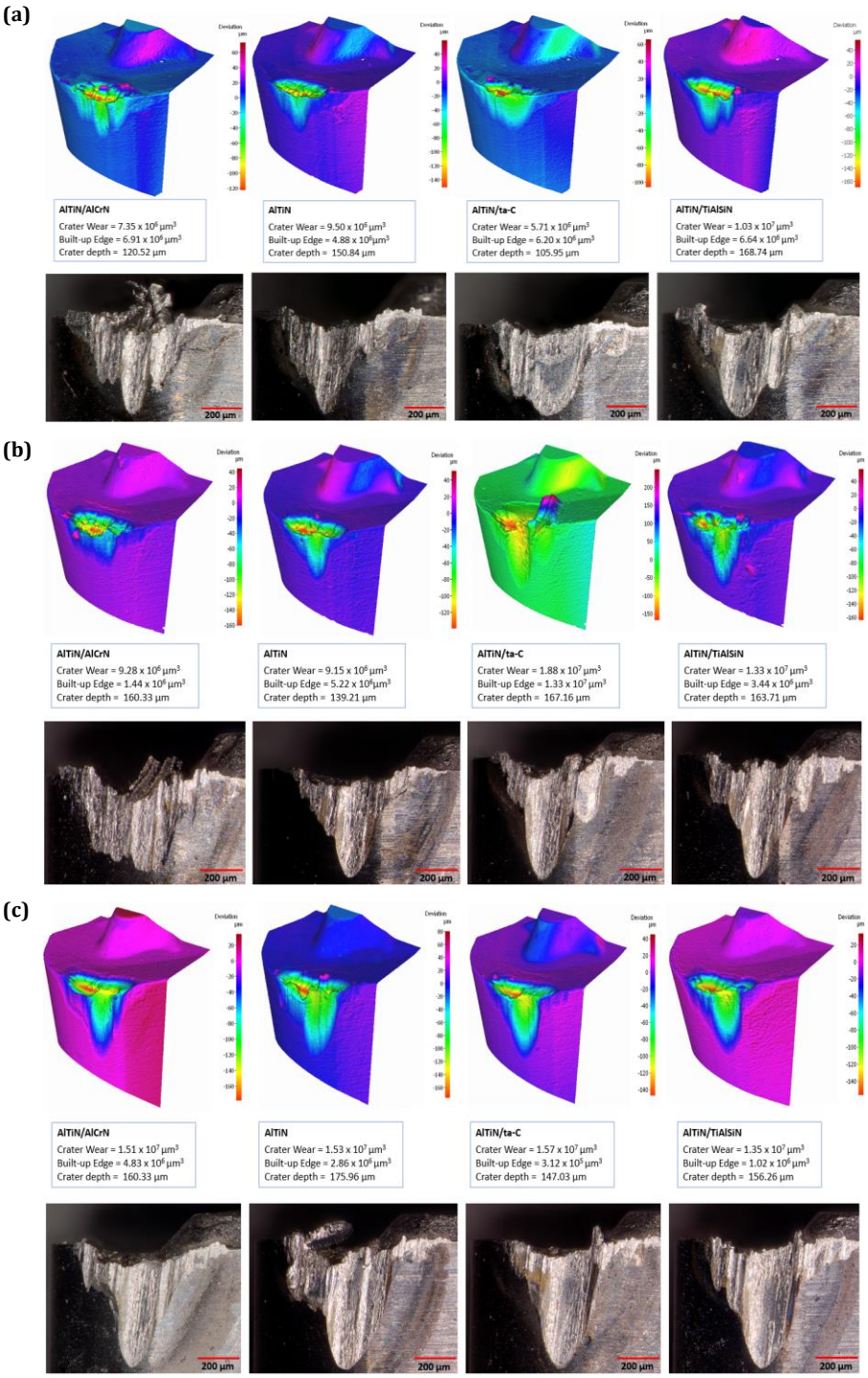


**Figure 3.10: Figure 5. Three-dimensional volumetric datasets and optical images of the coated tools highlighting the amount of crater wear and BUE formation after tool failure (end−of−life) at (a) 150 m/min, (b) 175 m/min, and (c) 200 m/min**

Surface roughness (Ra) measurements were taken an average of three times at all the cutting speeds after every cutting length pass to get an indication of the workpiece surface quality. Figure 6 depicts the surface roughness measurements taken at the cutting speeds of 150 m/min, 175 m/min, and 200 m/min. Measurements at 150 m/min were taken until close to the end of life (550 m). Overall, it can be noted that there is a decreasing trend of surface roughness values for all the coatings up to a cutting distance of approximately 150 m, with worsened surface quality and unpredictability observed past that distance. This phenomenon is similar to what was observed with the cutting forces, where cutting forces saw a rise and fluctuation past the approximate midway point. The AlTiN/AlCrN immediately stands out as consistently having the lowest surface roughness values throughout the whole cutting process, excluding the first pass (break-in period), decreasing from ~0.83 µm to the lowest value recorded at ~0.30 µm, and then observing an unpredictable trend in the range of ~0.37 µm to ~0.49 µm. It is well established in the literature that AlCrN coatings provide lubricious properties at high temperatures due to the formation of conducive oxides, which aid with reducing friction [44], and in turn result in improved workpiece surface quality. In contrast, the AlTiN/TiAlSiN coating on average imparted the worst workpiece surface quality, ranging from ~0.75 µm to ~1.16 µm, with rising deterioration as cutting length increased. The AlTiN/ta-C coating ranged from ~0.64 µm to ~0.95 µm, with a dipping trend up to 150 m of cutting length, followed by an increase up to its point of sudden failure (300 m). The base reference AlTiN coating too experienced a decreasing surface roughness trend followed by a mean rise and irregularity. A similar general trend of spike after first pass, drop, followed by a rise with irregularity was noted

at the speed of 175 m/min as well. The AlTiN/AlCrN coating once again was observed to impart the best surface quality on to the workpiece, with a sharp rise after the first pass (1.27 µm), decrementing to ~0.33 µm, and then increasing and pulsing within the range of ~0.49 µm and ~0.72 µm. The typical trend of the coatings experiencing a break-in period is not apparent from the results at 200 m/min as the high impact of the tool on workpiece negated that effect. Nevertheless, excluding the anomalous behavior of the AlTiN/TiAlSiN coating, there are two important trends to note: all coatings increasing in surface roughness (Ra), and the AlTiN/AlCrN coating persistently providing the best surface quality.

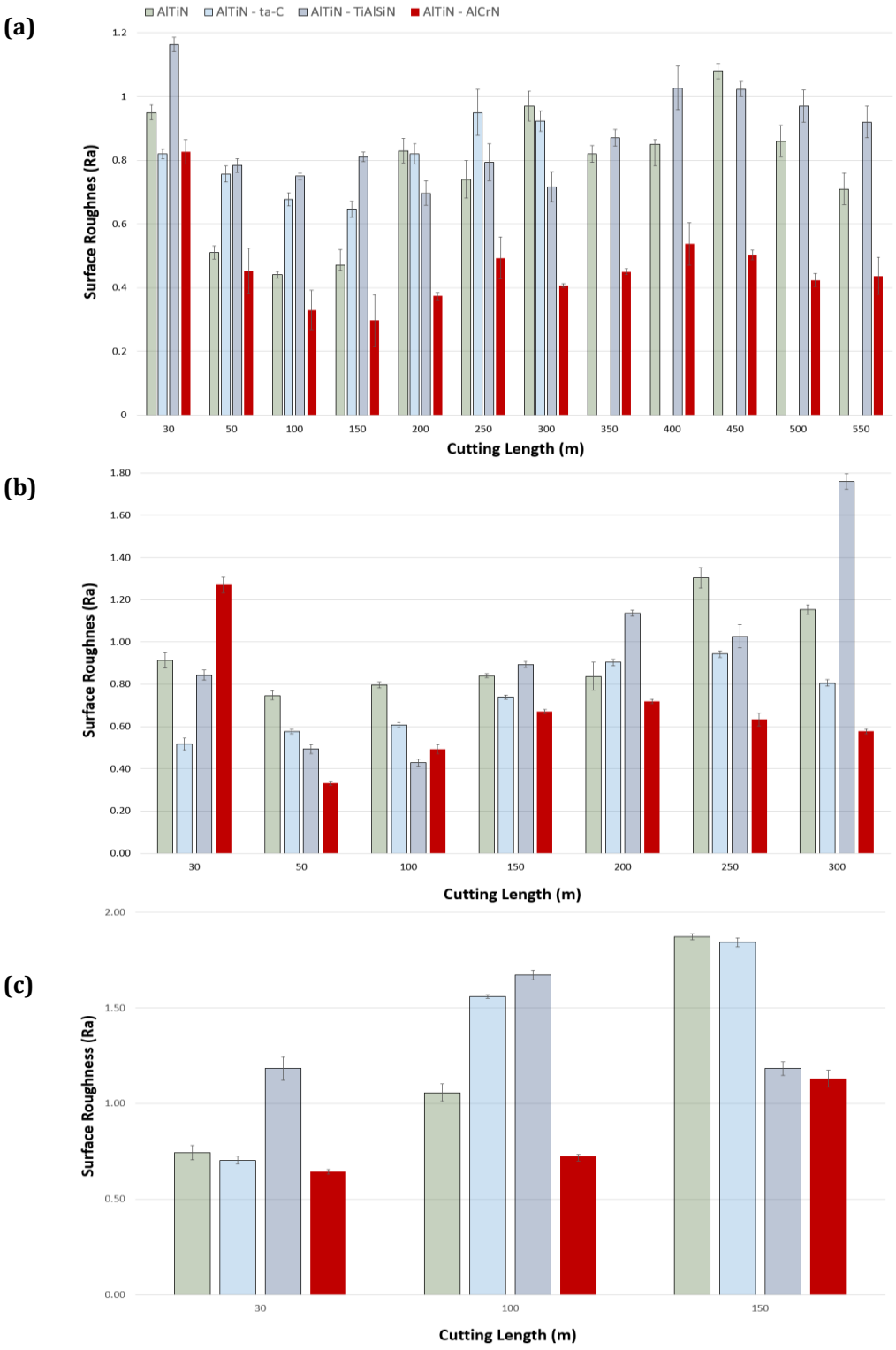


**Figure 3.11: Figure 6. Comparison of surface roughness of the workpiece after machining using the AlTiN/AlCrN-, base AlTiN-, AlTiN/ta-C-, and AlTiN/TiAlSiN-coated tools at the cutting speeds of (a) 150 m/min, (b) 175 m/min, and (c) 200 m/min**

### 3.3.3 Micromechanical Properties of the Coatings

This section covers the micromechanical properties of the coatings, as they give a good indication of how a coating would perform during a machining process, and serve as a basis to substantiate and explain the observed results. Table 5 provides details of the coatings' micromechanical properties, architecture, thickness, surface roughness, and other relevant properties. The coatings' H/E and $H^3/E^2$ ratios were calculated from the hardness (H) and elastic modulus (E) values obtained via a nanoindenter. These properties are often utilized to make inferences about a coating's resistance to wear. The H/E ratio represents a materials elastic strain to failure, or the measure of elasticity at the point of contact between the indenter tip and coating in this context, whereas the $H^3/E^2$ ratio is the coating's ability to resist plastic deformation. It has been reported that under heavy load cutting applications, with the dominant wear mechanism being adhesion, a stable adhesive layer forms on coatings with low H/E and $H^3/E^2$ ratios, resulting in reduced frictional forces [45]. This trend is the opposite of what is typically found—the higher the H/E and $H^3/E^2$ ratios, the better the wear resistance. Another indicator to consider is the plasticity index (PI), which is calculated based on the proportion of plastic work to the total work during indentation [46]. A higher PI indicates that the coating experienced more plastic deformation during indentation. In scenarios where abrasion is dominant, a high H/E ratio (indicating a lower PI) is usually desirable. However, in operations where adhesive wear is dominant, the opposite trend is observed. Studies [47] suggest that having a reserve of plasticity is necessary to dissipate the energy produced during friction, with a higher PI correlating with greater energy dissipation. Additionally, the findings of [48,49] support this trend in turning and milling operations, respectively, where adhesive wear is dominant. Hence, the

AlTiN/AlCrN coating having the smallest of these H/E and $H^3/E^2$ ratios and the highest PI translates to it attaining the best tool-life and workpiece surface quality. The AlTiN/ta-C coating, on the other hand, has the opposite trend, and that translates to it experiencing brittle failure during the machining process, and chips with staggered ridges and roughness within the spacings. The AlTiN/TiAlSiN coating had marginally higher hardness than the base AlTiN coating and had similar H/E and $H^3/E^2$ ratios. These properties when translated to the machining process entails the AlTiN/TiAlSiN coating having marginally shorter tool life as compared to the base monolayer coated tool. Other characterization tests discussed in the Materials and Methods Section have been discussed elsewhere by Syed et al. [39].

### 3.3.4 Tribological Performance

Chip tribological analysis is essential to perform machining at high cutting speeds as it adds an additional layer of depth to the understanding of tool–workpiece interaction and the associated variables—tool life, friction, and the workpiece surface quality imparted as a result [50]. An SEM was used to take high magnification images of the chips to characterize the back surface roughness, shear band morphology, and shape as they tend to be an excellent guide to gain insight into the tribological behavior at the tool–chip interaction zone. Figure 7 shows the visual representation of the back surface quality (magnification 1000×) and accompanying surface roughness (Sa) values extracted via an Alicona Infinite Focus G5 3D surface measurement system for all the coated tools and cutting speeds. By a visual inspection of the SEM images, several key features can be noted at each of the three cutting speeds: The AlTiN/AlCrN coating being a softer coating, with its micromechanical properties conducive to allowing for prolonged plastic deformation,

formed chips that had the smoothest back surface roughness and minimal crease lines. At the highest speed of 200 m/min, due to thermal deformation and stresses, small pockets of uneven spots started to appear. Chips collected from the initial pass of the AlTiN coating indicate that it experienced extensive tearing and had uneven spots as a result of chips sticking to the tool's surface [50,51]. The chips collected from machining via the AlTiN/ta-C coated tool had abrasion and occasional appearance of shred marks as the primary damage mechanism. This is owed to the AlTiN/ta-C coating having a relatively higher coefficient of friction as indicated in a previous work [39]. Chips formed via machining of Ti-5553 using AlTiN/TiAlSiN coated tools had shred marks and folds as the main mechanism of deterioration.

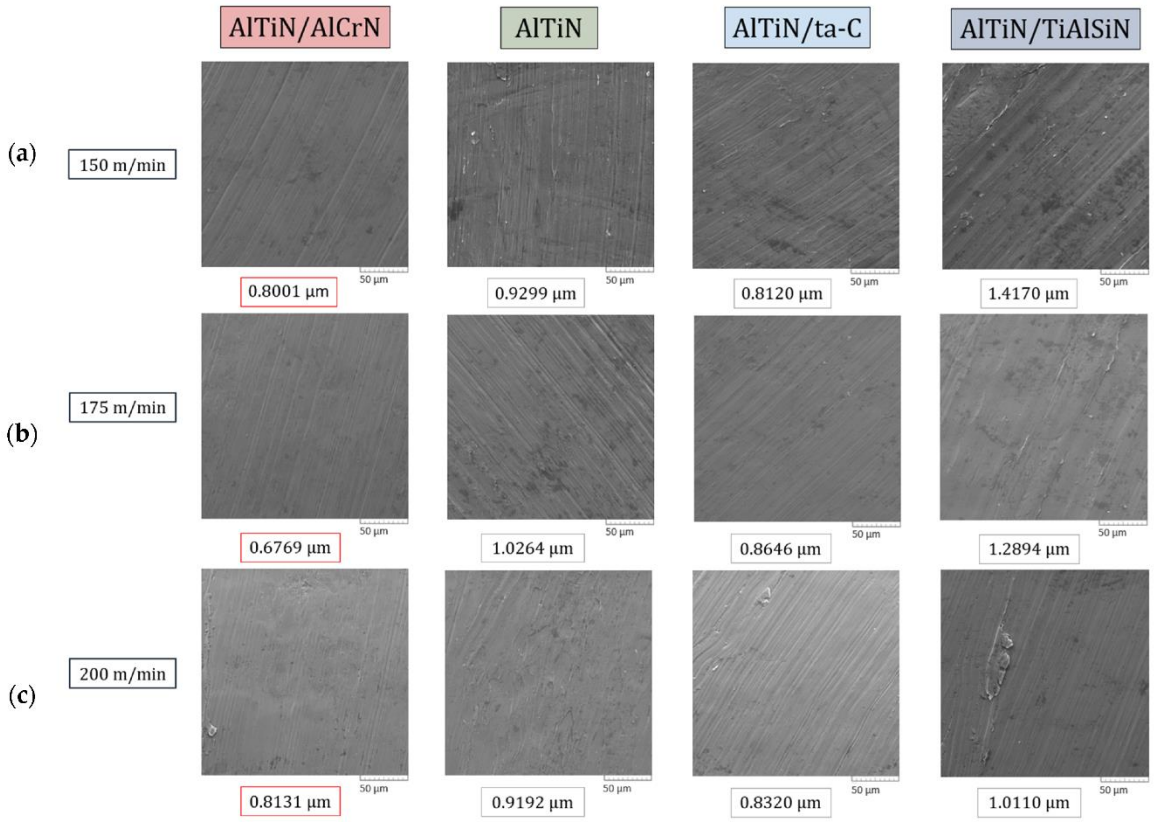


**Figure 3.12: Figure 7. SEM images and surface area roughness (Sa) values of chips collected after the first pass during the machining of Ti-5553 with AlTiN/AlCrN-, base AlTiN, AlTiN/ta-C-, and AlTiN/TiAlSiN-coated tools at the cutting speeds of (a) 150 m/min, (b) 175 m/min, and (c) 200 m/min. Magnification 1000×**

Visual inspection is only one of the many methods by which chip analysis can be performed. Back surface roughness (Sa) is another key indicator to help further understand the tribological behavior at the tool–chip interaction zone during a turning machining process. The general pattern is that of the back surface roughness values being in a particular range for each of the respective coatings: the worst chip back surface quality was found to be on the chips produced using the AlTiN/TiAlSiN coating, with an average value of ~1.239 μm, followed by the base AlTiN coating at ~0.959 μm, AlTiN/ta-C coating at ~0.836 μm, and AlTiN/AlCrN coating having the smoothest back surface roughness at ~0.763 μm. In a recent study by the authors [39], XPS analysis was performed on the rake face of the tools to understand diffusion/oxidation interaction between the workpiece and the cutting tool. The low surface roughness of the chips obtained by the AlTiN/AlCrN coating can partly be attributed to the formation of beneficial $Cr_2O_3$ and $(Al, Cr)_2O_3$ (due to $Cr_2O_3$ solubility in alumina) tribo-oxides. These tribo-oxides have been reported to provide lubricious and thermal barrier properties at high temperatures, which help with reducing friction at the tool–chip interaction zone and protect the tool substrate from thermal damage.

Shear bands of the chips shown in Figure 8 are of significance as they reveal information pertaining to the flow of chips as well as deformation behavior. The shear bands produced by the AlTiN/AlCrN coating experienced minor splitting indicative of plastic deformation with spacing between the ridges holistically smoother than the other three coatings. This relatively better morphology in the AlTiN/AlCrN chips may be owed to it having undergone prolonged plastic deformation and smoother chip flow due to low

friction at the tool–chip interface. The chips produced by the base AlTiN-coated tools had a tendency to experience extreme anisotropic deformation with inconsistent spacing between the ridge segments. In other words, the chip flow and deformation were not continuous. Shear bands collected after machining via the AlTiN/ta-C-coated tools had staggered segments with a continuous ridge line across the shear bands, and rough spacing in-between. The AlTiN/TiAlSiN coated tools produced chips that had an unpredictable pattern across the speeds: large spacing between the ridges at 150 m/min, variance in ridge sizes at 175 m/min, and staggered behavior at 200 m/min.

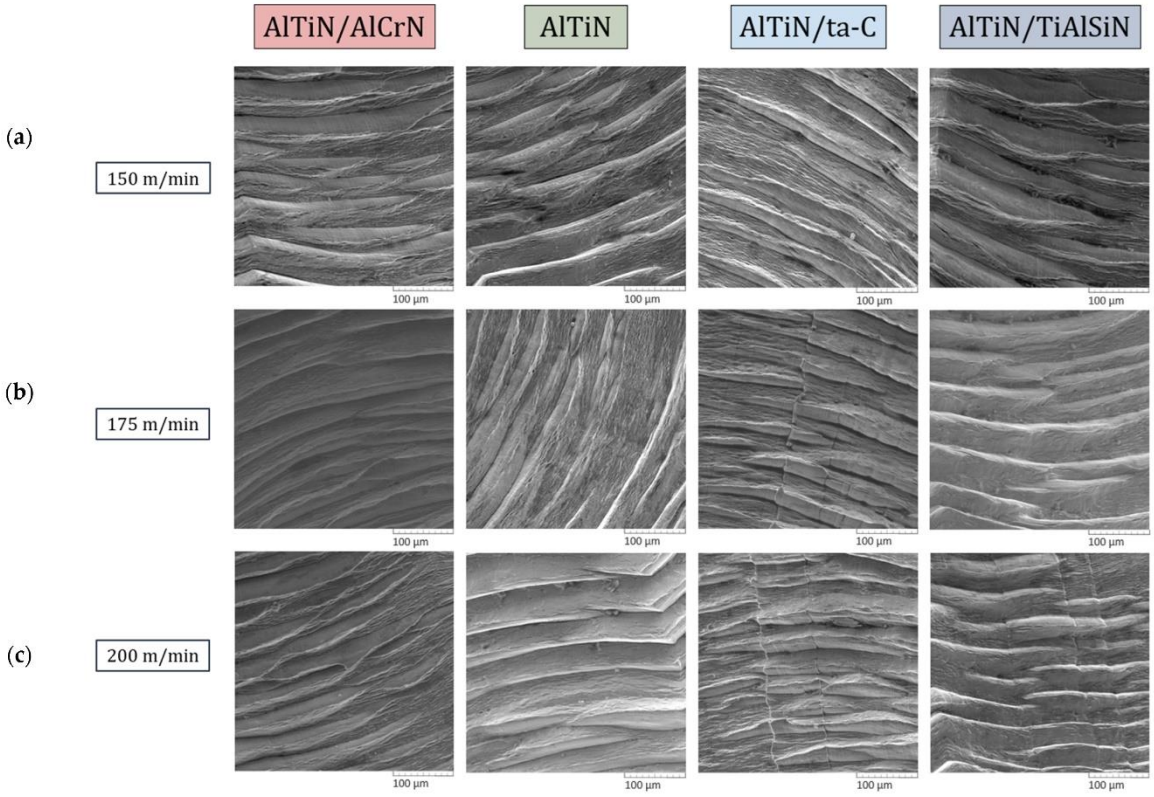


**Figure 3.13: Figure 8. Shear band morphological comparison of chips collected after the first pass during the machining of Ti-5553 with the AlTiN/AlCrN-, base AlTiN-, AlTiN/ta-C-, and AlTiN/TiAlSiN-coated tools at cutting speeds of (a) 150 m/min, (b) 175 m/min, and 200m/min. Magnification 600×**

## 3.4 Conclusions

This study investigated the high-speed finish-turning—150 m/min, 175 m/min, and 200 m/min—of Ti-5553 using novel mono/bi-layered WC cutting tools to fill a void that exists in the literature. The cutting tools involved are composed of a base monolayered AlTiN-coated tool, and AlCrN, ta-C, and TiAlSiN coatings each deposited on top of the base AlTiN coating on three separate cutting tools to form bi-layered AlTiN/AlCrN, AlTiN/ta-C, and AlTiN/TiAlSiN coatings, respectively. The following conclusions are drawn based on the analysis:

- A comparative analysis indicated that the AlTiN/AlCrN-coated tools obtained the longest tool life with an average improvement over the base reference of about 19% based on the average of the three cutting speeds.
- The AlTiN/ta-C coating's brittle nature led to it experiencing premature failure.
- The general trend for all the coatings was that of cutting forces remaining within a specified range up to the approximate midway point of tool life, after which a rise was observed due to geometrical deviations at the cutting tool edge.
- The mean lowest cutting force values obtained by the AlTiN/AlCrN-coated tools can be attributed to its optimal micromechanical properties permitting prolonged plastic deformation before failure.
- The most common wear mechanisms across the speeds were flank and crater wear, with the AlTiN/AlCrN coated tool having experienced the smallest crater wear volume and depth at 150 m/min.

- In general, all the coated tools experienced progressively worsening crater and flank wear with increasing speed, particularly at 200 m/min.
- The AlTiN/AlCrN-coated tools consistently, at all speeds, imparted the highest surface finish on the workpiece, whereas the AlTiN/TiAlSiN-coated tools frequently imparted the worst.
- The chip back surface roughness values were found to be within a specified range for each of the respective coatings; similar to what was observed with the workpiece surface roughness, the smoothest back surface roughness was that of chips obtained via machining using the AlTiN/AlCrN-coated tool as a result of conducive oxide formation and optimal micromechanical properties, and the worst by the AlTiN/TiAlSiN-coated tool due to its hard nature and constituent elements.

## 3.5 References

1. Kolli, R.; Devaraj, A. A Review of Metastable Beta Titanium Alloys. Metals 2018, 8, 506. https://doi.org/10.3390/met8070506.

2. Wang, L.; Wang, Y.; Xu, X.; Liu, C. Dynamic Behaviour and Shock-Induced Martensite Transformation in near-Beta Ti-5553 Alloy under High Strain Rate Loading. EPJ Web. Conf. 2015, 94, 02026. https://doi.org/10.1051/epjconf/20159402026.

3. Veeck, S.; Lee, D.; Boyer, R.; Briggs, R. The Castability of Ti-5553 Alloy: The Microstructure and Properties of Cast Titanium Alloy Ti-5553 Were Evaluated in a Joint Program by Howmet and Boeing. Adv. Mater. Process. 2004, 162, 47–49.

4. Micheletti, C.; Lee, B.E.J.; Deering, J.; Binkley, D.M.; Coulson, S.; Hussanain, A.; Zurob, H.; Grandfield, K. Ti–5Al–5Mo–5V–3Cr Bone Implants with Dual-Scale Topography: A Promising Alternative to Ti–6Al–4V. Nanotechnology 2020, 31, 235101. https://doi.org/10.1088/1361-6528/AB79AC.

5. Cotton, J.D.; Briggs, R.D.; Boyer, R.R.; Tamirisakandala, S.; Russo, P.; Shchetnikov, N.; Fanning, J.C. State of the Art in Beta Titanium Alloys for Airframe Applications. JOM 2015, 67, 1281–1303. https://doi.org/10.1007/S11837-015-1442-4/FIGURES/25.

6. Wagner, V.; Baili, M.; Dessein, G. The Relationship between the Cutting Speed, Tool Wear, and Chip Formation during Ti-5553 Dry Cutting. Int. J. Adv. Manuf. Technol. 2015, 76, 893–912. https://doi.org/10.1007/S00170-014-6326-1/METRICS.

7. Titanium 2005 Conference Proceedings. In Proceedings of the 21st Annual International Titanium Association, Scottsdale, Arizona, 25–27 September 2005.

8. Williams, J.C.; Boyer, R.R. Opportunities and Issues in the Application of Titanium Alloys for Aerospace Components. Metals 2020, 10, 705. https://doi.org/10.3390/met10060705.

9. Zhao, Q.; Sun, Q.; Xin, S.; Chen, Y.; Wu, C.; Wang, H.; Xu, J.; Wan, M.; Zeng, W.; Zhao, Y. High-Strength Titanium Alloys for Aerospace Engineering Applications: A Review on Melting-Forging Process. Mater. Sci. Eng. A 2022, 845, 143260. https://doi.org/10.1016/j.msea.2022.143260.

10. Arrazola, P.-J.; Garay, A.; Iriarte, L.-M.; Armendia, M.; Marya, S.; Le Maître, F. Machinability of Titanium Alloys (Ti6Al4V and Ti555.3). J. Mater. Process. Technol. 2009, 209, 2223–2230. https://doi.org/10.1016/j.jmatprotec.2008.06.020.

11. Lu, J.; Ge, P.; Zhao, Y. Recent Development of Effect Mechanism of Alloying Elements in Titanium Alloy Design. Rare Met. Mater. Eng. 2014, 43, 775–779. https://doi.org/10.1016/S1875-5372(14)60082-5.

12. Ezugwu, E.O.; Wang, Z.M. Titanium Alloys and Their Machinability—A Review. J. Mater. Process. Technol. 1997, 68, 262–274.

13. Nouari, M.; Makich, H. On the Physics of Machining Titanium Alloys: Interactions between Cutting Parameters, Microstructure and Tool Wear. Metals 2014, 4, 335–358. https://doi.org/10.3390/met4030335.

14. Filho, T.K.; He, Q.; Paiva, J.M.; Veldhuis, S.C. An Analysis of Different Cutting Strategies to Improve Tool Life When Machining Ti-5Al-5V-5Mo-3Cr Alloy. J. Manuf. Process. 2023, 102, 50–66. https://doi.org/10.1016/j.jmapro.2023.07.030.

15. Imam, M.A. The 12th World Conference on Titanium Presents Research and Applications of "Wonder Metal." JOM 2011, 63, 16–23. https://doi.org/10.1007/S11837-011-0166-3/METRICS.

16. Parida, A.K.; Maity, K. Analysis of Some Critical Aspects in Hot Machining of Ti-5553 Superalloy: Experimental and FE Analysis. Def. Technol. 2019, 15, 344–352. https://doi.org/10.1016/J.DT.2018.10.005.

17.ASM Material Data Sheet. Available online: https://asm.matweb.com/search/SpecificMaterial.asp?bassnum=mtp641 (accessed on 3 January 2023).

18. Machado, A.R.; Wallbank, J. Machining of Titanium and Its Alloys—A Review. Proc. Inst. Mech. Eng. Part B J. Eng. Manuf. 2016, 204, 53–60. https://doi.org/10.1243/PIME_PROC_1990_204_047_02.

19. Stephenson, D.A.; Agapiou, J.S. Metal Cutting Theory and Practice; Taylor & Francis: London, United Kingdom, 2018. https://doi.org/10.1201/9781315373119.

20. Chowdhury, M.S.I.; Chowdhury, S.; Yamamoto, K.; Beake, B.D.; Bose, B.; Elfizy, A.; Cavelli, D.; Dosbaeva, G.; Aramesh, M.; Fox-Rabinovich, G.S.; et al. Wear Behaviour of Coated Carbide Tools during Machining of Ti6Al4V Aerospace Alloy Associated with Strong Built up Edge Formation. Surf. Coat. Technol. 2017, 313, 319–327. https://doi.org/10.1016/j.surfcoat.2017.01.115.

21. Kaynak, Y.; Gharibi, A. The Effects of Cutting Parameters on Machining Performance of Titanium Alloy Ti-5553. Adv. Mater. Process. Technol. 2019, 5, 317–328. https://doi.org/10.1080/2374068X.2019.1585071.

22. Sun, Y.; Huang, B.; Puleo, D.A.; Jawahir, I.S. Enhanced Machinability of Ti-5553 Alloy from Cryogenic Machining: Comparison with MQL and Flood-Cooled Machining and Modeling. Procedia CIRP 2015, 31, 477–482. https://doi.org/10.1016/J.PROCIR.2015.03.099.

23. Tascioglu, E.; Gharibi, A.; Kaynak, Y. High Speed Machining of Near-Beta Titanium Ti-5553 Alloy under Various Cooling and Lubrication Conditions. Int. J. Adv. Manuf. Technol. 2019, 102, 4257–4271. https://doi.org/10.1007/S00170-019-03291-3/METRICS.

24. Kaynak, Y.; Gharibi, A.; Yılmaz, U.; Köklü, U.; Aslantaş, K. A Comparison of Flood Cooling, Minimum Quantity Lubrication and High Pressure Coolant on Machining and Surface Integrity of Titanium Ti-5553 Alloy. J. Manuf. Process. 2018, 34, 503–512. https://doi.org/10.1016/j.jmapro.2018.06.003.

25. Yan, D.P.; Hilditch, T.; Kishawy, H.A.; Littlefair, G. On Quantifying the Strain Rate During Chip Formation When Machining Aerospace Alloy Ti-5553. Procedia CIRP 2013, 8, 123–128. https://doi.org/10.1016/J.PROCIR.2013.06.076.

26. Kaynak, Y.; Gharibi, A.; Ozkutuk, M. Experimental and Numerical Study of Chip Formation in Orthogonal Cutting of Ti-5553 Alloy: The Influence of Cryogenic, MQL,

and High Pressure Coolant Supply. Int. J. Adv. Manuf. Technol. 2017, 94, 1411–1428. https://doi.org/10.1007/S00170-017-0904-Y.

27. Liu, E.; Wang, R.; Zhang, Y.; An, W. Tool Wear Analysis and Mapping Wear for Cryogenic Machining of Ti-5553 with Uncoated Cemented Carbide. Integr. Ferroelectr. 2022, 227, 28–38. https://doi.org/10.1080/10584587.2022.2065572.

28. Wang, L.; Li, R.; Liu, E.; Zhang, H. Experimental Research on Chip Morphology of Ti-5553 Cutting under High-Pressure Cooling. Integr. Ferroelectr. 2022, 229, 62–77. https://doi.org/10.1080/10584587.2022.2074224.

29. Liu, E.; Wang, R.; Zhang, Y.; An, W. Tool Wear Analysis of Cutting Ti-5553 with Uncoated Carbide Tool under Liquid Nitrogen Cooling Condition Using Tool Wear Maps. J. Manuf. Process. 2021, 68, 877–887. https://doi.org/10.1016/j.jmapro.2021.06.016.

30. Kaynak, Y.; Gharibi, A. Cryogenic Machining of Titanium Ti-5553 Alloy. J. Manuf. Sci. Eng. 2019, 141, 041012. https://doi.org/10.1115/1.4042605.

31. Yan, D.P.; Jin, X. Characterization of Shear Band Formation and Microstructure Evolution during Orthogonal Cutting of Ti-5553: Part I—Shear Angle, Strain and Strain Rate. J. Mater. Eng. Perform. 2020, 29, 4063–4074. https://doi.org/10.1007/S11665-020-04880-0/FIGURES/9.

32. Zhao, X.; Li, R.; Liu, E.; Lan, C. Effect of Cryogenic Cutting Surface Integrity on Fatigue Life of Titanium Alloy Ti-5553. Fer-roelectrics 2022, 596, 115–125. https://doi.org/10.1080/00150193.2022.2087254.

33. Liu, E.; Deng, S.; Zhang, C.; Zhang, H.; Wei, X. Simulation and Experimental Research on Tool Temperature Field for Low-Temperature Cutting of Ti-5553. Ferroelectrics 2020, 563, 139–147. https://doi.org/10.1080/00150193.2020.1760618.

34. Liu, E.; Wang, R.; Zhang, Y.; Lan, C. Surface Integrity Analysis of Ti-5553 under Different Cooling Strategies. Ferroelectrics 2022, 593, 51–62. https://doi.org/10.1080/00150193.2022.2076433.

35. Liu, E.; Xu, G.; Wang, N. Analysis of Surface Morphology of Ti-5553 Based on Wavelet Transform. Integr. Ferroelectr. 2021, 217, 129–140. https://doi.org/10.1080/10584587.2021.1911304.

36. ISO 3685:1993; Tool-Life Testing with Single-Point Turning Tools. ISO: Geneva, Switzerland, 1993. Available online: https://www.iso.org/standard/9151.html (accessed on 26 December 2023).

37. ISO 21920-3:2021; Geometrical Product Specifications (GPS)—Surface Texture: Profile—Part 3: Specification Operators. ISO: Geneva, Switzerland, 2021. Available online: https://www.iso.org/standard/72228.html (accessed on 9 June 2024).

38. ISO 14577-4:2016; Metallic Materials—Instrumented Indentation Test for Hardness and Materials Parameters—Part 4: Test Method for Metallic and Non-Metallic Coatings. ISO: Geneva, Switzerland, 2016. Available online: https://www.iso.org/standard/61823.html (accessed on 25 December 2023).

39. Syed, H.S.; De Paiva, J.M.; Veldhuis, S.C. Wear and Micromechanical Performance of Novel Mono/Bi-Layered PVD-Coated WC Tools in High-Speed Turning of Ti-5Al-5V-5Mo-3Cr Alloy. Int. J. Adv. Manuf. Technol. 2024, 133, 4939–4955. https://doi.org/10.1007/S00170-024-14045-1.

40. Lawn, B.R.; Borrero-Lopez, O.; Huang, H.; Zhang, Y. Micromechanics of Machining and Wear in Hard and Brittle Materials. J. Am. Ceram. Soc. 2021, 104, 5–22. https://doi.org/10.1111/JACE.17502.

41. Montazeri, S.; Aramesh, M.; Veldhuis, S.C. An Investigation of the Effect of a New Tool Treatment Technique on the Ma-chinability of Inconel 718 during the Turning Process. Int. J. Adv. Manuf. Technol. 2019, 100, 37–54. https://doi.org/10.1007/S00170-018-2669-3/METRICS.

42. Fatima, A.; Wasif, M.; Ahmed, A.; Yaqoob, S. Effect of Rake Face Surface of Cutting Tool on Tool Crater Wear. Manuf. Rev. 2023, 10, 15. https://doi.org/10.1051/MFREVIEW/2023013.

43. Hatt, O.; Crawforth, P.; Jackson, M. On the Mechanism of Tool Crater Wear during Titanium Alloy Machining. Wear 2017, 374–375, 15–20. https://doi.org/10.1016/J.WEAR.2016.12.036.

44. Galindo, R.E.; Endrino, J.L.; Martínez, R.; Albella, J.M. Improving the Oxidation Resistance of AlCrN Coatings by Tailoring Chromium Out-Diffusion. Spectrochim. Acta Part B At. Spectrosc. 2010, 65, 950–958. https://doi.org/10.1016/j.sab.2010.09.005.

45. Ding, F.; Wang, C.; Zhang, T.; Deng, Y.; Zhu, X. Adhesive Wear Mechanism of Coated Tools and Its Influence on Cutting Performance during Machining of Zr-Based

Bulk Metallic Glass. J. Mater. Res. Technol. 2023, 27, 5489–5506. https://doi.org/10.1016/j.jmrt.2023.11.073.

46. Beake, B.D. The Influence of the H/E Ratio on Wear Resistance of Coating Systems—Insights from Small-Scale Testing. Surf. Coat. Technol. 2022, 442, 128272. https://doi.org/10.1016/J.SURFCOAT.2022.128272.

47. Beake, B.D.; Fox-Rabinovich, G.S.; Veldhuis, S.C.; Goodes, S.R. Coating Optimisation for High Speed Machining with Advanced Nanomechanical Test Methods. Surf. Coat. Technol. 2009, 203, 1919–1925. https://doi.org/10.1016/J.SURFCOAT.2009.01.025.

48. Chowdhury, M.S.I.; Bose, B.; Rawal, S.; Fox-Rabinovich, G.S.; Veldhuis, S.C. Investigation of the Wear Behavior of PVD Coated Carbide Tools during Ti6Al4V Machining with Intensive Built up Edge Formation. Coatings 2021, 11, 266. https://doi.org/10.3390/COATINGS11030266.

49. Saciotto, V.; He, Q.; Guimaraes, M.C.; DePaiva, J.M.; Kohlscheen, J.; Fontana, L.C.; Veldhuis, S.C. A Comparative Study on Al0.6Ti0.4N Coatings Deposited by Cathodic Arc and HiPIMS in End Milling of Stainless Steel 316L. Coatings 2024, 14, 811. https://doi.org/10.3390/COATINGS14070811.

50. He, Q.; Depaiva, J.M.; Kohlscheen, J.; Veldhuis, S.C. Analysis of the Performance of PVD AlTiN Coating with Five Different Al/Ti Ratios during the High-Speed Turning of Stainless Steel 304 under Dry and Wet Cooling Conditions. Wear 2022, 492–493, 204213. https://doi.org/10.1016/j.wear.2021.204213.

51. He, Q.; DePaiva, J.M.; Kohlscheen, J.; Veldhuis, S.C. A Study of Mechanical and Tribological Properties as Well as Wear Per-formance of a Multifunctional Bilayer AlTiN PVD Coating during the Ultra-High-Speed Turning of 304 Austenitic Stainless Steel. Surf. Coat. Technol. 2021, 423, 127577. https://doi.org/10.1016/j.surfcoat.2021.127577.

# 4 Chapter 4: Conclusions, Contributions, and Future Directions

## 4.1 Conclusions

Ti-5553 is a relatively novel material often employed in the aerospace industry for its resilience and strength. However, its exceptionally high mechanical properties render it very difficult to cut. In addition, investigation of the effect of PVD-coated WC tools on the machining, particularly turning machining of Ti-5553, is very limited. Hence, a thorough investigation of the impact of novel mono/bi-layered WC PVD-coated tools on the finish-turning of Ti-5553 under high speeds was conducted. This study prioritized the wear, micromechanical, and tribological performance of four sets of coated tools, namely, AlTiN, bi-layered AlTiN/AlCrN, AlTiN/ta-C, and AlTiN/TiAlSiN coatings, and their resulting machining performance:

- A comparative analysis revealed that AlTiN/AlCrN-coated tools achieved the longest tool life, with an average improvement of approximately 19% over the base reference across three cutting speeds.
- For all coatings, cutting forces generally remained within a specified range until about midway through the tool's life, after which an increase was observed due to geometrical deviations at the cutting tool edge.
- The AlTiN/AlCrN-coated tools demonstrated the lowest mean cutting force values, attributed to their optimal micromechanical properties (H/E, $H^3/E^2$, and PI) supported by the micro scratch tests, allowing for prolonged plastic deformation before failure.

- The most common wear mechanisms at various speeds were flank and crater wear, with the AlTiN/AlCrN-coated tool showing the smallest crater wear volume and depth at 150 m/min.
- All coated tools experienced progressively worsening crater and flank wear with increasing speed, particularly at 200 m/min.
- AlTiN/AlCrN-coated tools consistently produced the highest surface finish on the workpiece at all speeds, while AlTiN/TiAlSiN-coated tools often resulted in the worst surface finish.
- A coating's tribological performance and tool life are greatly influenced by its inherent characteristics—its adaptation after the break-in period, its micromechanical properties, and the types of oxides formed by its constituent elements. The $Cr_2O_3$ oxides detected via XPS on the rake face of the AlTiN/AlCrN coated tool were indicative of in situ lubrication and thermal barrier properties during the machining of Ti-5553, which effectively protected the coated tool in the initial stages of cutting, thereby extending its tool life.
- Chip back surface roughness values were within a specified range for each coating. Similar to workpiece surface roughness, chips from machining with the AlTiN/AlCrN-coated tool had the smoothest back surface roughness due to beneficial oxide formation and optimal micromechanical properties, whereas the AlTiN/TiAlSiN-coated tool produced the roughest due to its hardness and composition.

## 4.2 Research Contributions

My research primarily focused on the application of novel PVD-coated tools for the finish-turning of Ti-5553, an alloy known for its difficult-to-cut nature. A detailed analytical study was conducted on the wear, and micromechanical characteristics of mono- and bi-layered PVD-coated tools during high-speed finish turning operations, resulting in the publication of two journal papers. The research contributes to improvement in the overall tool life and machinability performance of the Ti-5553 alloy, leading to improved efficiency and cost-effective manufacturing. The insights acquired from this research work hope to be of value to the Canadian manufacturing industrial sectors, particularly aerospace and biomedical, where the selection and application of such advanced materials and coatings are critical to maintaining a competitive edge in the global market.

## 4.3 Future Directions

Although the research conducted addressed many of the existing research gaps, the work can be built upon to investigate other limitations and potential directions of future development:

- The utilization of multiple process parameters such as depth of cut, feed rate, a wider range of cutting speeds, and more coated tool variants to find the most optimal machining parameters and conditions for the finish-turning of Ti-5553 may be considered.
- The Design of Experiment (DoE) approach could be utilized to systematically investigate the interactions between the various machining parameters and conditions to account for variability and increase the robustness of the results.

- A comparative analysis of lubricant types would aid in analyzing the effectiveness of heat dissipation and tool performance.
- Conducting further investigation into the performance of cohesion/adhesion behavior of the coatings to attain a better understanding of the deformation mechanics, particularly for AlTiN/ta-C due to its anomalous rise and fall nature as opposed to a continuous rise.
- Investigating how functionally graded cutting tools impact the machining efficiency of Ti-5553.
- Examining optimal cutting speed ranges for conducive lubricious and heat-dissipating tribe-oxides for prolonged tool life and excellent workpiece surface integrity.
- The use of the Finite Element Analysis (FEA) technique may be necessary to simulate a broad range of conditions to aid in selecting optimal cutting parameters for experimental analysis, as well as to generate thermal and stress models to gain further insights as to what goes on in the tool-workpiece interaction zone.